ÉCOLE DE TECHNOLOGIE SUPÉRIEURE
UNIVERSITÉ DU QUÉBEC

MANUSCRIPT-BASED THESIS PRESENTED TO
ÉCOLE DE TECHNOLOGIE SUPÉRIEURE

IN PARTIAL FULFILLMENT OF THE REQUIREMENTS FOR
THE DEGREE OF DOCTOR OF PHILOSOPHY
Ph.D.

BY
Jonathon SUMNER

TOWARDS IMPROVED RANS/$k-\varepsilon$ MODELLING OF TURBULENT INCOMPRESSIBLE FLOWS FOR WIND ENERGY APPLICATIONS

MONTREAL, AUGUST 17, 2012

BOARD OF EXAMINERS

THIS THESIS HAS BEEN EVALUATED

BY THE FOLLOWING BOARD OF EXAMINERS:

Prof. Christian Masson, Thesis director
Département de Génie Mécanique, École de Technologie Supérieure

Mr. Daniel Cabezón, Thesis co-director
Wind Energy Department, National Renewable Energy Centre of Spain

Prof. Saad Bennis, Committee president
Département de Génie de la Construction, École de Technologie Supérieure

Dr. Gregory S. Oxley, External examiner
Global Flow Solutions, Vestas Technology R&D

Prof. Louis Dufresne, Examiner
Département de Génie Mécanique, École de Technologie Supérieure

THIS DISSERTATION WAS PRESENTED AND DEFENDED

IN THE PRESENCE OF A BOARD OF EXAMINERS AND PUBLIC

ON JULY 23, 2012

AT ÉCOLE DE TECHNOLOGIE SUPÉRIEURE

ACKNOWLEDGEMENTS

First and foremost, I would like to sincerely thank Prof. Christian Masson for his guidance, mentorship, and, above all, willingness to let me set my own course. He has supervised both my master's and doctoral research and provided me with innumerable interesting opportunities over the last nine years. I am enormously grateful. I have enjoyed all of the projects we have been involved in together and look forward to many more in the future.

In the same breath, I must also acknowledge the kind support of my co-director Daniel Cabezón and thank him and his family for the truly warm welcome my family and I received in Spain. Muchísimas gracias pollo!

I would also like to recognize the financial support I have received from the Natural Sciences and Engineering Research Council of Canada both directly through the Postgraduate Scholarship program and indirectly through its funding of the Wind Energy Strategic Network. Without its support, none of this would have been possible.

To all my colleagues at ÉTS, CENER and Dawson: the next coffee is on me! A heartfelt thanks for the good times and enlightening discussions to Nicolas, Simon-Philippe, Hugo, Mary, Louis-Étienne, Chérif, Chris W., Jean-François, Chris R., Michelle, Mo, Joel, Nadim, y todos mis amigos espagnoles Philip, Marcelino, Ignacio, Anna Rosa, Julia, Roger, y Ines. Time indeed flies.

My entire extended family has always been incredibly supportive of my endeavours – despite the fact they sometimes take me to faraway places – and I have appreciated their encouragement greatly.

Lastly, to the two most important people in my life, my wife Annie and my daughter Molly, this is dedicated to you.

TOWARDS IMPROVED RANS/$k-\varepsilon$ MODELLING OF TURBULENT INCOMPRESSIBLE FLOWS FOR WIND ENERGY APPLICATIONS

Jonathon SUMNER

ABSTRACT

The advancement of wind energy as a viable and competitive alternative to traditional sources is dependent on the development of advanced modelling techniques to decrease both the cost of energy and the cost uncertainty. Of special importance in this effort is the improvement of wind energy assessment tools. While so-called linearized models have dominated this field in the past, models based on the Reynolds-Averaged Navier–Stokes (RANS) equations are becoming more popular, especially for difficult sites involving complex terrain and multiple wakes. Although RANS modelling is implicitly more appropriate for complex flows than its lower-order derivatives, refinements are required to better adapt it to the needs of the sector and improve accuracy. With that in mind, this dissertation strives to make fundamental improvements in the use of RANS-based models for the simulation of atmospheric and wake flows.

Despite common use of the RANS equations with $k-\varepsilon$ closure for simulations involving the atmospheric boundary layer, challenges remain in its implementation – even for the simplest case involving horizontally homogeneous conditions. Most notably, the distributions of turbulent kinetic energy and its dissipation rate have proved difficult to maintain near solid boundaries, particularly in wind energy and wind engineering applications where the near-wall grid is relatively coarse. In the first study of this dissertation, the origin of these errors is investigated and it is shown that by applying appropriate discretization schemes in conjunction with the Richards and Hoxey boundary conditions, truly invariant profiles of all flow properties can be obtained on such grids. Furthermore, based on this finding, a wall treatment for *practical* grids is proposed that could be implemented for non-homogeneous conditions.

The second study focuses on the physical modelling of atmospheric flows. The limited-length-scale $k-\varepsilon$ model proposed by Apsley and Castro for the atmospheric boundary layer is revisited with special attention given to its predictions in the constant-stress surface layer. The original model proposes a modification to the length-scale-governing ε equation that ensures consistency with surface-layer scaling in the limit of small ℓ_m/ℓ_{max} (where ℓ_m is the mixing length and ℓ_{max} its maximum) and yet imposes a limit on ℓ_m as ℓ_m/ℓ_{max} approaches one. However, within the equilibrium surface layer and for moderate values of z/ℓ_{max}, the predicted profiles of velocity, mixing length, and dissipation rate using the Apsley and Castro model do not coincide with analytical solutions. In view of this, a general ε transport equation is derived herein in terms of an arbitrary desired mixing-length expression that ensures exact agreement with corresponding analytical solutions for both neutral and stable stability. From this result, a new expression for the closure coefficient $C_{\varepsilon 3}$ can be inferred that shows it tends to a constant only for limiting values of z/L (where z is the height above ground and L is the Monin-Obukhov length); and, furthermore, that the values of $C_{\varepsilon 3}$ for $z/L \to 0$ and $z/L \to \infty$ differ by a factor of exactly two.

Wake modelling also plays an important role in wind energy assessment. These models must be reasonably accurate – to minimize financial risk – and yet economical so that many layouts can be tested within reasonable time. While numerous such models have been proposed, an especially attractive approach is based on the solution of the RANS equations with two-equation turbulence closure and an actuator disk representation of the rotor. The validity of this approach and its inherent limitations however remain to be fully understood. In the final study, detailed wind tunnel measurements in the wake of a porous disk (with similar aerodynamic properties as a turbine rotor) immersed in a uniform flow are compared with the predictions of several turbulence closures, including a newly proposed one. Agreement with measurements is found to be excellent for all models. This unexpected outcome appears to derive from a fundamental difference in the turbulent nature of the homogeneous wind tunnel flow and that of the atmospheric boundary layer. This result suggests that the largest source of uncertainty in turbulence modelling remains the production term and leads to a discussion on similarity requirements for wind tunnel testing.

Keywords: wind energy, atmospheric surface layer, computational fluid dynamics, turbulence modelling, $k-\varepsilon$ closure, finite volume method, discretization error, wall treatment, mixing length, stably-stratified flow, wind turbine wakes, wind tunnel, actuator disk.

ÉVALUATION ET AMÉLIORATION DE LA MODÉLISATION DES ÉCOULEMENTS INCOMPRESSIBLES ET TURBULENTS À PARTIR DES ÉQUATIONS DE NAVIER–STOKES MOYENNÉES AVEC LA FERMATURE $k-\varepsilon$ POUR LES APPLICATIONS ÉOLIENNES

Jonathon SUMNER

RÉSUMÉ

La promotion de l'énergie éolienne comme une alternative viable et compétitive aux sources traditionnelles est dépendant du développement des techniques de modélisation avancées qui vont diminuer à la fois le coût de l'énergie et l'incertitude reliée à son évaluation. D'une importance particulière dans cet effort est l'amélioration des outils d'évaluation de la production des projets éoliens. Bien que des modèles linéarisés ont dominé ce domaine dans le passé, les modèles basés sur les équations de Navier–Stokes moyennées (RANS) sont de plus en plus populaires, surtout pour les sites difficiles où les effets de topographie et de sillage sont importants et se mélangent. Cependant, même si la modélisation RANS est implicitement plus appropriée pour les écoulements complexes que ses dérivés d'ordre inférieur, des améliorations sont nécessaires pour l'adapter aux besoins du secteur et améliorer la précision. Avec cela à l'esprit, cette thèse vise à apporter des améliorations fondamentales en ce qui concerne l'utilisation de modèles basés sur les équations RANS pour la simulation des écoulements atmosphériques et en sillage d'une éolienne.

Malgré l'utilisation courante des équations RANS avec le modèle $k-\varepsilon$ comme fermeture pour les simulations en couche limite atmosphérique, des défis subsistent dans la mise en œuvre de cette approche – même pour le cas le plus simple impliquant des conditions homogènes. Plus particulièrement, les distributions d'énergie cinétique turbulente et son taux de dissipation se sont révélées difficiles à maintenir à proximité des frontières solides, ce qui est surtout problématique quand les maillages à proximité de la paroi sont relativement grossiers. Dans la première étude de cette thèse, l'origine de ces erreurs est investigué et il est démontré qu'en appliquant des schémas de discrétisation appropriées et les conditions aux frontières de Richards et Hoxey, des profils invariants de toutes les propriétés d'écoulement peuvent être obtenus sur de tels maillages. En outre, grâce à ce travail, un traitement de paroi pour les maillages *pratiques* est proposé qui peut être appliqué aux conditions non-homogènes.

La deuxième étude se concentre sur la modélisation physique des écoulements atmosphériques. Le modèle $k-\varepsilon$ modifié de Apsley et Castro pour la couche limite atmosphérique est revisité avec une attention particulière à ses prédictions dans la couche limite de surface où le cisaillement est constant. Ces auteurs ont proposé une modification à l'équation de ε (qui détermine l'échelle de longueur des mouvements turbulents) afin d'imposer une limite sur la longueur de mélange en respectant toutefois la similitude près de la paroi. Cependant, des simulations de la couche limite de surface avec cette fermeture peuvent donner des profils de vitesse, longueur de mélange, et taux de dissipation de turbulence qui ne coïncident pas avec les solutions analytiques. Compte tenu de cela, une équation de ε générique est dérivée en termes d'une

distribution de la longueur de mélange arbitraire qui assure la concordance exacte avec les solutions analytiques correspondantes pour des conditions de stratification thermique neutre ainsi que stable. De ce résultat, une nouvelle expression pour le coefficient de fermeture $C_{\varepsilon 3}$ peut être déduite démontrant que ce coefficient n'est constant que pour des valeurs extremes de z/L (où z est la distance du sol et L est la longueur de Monin-Obukhov). En fait, $C_{\varepsilon 3}$ varie d'un facteur de deux entre les limites de $z/L \to 0$ et $z/L \to \infty$.

La modélisation du sillage d'une éolienne a aussi un rôle important à jouer dans l'évaluation d'un projet éolien. Ces modèles doivent être assez précis – afin de minimiser les risques financiers – et pourtant économique de telle sorte que de nombreuses configurations peuvent être évaluées dans un délai raisonnable. Tandis que plusieurs modèles de ce genre ont été déjà proposés, une approche particulièrement intéressante est basée sur la solution des équations RANS avec une fermeture à deux équations et où l'action du rotor est modelisée par un disque actuateur. La validité d'une telle approche et ses limitations inhérentes reste toutefois à être pleinement comprises. Dans la dernière étude, des mesures détaillées en soufflerie dans le sillage d'un disque poreux (avec les mêmes propriétés aérodynamiques d'une éolienne) immergé dans un écoulement uniforme sont comparées avec les prévisions de plusieurs fermetures, y compris une nouvelle proposition. L'accord avec les mesures est jugé excellent pour tous les modèles. Ce résultat inattendu semble provenir d'une différence fondamentale dans la nature turbulente de l'écoulement en soufflerie et celle de la couche limite atmosphérique. De plus, ce résultat suggère que la plus grande source d'incertitude dans la modélisation de la turbulence reste dans le terme de production et conduit à une discussion sur les exigences de similarité pour des essais en soufflerie.

Mots-clés: énergie éolienne, couche limite de surface, modélisation numérique en dynamique des fluides, modélisation de la turbulence, la fermature $k-\varepsilon$, méthodes aux volumes finies, erreur de discretisation, traitement à la paroi, longueur de melange, stratification thermique stable, sillages des éoliennes, soufflerie, disque actuateur.

CONTENTS

LIST OF TABLES

LIST OF FIGURES

LIST OF SYMBOLS

Co-ordinates

r	Radial direction
θ	Azimuthal direction
x	Cartesian
y	Cartesian
z	Cartesian

Greek symbols

α	Coefficient of thermal expansion, 1/K
α	Interpolation factor
β	RNG $k-\varepsilon$ model coefficient
β	Surface-layer scaling parameter
ε	Turbulence dissipation rate, m^2/s^3
γ	Diffusion coefficient
θ'	Fluctuating part of decomposed potential temperature, K
θ_*	Characteristic potential temperature, K
Θ	Mean potential temperature, K
χ	Step function
κ	von Karman constant
η	RNG $k-\varepsilon$ model parameter
η_0	RNG $k-\varepsilon$ model coefficient
Π_k	Turbulence production rate, m^2/s^3
ϕ	General scalar
ϕ_ε	Universal similarity function
ϕ_m	Universal similarity function
ρ	Fluid density, kg/m^3
σ_ε	$k-\varepsilon$ model coefficient
σ_k	$k-\varepsilon$ model coefficient
σ_θ	Turbulent Prandtl number
σ_u	Standard deviation of U velocity component, m/s
τ'	Kinematic Reynolds stress tensor, m^2/s^2
τ_ε	Relaxation time, s
τ_D	Modified relaxation time, s
τ'	Kinematic shear stress, m^2/s^2
ν	Kinematic viscosity, m^2/s
ν_t	Turbulent (eddy) viscosity, m^2/s
ζ	Non-dimensional height, $= z/\ell_{max}$

Roman symbols

a	Axial induction factor
A_{disk}	Disk (or rotor) area, m^2
A_{wake}	Area of wake measurement, m^2
A_{wt}	Wind tunnel cross-sectional area, m^2
c_p	Specific heat at constant pressure, $m^2/s^2/K$

C_D	Drag coefficient
$C_{\varepsilon 1}$	$k-\varepsilon$ model coefficient
$C_{\varepsilon 2}$	$k-\varepsilon$ model coefficient
$C_{\varepsilon 3}$	$k-\varepsilon$ model coefficient
$C_{\varepsilon 4}$	$k-\varepsilon$ model coefficient
C_μ	$k-\varepsilon$ model coefficient
C_P	Power coefficient
C_T	Thrust coefficient
D	Diameter, m
$\vec{f}$	Body force, N
f_ε	Wall function to correct ε source term in k transport equation
f_{ε^2}	Wall function to correct ε source term in ε transport equation
$f_{\nabla\varepsilon}$	Wall function to correct Laplacian term in ε transport equation
f_G	Wall function to correct G source term in k transport equation
$f_{G\varepsilon}$	Wall function to correct G source term in ε transport equation
$f_{\nabla U}$	Wall function to correct Laplacian term in momentum equation
f	General wall function
F	Weighting function
g	Gravitational field strength, N/m
G_k	Turbulence production rate, m^2/s^3
H	Hub height, m
$\mathbf{I}$	Identity matrix
I	Imbalance or residual, 1/m
I_{atm}	Atmospheric turbulence intensity
I_U	Streamwise turbulence intensity
k	Turbulent kinetic energy, m^2/s^2
ℓ	Length scale, m
ℓ_ε	Length scale related to dissipation of k, m
ℓ_m	Mixing length, m
ℓ_{max}	Maximum mixing length, m
ℓ_t	Length scale related to transport of k, m
L	Monin-Obukhov length, m
L	Length scale, m
$\hat{n}$	Cell face normal
p	Modified mean pressure, Pa or m^2/s^2 (if normalized by fluid density)
p_{wake}	Wake pressure, Pa
P_k	Turbulence production rate, m^2/s^3
Q_H	Heat flux, W/m^2
R	RNG $k-\varepsilon$ model parameter
Re_t	Turbulent Reynolds number
R_f	Flux Richardson number based on ratio of buoyant to shear turbulence production rate
R'_f	Flux Richardson number based on ratio of buoyant to total turbulence production rate
R_{wake}	Radius of wake measurements, m
$\vec{s}_f$	Cell face area vector, m^2

S	Source term
$\overline{S}$	Volume-average of source term
$\mathbf{S}$	Mean strain rate tensor, 1/s
T	Thrust, N
$\vec{U}$	Mean velocity vector with components (U,V,W), m/s
u^*	Friction velocity, m/s
$\vec{u}'$	Fluctuating part of decomposed velocity vector with components (u',v',w'), m/s
u_0	Velocity scale, m/s
u^*_{sl}	Friction velocity related to shear stress τ' that drives surface-layer flow, m/s
u^*_g	Ground friction velocity based on wind speed in wall-adjacent cell, m/s
U_∞	Freestream flow speed, m/s
U'	Unmeasured flow speed, m/s
U_{ref}	Mean horizontal wind speed at reference height, m/s
U_{wake}	Measured wake flow speed, m/s
ΔV	Cell volume, m^3
Δz	Cell height, m
z_0	Aerodynamic roughness length, m
z^+	Non-dimensional wall-normal distance, $= u^* z/\nu$
z_{ref}	Reference height, m
Subscripts	
CV	Control volume
f	Refers to a cell face
n	Refers to a cell face between P and N
NT	Refers to cell adjacent to top boundary
N	Refers to 'north' neighbour
P	Refers to current cell
s	Refers to cell face between P and S
S	Refers to 'south' neighbour
t	Refers to top boundary of computational domain
w	Refers to wall boundary, *i.e.* at z_0

INTRODUCTION

0.1 Context

The new millenium has seen the beginning of a global energy revolution. The spectre of peak oil, heightened concerns regarding pollution, greenhouse gas emissions and climate change, and attractive government subsidies are stimulating the development of a new market for sustainable energy sources. For the first time, onshore wind has been recognized as a potentially competitive primary electricity generation source by the International Energy Agency (IEA, 2010b), while renewables as a sector have recently experienced incredible growth (IEA, 2011). Wind-based energy conversion systems remain the most economically viable option and make the largest contribution to the clean energy movement (in terms of installed capacity). As energy demands climb and the cost of traditional sources increases, wind energy will not only see its capacity grow but also its market share: it is forecast to provide as much as 13% of worldwide electricity needs by 2035 (IEA, 2010a).

At first glance, this outlook may seem overly optimistic. In fact, the wind energy sector has been growing at a breakneck pace since the mid-nineties: worldwide cumulative installed capacity grew at an average rate of nearly 30% annually in the period from 1996 to 2010, as shown in figure 0.1 (Pullen and Sawyer, eds., 2010). Even if the year-on-year growth rate has recently slowed, the above projections remain realistic. This is predicated by the fact that while wind energy has long established itself as an ecologically sound alternative to the trifecta of oil, coal, and gas, it is rapidly becoming an economically competitive option as well.

However, despite generally favourable socio-economic conditions and a relatively mature technology, the wind energy industry faces several obstacles to increasing penetration levels and attaining absolute cost parity. These have been enumerated by the European Wind Energy Technology Platform and translated into a set of strategic research and development objectives (TPWind, 2008). Among the numerous initiatives proposed, one of the predominant themes centres around the reduction of uncertainties in wind resource assessment, improved predic-

tion of wind farm energy production, and better evaluation of turbine loading. Furthermore, implicit to the objective of attaining cost parity is the idea of optimal exploitation.

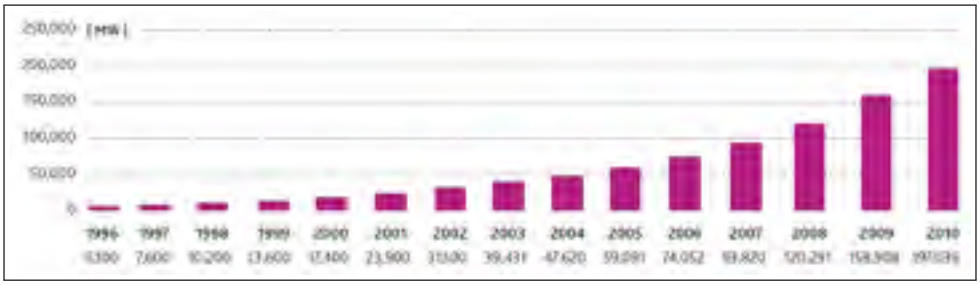

Figure 0.1 Global cumulative installed wind capacity 1996–2010.
From: Pullen and Sawyer, eds. (2010)

0.1.1 Technical challenges

The common thread is a need for improved modelling. Consider first wind resource assessment. Evaluation of site suitability is generally based on direct observation via a short measurement campaign ($\sim$1 year) where wind speed and temperature statistics are recorded at a few discrete locations and at several heights. The compiled data is then correlated to long-term regional observations to improve climatological representivity (Nielsen *et al.*, 2001) upon which energy projections may then be based. The end result is a characterization of the wind resource, in terms of direction, frequency and intensity, at the measurement locations only. The challenge is to spatially extrapolate these observations to the entire region of interest. The importance of accuracy in this work is underlined by the fact that energy production is proportional to the cube of wind speed: a 1% uncertainty in the extrapolated independent variable becomes a 3% uncertainty in the dependent variable.

The problem of micro-siting turbines – that is, the determining of optimal positions – is doubly challenging given the implicit nature of the task: turbines themselves affect the local resource by removing kinetic energy and increasing downstream turbulence[1]. As topographic influences become more important, the combined effect of multiple wakes and surface conditions on flow properties becomes increasingly difficult to predict leading to appreciable uncertainty in the

[1] A good wind farm flow model might be simply defined as one that provides accurate predictions of these two effects.

forecasted energy production. To further complicate the issue, turbine positioning is subject to loading requirements which are highly dependent on both the average wind velocity and the level of turbulence. While accurately extrapolating the mean velocity can be a difficult task in and of itself, it is considerably easier than extrapolating the energy contained in the turbulent fluctuations about the mean.

0.1.2 The need for advanced models

It is worth noting that the most common approach for wind energy assesment still involves the use of a *linearized* model – one that is based on a simplified form of the equations governing flow fluid – such as WAsP (Troen and Petersen, 1989) or MS-Micro (Taylor *et al.*, 1983). Although these models are, to some extent, a reflection of the available computing power at the time of their development, they are clearly inspired by early-generation wind farms. They are valid for thermally neutral flow over gently sloping terrain and low hills and perform very well when predicting the flowfield for cases that conform to this limited parameter space (Ayotte, 2008). However, the modern wind energy industry is expanding and looking to exploit both offshore and mountainous sites. As the terrain becomes more complex, non-linear effects such as recirculation become dominant flow features and linearized models are ill-suited. In fact, the calculations of Ayotte (2008) over smooth and rough two-dimensional hills suggest that such models yield unacceptably large error for slopes greater than 0.2.

As may be surmised from the preceding, advanced mathematical models will be required to adequately address the technical challenges the wind energy sector presently faces. To this end, computational fluid dynamics (CFD) – the field dedicated to solving the partial differential equations governing fluid flow by approximate numerical means – is being increasingly used to deal with the inherent complexity of atmospheric flows and their interaction with turbines, both individually and in large groups. Although use of CFD is expected to improve the accuracy of resource predictions in areas where flow separation and thermal effects are characteristic of the flow (Landberg *et al.*, 2003), this approach has never been the tool of choice of wind energy specialists and its pace of adoption remains slow for a variety of reasons. At the research level, CFD has long been used to predict the flow over complex terrain (see Bit-

suamlak *et al.* (1999) for a concise review) and wind energy related applications can be found in the recent literature. Hashimoto *et al.* (2007) applied CFD to the problem of ideal turbine siting, not only for the improved flowfield representation but also for its ability to estimate turbulence properties. Further examples can be found of CFD being used to help design measurement campaigns in the selection of proper measurement sites (Bechmann *et al.*, 2007) and in numerical site calibration (Brodeur and Masson, 2008). Palma *et al.* (2008) have provided guidance on the use of CFD in combination with conventional techniques for wind resource assessment and micro-siting in another recent case study. The development of new commercial CFD software marketed specifically to the wind energy sector will help build confidence in these methods and contribute to increased use by industry.

The overarching objective of the present work is to support this paradigm shift. In particular, the goal is to improve modelling techniques related to wind energy assessment in order to reduce cost uncertainty and the associated financial risks. Diminishing such hurdles opens the door to greater investment which supports the ultimate end of reducing dependence on fossil fuels and developing a more sustainable energy mix.

0.2 Scope and methodology

At the scale of wind farms, the application of CFD techniques is largely focused on the prediction of the flowfield over topography and on the evaluation of wind turbine wakes. A slightly more precise statement of the dissertation objectives is then to improve modelling of a) atmospheric flows, and b) the rotor-wind interaction. Research in these areas is generally divided along two lines: those who are interested in *describing*, in as much detail as possible, the time-varying turbulent structures that arise from the interactions of the wind with terrain and with an operating rotor, and those who are primarily interested in *modelling* such effects for macroscopic analyses. While the former group often employs high-order transient numerical methods based on large- or detached-eddy simulation to investigate the development and dissipation of vortical structures, the latter group is more interested in modelling the energy available, the extraction process, and its influence on far-wake turbulent flow properties in a time-averaged sense. Immediately, then, a distinction in methodologies can be made based on

physical realism; the present work falls squarely into the latter category where the interest is simply in the "average" flow.

0.2.1 Conservation laws and mathematical modelling

The nature of turbulent flows is such that an exact solution to the governing equations is simply impossible to attain, especially at high Reynolds number (Gatski and Rumsey, 2002). However, in many instances one is satisfied with modelling the effects of turbulence on the mean flow and, although use of large-eddy simulation (LES) for wind energy applications has started in earnest, the majority of models are based on the steady, incompressible Reynolds-Averaged Navier–Stokes (RANS) equations derived from the principles of conservation of mass and momentum:

$$\nabla \cdot \vec{U} = 0, \tag{1}$$

$$\nabla \cdot \vec{U}\vec{U} = -\nabla p + \nabla \cdot \boldsymbol{\tau}' + \vec{f}. \tag{2}$$

Here, $\vec{U}$ represents the mean velocity vector and p is the modified mean pressure (normalized by fluid density) (Pope, 2000). $\vec{f}$ represents a body force (*e.g.* Coriolis, buoyancy, *etc.*). $\boldsymbol{\tau}'$ is the deviatoric component of the kinematic Reynolds stress tensor. It appears as part of the time-averaging process and represents the turbulent transport of momentum. It is often assumed to dominate the viscous terms which have been neglected.

The rank-2 stress tensor is symmetric and introduces six new unknowns – the covariances of the time-varying components of the velocity field: $\overline{u'u'}$, $\overline{u'v'}$, $\overline{u'w'}$, $\overline{v'v'}$, $\overline{v'w'}$, and $\overline{w'w'}$. The four RANS equations contain thus a total of ten unknowns and are *open*. To close the system, the Boussinesq linear (or isotropic) eddy-viscosity hypothesis is often applied

$$\tau'_{ij} = -\overline{u'_i u'_j} = 2\nu_t S_{ij} - \frac{2}{3} k \delta_{ij} \tag{3}$$

where S_{ij} is the mean strain rate tensor, the components of which are

$$S_{ij} = \frac{1}{2}\left(\frac{\partial U_i}{\partial x_j} + \frac{\partial U_j}{\partial x_i}\right) \tag{4}$$

and the eddy viscosity, ν_t, must be modeled. The isotropic part of the stresses related to the turbulent kinetic energy, *i.e.* $2k/3$, can be subsumed by the pressure term (Gatski and Rumsey, 2002) – thus "modifying" it – as their action on the flow is the same and pressure loses its meaning as a thermodynamic variable for incompressible flows (Pope, 2000). This leaves

$$\boldsymbol{\tau}' = 2\nu_t \mathbf{S}. \tag{5}$$

If desired, viscous effects can be reintroduced by replacing ν_t with an effective viscosity $\nu_{eff} = \nu_t + \nu$.

The most popular closure of this type is the standard $k-\varepsilon$ model of Jones and Launder (1972) wherein the eddy viscosity is given by

$$\nu_t = C_\mu \frac{k^2}{\varepsilon} \tag{6}$$

and C_μ is a closure coefficient. The turbulent kinetic energy, k, and its dissipation rate, ε, are each modelled with transport equations. In steady form,

$$\nabla \cdot k\vec{U} = \nabla \cdot \left(\frac{\nu_t}{\sigma_k}\nabla k\right) + P_k - \varepsilon, \tag{7}$$

$$\nabla \cdot \varepsilon\vec{U} = \nabla \cdot \left(\frac{\nu_t}{\sigma_\varepsilon}\nabla \varepsilon\right) + C_{\varepsilon 1} P_k \frac{\varepsilon}{k} - C_{\varepsilon 2}\frac{\varepsilon^2}{k} \tag{8}$$

where $C_{\varepsilon 1}$, $C_{\varepsilon 2}$, σ_ε, and σ_k are closure coefficients and again ν_t could be replaced by ν_{eff} to account for viscous action. P_k is a source term representing the rate of production of k,

$$P_k = 2\nu_t S_{ij} S_{ij}. \tag{9}$$

0.2.2 Justification of approach

In some sense, RANS modelling appears to be a half measure. Yes, the non-linearity of the fluid flow equations is maintained and basic conservation laws respected, but the description of turbulence is inherently limited. This is a considerable drawback given the importance of turbulence in many flows. Why not then use eddy-resolving schemes directly?

For the moment, the simple answer is that RANS-based modelling is both more practical and more mature. This situation is admittedly transient; on a horizon of five to ten years eddy-resolving techniques may well come to dominate atmospheric flow modelling for wind energy applications. Certainly, research on the use of LES for such purposes is increasing and the recent works of *e.g.* Brasseur and Wei (2010) and Meyers and Meneveau (2012) make this prediction all the more plausible. LES is analogous to direct numerical simulation for high Reynolds number flows as a large fraction of the turbulent kinetic energy is directly resolved (see Pope (2000); Sagaut (2006) for review of method). Sub-grid scale models are used to handle turbulence at scales smaller than some filter width, which is often the grid itself. At this scale, the eddy-viscosity concept has more relevance and the assumption of isotropy may be valid. Although many problems associated with RANS closure can be avoided using an LES-based approach, the computational effort is considerably greater. In a review on the use of LES for flow over complex terrain, Wood (2000) concluded that true LES of atmospheric boundary layer flow over a three-dimensional, rough surface of arbitrary shape was still a long way off based on the grid refinement and averaging time required to properly resolve non-linear interactions at all scales and obtain meaningful turbulence statistics. Citing the work of Chow and Street (2004) (see Chow and Street (2009) for most recent developments) and Chow *et al.* (2006) regarding LES modelling of flow over Askervein and a valley in the Alps, Ayotte (2008) also concludes that direct use of LES specifically for wind energy is not yet feasible, although concedes that at some point it will likely be used as part of wind farm design. As a case in point, Uchida and Ohya have developed an LES-based model for analyzing neutral flow over variable orography (Uchida and Ohya, 1999, 2003) and applied it to the problem of proper site selection (Uchida and Ohya, 2006).

The difficulties in applying LES to wall-bounded flows are largely due to impractical grid requirements in the near-wall region (Piomelli and Balaras, 2002; Piomelli, 2008) – the region of greatest importance for wind energy purposes. Hybrid RANS/LES methods, in which the near-wall flow is modeled using a RANS approach that is coupled to an LES model away from the surface, appear to offer a way out. Silva Lopes and Palma (2002) were the first to analyze Askervein using such an approach and a later paper by Silva Lopes *et al.* (2007) elaborates on the strengths and weaknesses of using a hybrid scheme. More recently, Bechmann and Sørensen (2010) have also applied a hybrid model to Askervein that uses an unsteady RANS/$k-\varepsilon$ closure in the near-wall region and LES with $k-\varepsilon$ acting as a sub-grid model for the outer layer. Validation with the Askervein data shows, as reported by others, that calculations using standard RANS/$k-\varepsilon$ result in an underestimation of hill top wind speeds and leeside turbulent kinetic energy while the proposed hybrid RANS/LES approach yielded excellent agreement with these measurements.

This cursory review on the topic of LES reveals the progress, the possibilities, and the roadblocks. The near-certain eventuality of LES supplanting RANS for atmospheric flow modelling would, on the surface, diminish the importance of the work presented here and the continued push for better RANS turbulence closures in both the wind energy and wind engineering fields. But this should not be seen as the case. Firstly, RANS modelling is something of a bridge to more advanced techniques: a jump from linearized solvers to LES is simply not in the cards. Secondly, for the reasons mentioned above, LES is some time away from being truly practical and an interim solution is required to deal with complex cases; the RANS equations coupled with two-equation closure appear to be the most suitable approach (Bechmann *et al.*, 2011). Thirdly, as mentioned above, RANS (or more specifically URANS) models have an important role to play in hybrid schemes.

There is another, perhaps subtle, reason for continued research in RANS-based flow modelling: as computing power increases and LES becomes feasible, RANS simulations will too become that much more economical. It is in this context that one might envision the use of RANS-based models for the optimization of wind farms; an application that depends on relatively accurate

modelling and one in which LES will surely be unable to make any significant contribution for the foreseeable future. Given that even modest increases in production can yield significant financial gains, there is a strong impetus to develop modelling tools which accurately predict the mean flow properties within a park and that can subsequently be incorporated as part of a scheme to systematically improve layouts.

Given these arguments, this thesis aims to resolve some fundamental issues related to RANS/$k-\varepsilon$ modelling of flows for wind energy assessment purposes.

0.3 Thesis organization

This dissertation is presented as a series of manuscripts. In the first article, the basic problem of simulating a steady, incompressible, horizontally homogeneous, and neutrally stratified surface-layer flow with the RANS equations and $k-\varepsilon$ closure is considered. Historically, the simulation of such flows has proved surprisingly problematic which is particular given the availability of an analytical solution. Chapter 1, entitled *$k-\varepsilon$ simulations of the neutral atmospheric boundary layer: analysis and correction of discretization errors on practical grids*, treats this problem directly.

In the second article, *The Apsley and Castro limited-length-scale $k-\varepsilon$ model revisited for improved performance in the atmospheric surface layer*, the surface-layer model presented in Chapter 1 is adapted to account for more realistic conditions. In general, the *mixing length* – a parameter related to the maximum size of turbulent eddies – is predicted to increase proportionally with height above ground in the standard $k-\varepsilon$ model but, in reality, cannot increase indefinitely. Rather, it tends to be bounded by some physical constraint: stable stratification, boundary layer depth, *etc*. Regardless of the source of the limit, the standard model must be modified to account for this action. This has proven tricky in the past, and here a single modified formulation of the $k-\varepsilon$ model is proposed that can reproduce both neutral length-limited and stable surface layers. This is of special importance to offshore wind farms where stable conditions are common, rotor diameters are large and hub heights relatively low: wind shear effects become quite important and must be accurately reproduced.

In the closing chapter on the *Evaluation of RANS modelling of wind turbine wake flow using wind tunnel measurements*, the actuator disk concept is added to the RANS/eddy-viscosity framework for the purpose of wake analysis. This topic is something of a minefield: this combination of models has previously been shown to have fundamental flaws. Here, a modified closure is proposed, that hopes to partially address the known issues, and wind tunnel experiments are solicited as a means to evaluate several two-equation turbulence closures.

Following the dissertation conclusions, two additional and more practical case studies are presented as annexes. Annex I provides a summary of several wind flow simulations over the small isolated island of Bolund while the simulations presented in Annex II concern the flow through an entire wind farm situated in moderately complex terrain. Most importantly, the suitability of RANS-based models for wind resource assessment and for the estimation of wind farm power performance is assessed by comparing predictions with field measurements.

LITERATURE REVIEW

Foreword

The following chapter presents an overview of the application of CFD for wind energy assessment and is based largely on the survey published by Sumner *et al.* (2010). More critical discussions of the literature as it relates to the research presented herein are contained in the manuscripts. The following serves to provide context to the work and highlight the contributions of this dissertation.

0.4 RANS modelling of atmospheric flows

0.4.1 Homogeneous conditions

The simplest atmospheric flow is that of the idealized surface layer wherein the shear stress and sensible heat flux are assumed constant with height, there is no pressure gradient in the flow direction, and the velocity distribution is logarithmic or perhaps log-linear. Although rarely observed, this *model* of the flow in the lowest portion of the atmosphere has importance for CFD applications not only in the validation of codes but also as the approach flow in both wind engineering and wind energy simulations.

It is only recently that idealized surface-layer flows have been accurately simulated using common CFD techniques. Richards and Hoxey (1993) made the most important contribution to this effort by defining the appropriate boundary conditions for the $k-\varepsilon$ model (for neutral conditions). Several others have since commented on lingering difficulties related to wall function implementation issues (Blocken *et al.*, 2007) and unexpected near-wall distributions of turbulent kinetic energy (Hargreaves and Wright, 2007). Fortuitously, problems in specifying proper boundary conditions have become less relevant with the recent availability of high-quality, open-source CFD software that allows users to modify the source code directly. On the other hand, the problems with respect to the turbulent kinetic energy distribution have been more difficult to resolve and have been the focus of several recent works (by *e.g.* Gorlé *et al.* (2009) and Parente *et al.* (2011)).

The challenge in modelling surface-layer flows is somewhat increased when the heat flux is non-zero. Until lately, the effect of atmospheric stability has been somewhat overlooked by the wind energy community. It may, however, be an important factor for offshore installations as stable thermal stratification is common and wind shear effects are exacerbated by very large rotors. Additionally, Eidsvik (2005) postulates that stability effects in mountainous terrain may lead to large uncertainties for RANS models. Efforts have already been made to incorporate buoyancy effects in a RANS/$k-\varepsilon$ framework. The modification proposed by Rodi (1987) wherein a buoyancy-dependent term is added to the transport equations is commonly used; however, the value chosen for the closure coefficent $C_{\varepsilon 3}$ varies greatly. Freedman and Jacobson (2003) have since shown that, in fact, any constant value for $C_{\varepsilon 3}$ is inconsistent with similarity theory. Alinot and Masson (2005) have thus proposed a polynomial expression for $C_{\varepsilon 3}$ in the dimensionless stability parameter z/L, where z is height above ground and L the Monin-Obukhov length, based on surface-layer similarity profiles.

0.4.2 Heterogeneous conditions

Most current use of CFD for flow simulations in complex terrain entails the solution of the incompressible RANS equations with two-equation turbulence closure. Often, thermal effects and the Coriolis force are neglected. Lower-order turbulence models are avoided as they appear to lack the sophistication required to handle recirculation whereas higher-order methods require longer computing times. As mentioned already, the $k-\varepsilon$ model, and variants thereof, are presently the most popular closures.

Many authors have previously reported on the known weaknesses of the standard model which, in the context of flow over complex terrain, tend to manifest as an overestimation of turbulent kinetic energy and an underestimation of mean flow recirculation. To try to remedy these issues, variations on the $k-\varepsilon$ theme are common. Chen and Kim (1987) modified the ε equation by adding a new production term in an effort to balance turbulence production for highly strained flows. In their derivation of the RNG $k-\varepsilon$ model, Yakhot and Orszag (1986) and Yakhot and Smith (1992) modified the standard ε equation in a similar manner.

Maurizi (2000) has tested these two versions of the $k-\varepsilon$ model, along with its standard form, for flow over two-dimensional valleys using wind tunnel data from the RUSVAL experiment. For gentle slopes with attached flow, all three models yield similar results for the mean velocity field. However, when recirculation is present, the mean flow solution is much more sensitive to the ε transport equation and results between the models vary considerably; the RNG version yields the best agreement with data. Considering the prediction of turbulent kinetic energy, differences are present even for attached flow, and none of the models provide consistently better predictions. For the Reynolds stresses, the RNG model again appears to provide the best results, however Maurizi suggests a transport equation for $\overline{u'w'}$ be included to overcome some fundamental problems with the modelling of this quantity under the eddy-viscosity concept. It is further recommended that for flows involving recirculation, the RNG model should be used.

Ying *et al.* (1994) have performed a similar analysis over the two-dimensional analytical hill from the RUSHIL experiment by solving the compressible RANS equations again using three closure schemes: the standard $k-\varepsilon$ model, an algebraic Reynolds stress model (ARSM) and an extended $k-\varepsilon-\overline{u'w'}$ model that includes a transport equation for the $\overline{u'w'}$ stress component. All the closure schemes provide reasonable and roughly equivalent results for the mean velocity field but, again, large discrepancies are observed in the calculated turbulent shear stress. Focusing on predictions at the hilltop, both the standard model and the ARSM provide poor underestimations of $\overline{u'w'}$ while the $k-\varepsilon-\overline{u'w'}$ model provides satisfactory results. The improvement is attributed to the ability of second-order closure to account for advection of upstream turbulence.

While some researchers have focused on modifying the ε equation, others have taken a closer look at the prescription of the time scale used in the definition of eddy-viscosity. Whereas standard $k-\varepsilon$ uses

$$\nu_t = C_\mu k \tau_\varepsilon \tag{10}$$

with the *relaxation time* being defined as

$$\tau_\varepsilon = \frac{k}{\varepsilon}. \tag{11}$$

Durbin (1996) proposed imposing a *realizability* constraint,

$$\tau = \min\left[\tau_\varepsilon, \tau_D\right] \tag{12}$$

with

$$\tau_D = \frac{2}{3C_\mu\sqrt{2|\mathbf{S}|^2}}$$

Nagano *et al.* (2001) and Nagano and Hattori (2003) have developed this idea further and proposed various mixed time scale models based on mean strain rate and vorticity tensors (referred to as the $\mathbf{S}$ model and Ω model, respectively, and $\mathbf{S}-\Omega$ for their hybrid).

Despite some success using the revised non-linear $k-\varepsilon$ model proposed by Shih *et al.* (1995) for flow over a curved hill (Lun *et al.*, 2003), numerical stability problems prompted Lun *et al.* to evaluate these improved linear $k-\varepsilon$ models for wind energy predictions in complex terrain (Lun *et al.*, 2007). For flow over a single isolated hill, the Durbin model predicts upstream turbulent kinetic energy well, but severely underestimates its magnitude in the wake. Conversely, the Ω model performs well in the wake, but overestimates k upstream. In terms of mean velocity, the Ω model is in good agreement with measurements whereas the Durbin model grossly overestimates the size of the recirculation zone behind the hill. Use of the mixed time scale model $\mathbf{S}-\Omega$ somewhat corrects the overestimation of k at the hill top and generally improves estimates of separation and reattachment points in the hill wake. From this analysis and others, Lun *et al.* conclude that the $\mathbf{S}-\Omega$ version performs best; Muramaki *et al.* (2003) have integrated this approach as part of a wind turbine micro-siting scheme.

In his analysis of computational wind energy assessment methods, Ayotte (2008) has also simulated flow over symmetric two-dimensional hills of various slope using a full Reynolds stress transport model (RSTM) and compared with wind tunnel data. Mean flow predictions are in excellent agreement with measurements except in the wake region for large slopes where the mean flow recovers too quickly. This points to limitations in the RANS approach that will not likely be overcome by any of the above treatments and suggests the need for more advanced eddy-resolving techniques, especially if accurate turbulence predictions are desired. It was

further confirmed that the predicted mean velocity is relatively insensitive to the closure used: tests indicate that two-equation $k-\varepsilon$ and full second-order closures yield negligibly different results.

Considering flow over real terrain, Kim and Patel (2000) have investigated the performance of RNG $k-\varepsilon$ by simulating neutral flow through the Sirhowy Valley in Wales, over an embankment on the Rhine in Germany, and over Askervein hill in Scotland. The choice of RNG was motivated by case studies involving flow over a triangular ridge and several two-equation closure schemes. In general, the RNG-based model best predicted mean velocity and turbulence characteristics, including the size and shape of recirculation zones. In a separate work, Kim *et al.* (2000) presented further case studies using the RNG model for Cooper's Ridge, Kettles Hill, Askervein hill, and the Sirhowy Valley. For Cooper's Ridge, the simulation results for mean wind speed at 3 m above ground level show good agreement with measurements on the windward slope and at the hill top. Similar conclusions can be made for the flow prediction over Kettles Hill. For Askervein, predicted 10-m velocities are in good agreement, even on the leeside, although hill top wind speeds are underestimated. Some problems predicting hill top and leeside turbulence are noted. The Sirhowy Valley simulations further demonstrate the ability of the RNG model to predict separation and reattachment. El Kasmi and Masson have also applied the RNG model to simulate the flow over Blashavel hill using a set of closure coefficients calibrated for the atmospheric boundary layer (El Kasmi and Masson, 2010).

Starting with Raithby *et al.* (1987), many RANS models (*e.g.* Kim and Patel (2000); Castro *et al.* (2003); Eidsvik (2005); Undheim *et al.* (2006); Prospathopoulos and Voutsinas (2006); Laporte (2008)) have been evaluated using the Askervein Hill experiment (see Taylor and Teunissen (1987) for description, Mickle *et al.* (1988) for data). Castro *et al.* (2003) have carried out a grid dependence study using the standard $k-\varepsilon$ model in addition to unsteady RANS calculations to investigate low-frequency, time-dependent effects in the lee of the hill. Mean velocities at 10 m are well predicted, but k is overestimated in the upstream region. More recently, Eidsvik (2005) presented a down-scaling method for wind power estimation in mountainous terrain for near-neutral flows based, at the smallest scale, on a RANS/$k-\varepsilon$ approach

which is validated using the Askervein data. To account for the anisotropy of turbulence, Eidsvik employs the non-linear algebraic stress model proposed by Gatski and Speziale (1993). As for Castro *et al.*, mean velocity predictions agree well with measurements at 10 m, even in the lee of the hill. Upstream turbulence is correctly predicted, however hill top values underestimate observations. Prospathopoulos and Voutsinas (2006) have used the Askervein case to develop guidelines for RANS simulations in complex terrain.

An extensive wind flow measurement campaign over the small, isolated island of Bolund has recently been carried out by Risø DTU to provide a new database for the validation of flow models over real topography (Berg *et al.*, 2011). A blind comparison based on these measurements has underlined the challenges involved in making flow predictions over complex terrain (Bechmann *et al.*, 2011). Importantly, the lower bound of the average speed-up error for two-equation RANS closures was pegged at 6.5% for estimates in the *outer layer*, sufficiently far from ground, and roughly 10% overall. While this result is significantly better than that of linearized models and somewhat better than LES, there remains considerable room for improvement.

In addition to variable surface roughness and orography, complex terrain also implies the possible presence of forested regions. Given that forest canopies absorb momentum over a finite depth, a distributed drag force is a more appropriate boundary condition than simply incorporating a displacement height within the velocity wall function (Ayotte, 2008). Lopes da Costa *et al.* (2006) used the extended $k-\varepsilon$ model of Svensson and Häggkvist (1990) and an additional drag term in the momentum equation to study the wind over two moderately complex sites with forest cover. Comparisons with wind data above the forest highlight the importance of incorporating the distributed effect of canopies when predicting mean wind speed and turbulence properties. Dalpé and Masson (2008) have implemented a similar approach with the modified $k-\varepsilon$ closure of Katul *et al.* (2004). Results of one-dimensional simulations within and above three different forests are in good agreement with measurements. Ayotte (2008) has implemented second-order closure and compared with LES calculations for flow over a forested hill. Here, the problems observed for an unforested hill are somewhat exacerbated:

the increased drag causes the flow to be more prone to separation. The influence of eddies with length scales related to the hill and canopy are not adequately modeled with a RANS approach.

Considering the ensemble, it is interesting to note that, for the purposes wind resource assessment, it appears the exact closure scheme has little impact on the predicted mean flow velocity for locations of interest for simple cases (*i.e.* an isolated hill top) although the RNG variant seems best at dealing with flow recirculation. As alluded to in the introduction, the accurate prediction of turbulent properties is much more difficult and there is considerably less agreement between closure schemes. Given the importance of turbulence predictions for the evaluation of turbine loads, the use of an additional transport equation for $\overline{u'w'}$ seems prudent and worth further investigation.

0.5 RANS modelling of wind turbine wakes

Extensive reviews of the modelling of wind turbine wakes have been previously reported by Crespo *et al.* (1999), by Vermeer *et al.* (2003), and more recently by Sanderse *et al.* (2011). Here, the focus is on developments involving the use of CFD for the modelling of far wakes in the context of wind farms. As mentioned previously, far-wake modelling is dominated by actuator disk methods as the action of the blades need only be accounted for in an average sense. Methods for specifying forces applied by the actuator disk on the flow vary; usually constant loading is assumed or blade-element momentum theory is applied (see Mikkelsen (2003)), although the choice of method appears to have little effect on resolved far wake properties (El Kasmi and Masson, 2008). There are also differences in the application of the rotor thrust within a finite volume scheme: it generally appears either as a "volume" force or as a discrete pressure discontinuity.

0.5.1 Single wake

Considering a single isolated rotor in a uniform flow, Sørensen *et al.* (1998) have used the actuator disk concept to analyze wind turbine wake states for laminar conditions; however, most current analyses incorporate turbulence effects. Standard $k-\varepsilon$ closure typically underestimates the velocity defect as turbulent diffusion is too high in the wake region. El Kasmi and Masson

(2008) have applied the Chen and Kim modified ε equation to a discrete volume around the rotor to correct this weakness and improve wake predictions for a single turbine. The Chen and Kim modification effectively limits the turbulent kinetic energy (and viscosity) in this region as the new ε source term is a function of the turbulence production rate.

Cabezón *et al.* (2009) have presented a comparison of single-wake RANS simulations using various two-equation closure schemes, as well as RSTM, for the Sexbierum experiment. They have shown that while standard $k-\varepsilon$ grossly underestimates the velocity defect, the use of the El Kasmi and Masson approach greatly improves predictions. The realizable model proposed by Shih *et al.* also performs well. In both cases, the improvement is explained by an increase in the dissipation rate in the region of the rotor. In terms of velocity defect, the results are comparable to RSTM and in good agreement with data. All models tend to underestimate turbulence intensity, especially in the near wake, except along the axis of rotation where agreement with measurements is better. With respect to wake turbulence intensity, an earlier study by Gómez-Elvira *et al.* (2005) looked at the anisotropy of wake turbulence using the Sexbierum case with an explicit algebraic stress model. Prospathopoulos *et al.* (2009) have carried out a similar analysis to Cabezón *et al.* using the Nibe wake data and $k-\omega$ closure for both neutral and stable conditions. Here, the El Kasmi and Masson and Durbin corrections both improve velocity defect predictions.

However, as Réthoré (2009) argues, non-physical increases in ε to temper overestimations of ν_t makes application of these methods somewhat dubious for multiple wakes. More generally, Réthoré has exposed some fundamental problems with the use of the acuator disk/eddy-viscosity concepts for modelling wind turbine wakes that suggest a completely different approach may be needed. One possibility is LES. Although the eddy-viscosity concept may be used for sub-grid models, the context in which it is applied is more appropriate and should not pose the same problems (Réthoré, 2009). Jimenez *et al.* (2007) have implemented a simplified LES/actuator disk approach and comparisons of calculated turbulence properties are in good agreement with experimental data. RSTM may also be an attractive solution.

0.5.2 Multiple wakes

The objective of wake modelling, at the scale of wind farms, is to accurately predict the velocity defect and increase in turbulence to better model power variations and fatigue loading. Early approaches to accounting for the velocity defect in micro-siting relied on empirically derived guidelines outlining minimum distances between turbines in an array (Patel, 1999). Using an actuator disk approach to analyze a two-row array, Ammara *et al.* (2002) have shown these guidelines to be overly conservative. Barthelmie *et al.* (2009) have carried out a comparison of wind farm models, ranging from engineering to full CFD models, for predicting power losses due to wake effects in the large Horns Rev wind park. Although models are not specifically identified in the presented results, the RANS/$k-\varepsilon$ models tend to overpredict wake losses for narrow measurement sectors; wider sectors yield better agreement with data. Barthelmie *et al.* (2007) have also published a summary of developments on the use of actuator disks to study wakes within a wind farm. To be sure, accurately predicting cumulative wake effects remains a challenge.

0.6 Contributions

Despite the impressive body of work dedicated to atmospheric and wake flow modelling, there is no dearth of new research directions. It would certainly be tempting to address the problem of modelling flow through wind farms situated in arbitrarily complex terrain directly and some attention is directed towards that end herein. However, the primary focus is on simpler cases where, perhaps surprisingly, difficulties persist. A case in point: the exact[2] reproduction of neutral similarity profiles appears to be impossible without the use of excessively fine grids (Gorlé *et al.*, 2009). Whereas proposals have been made to minimize this problem, the contribution of the first study of this dissertation is an in-depth analysis of the source of the error. It is found to stem from approximations commonly used in the finite-volume discretization of the governing equations; a conclusion supported by the work of Richards and Norris (2011). Furthermore, a novel remedy is proposed such that near-exact distributions are obtained on *practical* grids. In the same vein, the second work is also concerned with surface-layer flows, however the

[2]Here, the term *exact* is used in a numerical sense, *i.e.* the difference with theory is trivial.

attention is on physical modelling and calibration of the turbulence closure to reproduce observations. More specifically, a comprehensive formulation of the $k-\varepsilon$ model is derived that is capable of exactly[3] reproducing both neutral length-limited and stable surface-layer flows.

Central to the ultimate objective of improving energy predictions is the refinement of far-wake models. Despite limitations in actuator-disk/eddy-viscosity modelling that seem to preclude the development of a general and accurate closure, the popularity and computational efficiency of such an approach beg for a reasonable solution. This is the backdrop against which the third study has been carried out. For the reasons mentioned previously, lower-order RANS modelling is likely a mainstay, at least in the near to medium term, and the goal of this work is to try to improve accuracy in light of the known issues. To this end, a new modified $k-\varepsilon$ closure is presented, similar to that of El Kasmi and Masson (2008), which aims at sidestepping the fundamental problem of an excessive eddy viscosity in the wake.

More generally, the aim of the final study is to contribute to the understanding of the applicability (or not) of RANS/two-equation closures by comparing model predictions with observations. Again, a simple case is considered based on extensive wind tunnel measurements carried out at Polytech'Orléans (Espana, 2009) of the flow properties in the wake of a porous disk placed in a uniform flow. As will be shown, comparing model predictions with these observations is unfortunately uninformative in this case: all models accurately predict wake properties. As it turns out, the primary contribution of this work is the proposed refinements to the testing procedure based on a detailed analysis of the determination of freestream properties from wake measurements and a discussion of similarity requirements.

Additionally, two case studies involving RANS simulations of flow over moderately complex terrain are considered. In the first, a summary of submissions to the Bolund blind comparison of flow models is presented. In the second, power production estimates for a Spanish wind farm based on several closure schemes (including a stress transport model) and two distinct actuator disk implementations are compared with measurements. Here, the aims are to bench-

[3]Here, the term *exact* is used in a mathematical sense, *i.e.* the theoretical distributions of flow properties are solutions of the model equations.

mark RANS modelling of flow over complex terrain and to contribute to the relatively limited existing literature on the topic of wind farm performance evaluation.

CHAPTER 1

$k-\varepsilon$ SIMULATIONS OF THE NEUTRAL ATMOSPHERIC BOUNDARY LAYER: ANALYSIS AND CORRECTION OF DISCRETIZATION ERRORS ON PRACTICAL GRIDS

Jonathon Sumner[1] and Christian Masson[1],

[1]Département de Génie Mécanique, École de Technologie Supérieure, 1100 Notre-Dame Ouest, Montreal, Quebec, Canada H3C 1K3

Article published online November 2011 by Wiley-Blackell in the *International Journal for Numerical Methods in Fluids*, DOI: 10.1002/fld.2709.

Foreword

In this chapter, the fundamental problem of simulating a steady, incompressible, shear-driven, boundary-layer flow using the RANS equations with standard $k-\varepsilon$ closure is analyzed in depth. Although this topic is well-founded in theory and has been previously discussed in the literature, most notably by Richards and Hoxey (1993), is has nonetheless attracted new attention recently (by *e.g.* Blocken *et al.* (2007); Hargreaves and Wright (2007); Gorlé *et al.* (2009); Richards and Norris (2011); Parente *et al.* (2011)). This renewed interest in such a basic flow has been largely motivated by the inability of many commercial CFD solvers to exactly reproduce the known analytical solution, raising questions regarding their general validity for atmospheric flows.

As it turns out, the errors in predicted velocity and turbulence properties can be significantly reduced with properly specified boundary conditions. The most stubborn case is the near-wall turbulent kinetic energy profile, which often contains a sharp anomalous peak in the first few cells. In the following, a systematic analysis of common finite-volume discretization schemes is presented to illustrate the source of this error and demonstrate how it may be remedied.

Abstract

The RANS/$k-\varepsilon$ approach is the popular and practical choice for carrying out simulations involving the atmospheric boundary layer. However, despite its widespread use, implementation of this approach is not without its challenges – even when considering the simplest case of horizontally homogeneous conditions. Most notably, the distributions of turbulent kinetic energy and its dissipation rate have proved difficult to maintain near solid boundaries, particularly in wind engineering applications where the near-wall grid is relatively coarse. In this work, the origin of these errors is investigated and it is shown that by applying appropriate discretization schemes in conjunction with the Richards and Hoxey boundary conditions, truly invariant profiles of all flow properties can be obtained on such grids. Furthermore, based on this finding, a wall treatment for coarse grids is proposed that could be implemented for non-homogeneous conditions. All simulations are carried out using OpenFOAM-1.6.x.

1.1 Introduction

Simulation of atmospheric boundary layer (ABL) flow is a topic of increasing interest within the computational fluid dynamics community. An accurate description of the mean turbulent flow within the first few hundred metres of the atmosphere is especially pertinent in the analysis of pollutant dispersion, in the evaluation of wind-induced loading on structures, and in determining site-suitability for wind energy projects. Although large-eddy simulation is becoming increasingly popular, the RANS approach remains the practical tool of choice for such work. Within this context, by far the most popular closure scheme is the $k-\varepsilon$ turbulence model of Jones and Launder (1972).

Numerically reproducing ABL flow using a RANS/$k-\varepsilon$ approach can be divided into two main tasks: the derivation of appropriate boundary conditions and model constants, and their numerical implementation. The first task has been fully addressed by Richards and Hoxey (1993) (RH) and the widely accepted best practice for simulating neutral equilibrium surface layer flow using the $k-\varepsilon$ model is laid out in their oft-cited paper (Franke *et al.*, 2007). Their

boundary conditions and prescription of model constants are mathematically consistent and ensure the inflow profiles are an exact solution of the model equations.

The second task has been more difficult to address. Maintaining turbulence properties under horizontally homogeneous conditions has proved problematic (Richards and Younis, 1990; Richards *et al.*, 2002; Riddle *et al.*, 2004; Blocken *et al.*, 2008), largely due to challenges in implementing the full RH conditions in commercial software (Franke *et al.*, 2007; Blocken *et al.*, 2007; Hargreaves and Wright, 2007). The presence of streamwise gradients in flow properties can thus often be attributed to the use of an inconsistent set of boundary conditions or to limitations in k_s-type wall functions for simulating ABL flow, or both, which initiates the development of an internal boundary layer at the domain inlet (see arguments by Blocken *et al.* (2007)). Recently, Hargreaves and Wright (2007) have addressed these problems by implementing the full RH boundary conditions, as well as a commonly used subset, in Fluent^{TM}, to highlight the importance of using the full set and to demonstrate how to better maintain inlet profiles over flat terrain using commercial software. They significantly reduced the presence of streamwise gradients everywhere except the near-wall region where a spike in the k distribution persists along with an overestimation of ε and an (albeit much smaller) underestimation of U. Even so, many of the original implementation difficulties with commercial software may be considered overcome and, at the same time, the recent availability of high-quality open-source CFD software obviates such challenges as users can modify the source code.

The unmitigated spike in k is often attributed to an overestimation of the turbulence production term in the first few cells nearest the wall. More precisely, it is likely due to an imbalance between calculated production and dissipation terms stemming from the fact that both are dependent on quantities that vary rapidly as $z \to 0$ and are thus poorly approximated using standard finite volume method (FVM) discretization schemes unless cell heights are exceedingly small. This leads to a third task: treatment of the inevitable discretization errors that arise due to the use of coarse grids recurrent in wind engineering applications. This last topic has received less attention and is the focus of the present study.

This work thus aims to clearly identify the source of and provide corrections for numerical errors near solid boundaries that arise when using the $k-\varepsilon$ turbulence model for ABL flow. Strategies are suggested herein which aim to yield truly horizontally homogeneous distributions of all turbulent flow properties on *practical* grids; grids which, for whatever reason (*e.g.* computational time, memory requirements, *etc.*), do not have sufficient fineness to properly resolve strong near-wall gradients in flow properties. Specifically, wall-damping-style functions are proposed, in the spirit of low-*Re* $k-\varepsilon$ models (Lam and Bremhorst, 1981; Chien, 1982), to adjust the source terms in the k and ε transport equations to correct for discretization errors. Furthermore, it is proposed to correct diffusion terms in the ε and momentum equations by replacing piecewise linear approximations with other weighting schemes inspired by analytically derived near-wall distributions of these quantities. Since it is postulated that these errors are entirely numerical in nature, all corrections are formulated purely in terms of grid geometry. Although the open-source CFD software OpenFOAM (OpenCFD, 2009b) has been used to analyze and develop improved discretization schemes, by interpreting them in terms of corrections to standard discretization methods (at least partial) implementation in commercial software should be possible.

The following section summarizes the RANS/$k-\varepsilon$ model as applied to surface layer flow. Section 1.3 outlines the case study used for the analysis of discretization error and a review of boundary conditions is given in section 1.4. Section 1.5 presents, term-by-term, the discretization of the governing equations and derivation of the required corrections. Simulations with corrected discretization schemes and a newly proposed wall treatment are also included.

1.2 Governing equations

1.2.1 RANS equations with $k-\varepsilon$ closure

Neglecting molecular viscosity, the Reynolds-averaged mass and momentum conservation equations for the steady motion of an incompressible fluid are

$$\nabla \cdot \vec{U} = 0, \tag{1.1}$$

$$\nabla \cdot \vec{U}\vec{U} = -\nabla p + \nabla \cdot \boldsymbol{\tau}' \tag{1.2}$$

where

$$\boldsymbol{\tau}' = 2\nu_t \mathbf{S} \tag{1.3}$$

is the kinematic Reynolds stress tensor and the Boussinesq eddy-viscosity assumption has been applied. $\vec{U}$ represents the mean velocity vector with components (U,V,W) and p is a modified mean pressure (Pope, 2000). $\mathbf{S}$ is the mean strain rate tensor.

The turbulent viscosity ν_t is calculated in the $k-\varepsilon$ model as

$$\nu_t = C_\mu \frac{k^2}{\varepsilon} \tag{1.4}$$

where k and ε are deduced from transport equations:

$$\nabla \cdot k\vec{U} = \nabla \cdot \left(\frac{\nu_t}{\sigma_k} \nabla k \right) + G_k - \varepsilon, \tag{1.5}$$

$$\nabla \cdot \varepsilon\vec{U} = \nabla \cdot \left(\frac{\nu_t}{\sigma_\varepsilon} \nabla \varepsilon \right) + C_{\varepsilon 1} G_k \frac{\varepsilon}{k} - C_{\varepsilon 2} \frac{\varepsilon^2}{k} \tag{1.6}$$

with

$$G_k = 2\nu_t \mathbf{S} : \mathbf{S} \tag{1.7}$$

and the molecular viscosity disregarded.

In addition to the original model constants (C_μ, σ_k, σ_ε, $C_{\varepsilon 1}$, $C_{\varepsilon 2}$) proposed by Jones and Launder, several alternative sets have been proposed for atmospheric flows (Crespo *et al.*, 1985;

Richards and Hoxey, 1993; Apsley and Castro, 1997; Bechmann and Sørensen, 2010). From a mathematical standpoint, any set that satisfies the governing equations and is employed consistently in the formulation of boundary conditions is appropriate (Richards and Hoxey, 1993; Franke *et al.*, 2007).

1.2.2 Two-dimensional surface layer flow

For the sake of simplicity, the present analysis is limited to two-dimensional flow where the x axis is defined by the mean wind direction and the z axis is normal to the ground. Assuming a constant shear stress, zero pressure gradient and horizontal homogeneity, the governing equations simplify to

$$\nu_t \frac{\partial U}{\partial z} = u^{*2}, \tag{1.8}$$

$$\frac{\partial}{\partial z}\left(\frac{\nu_t}{\sigma_k}\frac{\partial k}{\partial z}\right) + G_k - \varepsilon = 0, \tag{1.9}$$

$$\frac{\partial}{\partial z}\left(\frac{\nu_t}{\sigma_\varepsilon}\frac{\partial \varepsilon}{\partial z}\right) + C_{\varepsilon 1} G_k \frac{\varepsilon}{k} - C_{\varepsilon 2}\frac{\varepsilon^2}{k} = 0 \tag{1.10}$$

with

$$G_k = \nu_t \left(\frac{\partial U}{\partial z}\right)^2 \tag{1.11}$$

and $u^* = \sqrt{\tau'_w}$ is the characteristic friction velocity of the surface layer related to the kinematic wall shear stress (Richards and Hoxey, 1993).

If model constants are chosen such that

$$\sigma_\varepsilon = \frac{\kappa^2}{(C_{\varepsilon 2} - C_{\varepsilon 1})\sqrt{C_\mu}} \tag{1.12}$$

where κ is the von Karman universal constant, equations (1.13)–(1.15) are an exact solution of equations (1.8)–(1.10) and correspond to fully developed, neutrally stratified surface-layer

flow (Richards and Hoxey, 1993).

$$U(z) = \frac{u^*}{\kappa} \ln\left(\frac{z}{z_0}\right) \tag{1.13}$$

$$k(z) = \frac{u^{*2}}{\sqrt{C_\mu}} \tag{1.14}$$

$$\varepsilon(z) = \frac{u^{*3}}{\kappa z} \tag{1.15}$$

1.3 Case study

For the purposes of comparison, Task 1 of the blind test case proposed by Richards *et al.* (2002) as part of the Computational Wind Engineering 2000 Conference Competition has been chosen. The objective is straightforward: to maintain equilibrium inlet profiles of all flow properties in an empty domain. The atmospheric parameters that define the inlet conditions are listed in table 1.1. The model constants used for the simulations, which satisfy condition (1.12), are given in table 1.2.

Table 1.1 Inlet profile characteristics

Reference height, z_{ref}	6 m
Aerodynamic roughness length, z_0	0.01 m
Displacement height, d	0 m
Reference mean wind speed, U_{ref}	10 m/s
κ	0.40

Table 1.2 $k-\varepsilon$ model constants

C_μ	$C_{\varepsilon 1}$	$C_{\varepsilon 2}$	σ_k	σ_ε	κ
0.09	1.44	1.92	1.0	1.1111	0.40

Hargreaves and Wright (2007) also used this test case and a quasi-2D version of their grid is reproduced for the present work. This grid is practical and representative of what would be used to discretize an upstream fetch in a typical wind engineering application. The domain

length and height are 5000 m and 500 m, respectively. The horizontal direction is uniformly discretized using 500 cells whereas 50 cells are used to discretize the vertical direction. Cell heights are geometrically expanded, starting with a near-wall cell height of 1 m, using a ratio of 1.076.

1.4 Boundary conditions

Inlet

The profiles of velocity, turbulent kinetic energy and its dissipation rate are given by equations (1.13)–(1.15), respectively.

Outlet

All variables assume a fully-developed condition in the flow direction.

Surface: Equilibrium conditions

Control volumes adjacent to the bottom and top boundaries are illustrated in figure 1.1. A common interpretation of the RH conditions involves explicitly assuming $G_k = \varepsilon$ in the near-wall cell (Undheim *et al.*, 2006; Brodeur and Masson, 2008). Under this assumption, the turbulent kinetic energy and its dissipation rate can be directly specified as

$$k_P = \frac{u_g^{*2}}{\sqrt{C_\mu}}, \tag{1.16}$$

$$\varepsilon_P = \frac{u_g^{*3}}{\kappa z_P} \tag{1.17}$$

where u_g^* is the local friction velocity based on the near-ground velocity,

$$u_g^* = \frac{\kappa U_P}{\ln(z_P/z_0)}. \tag{1.18}$$

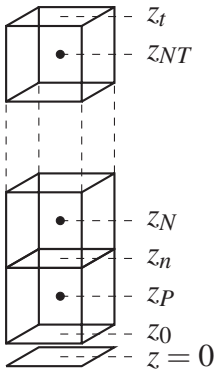

Figure 1.1 Control volumes adjacent to the surface and top boundaries. The second near-wall cell is labeled with respect to the wall-adjacent cell. The region between $z = 0$ and $z = z_0$ is not resolved

Richards and Hoxey suggest the wall shear stress also be specified based on local conditions (*i.e.* $\tau'_w = u_g^{*2}$). This quantity is approximated through finite differencing with

$$\tau'_w = \nu_{t,w} \left.\frac{\partial U}{\partial z}\right|_{z=z_0} \approx \nu_{t,w} \frac{(U_P - U_w)}{(z_P - z_0)} \tag{1.19}$$

where the turbulent viscosity in the surface layer can be expressed as

$$\nu_t = \kappa u_g^* z. \tag{1.20}$$

Equating the two expressions for τ'_w and taking $\nu_{t,w} = \nu_{t,P}$, the wall velocity must be set according to

$$U_w = U_P - \frac{u_g^*}{\kappa} \frac{(z_P - z_0)}{z_P}. \tag{1.21}$$

By definition, the velocity should be zero at $z = z_0$ and this condition is respected in the calculation of u_g^*. However, in the discretization of the governing equations, the wall velocity only appears in gradient calculations and, given the highly non-linear fashion in which U varies towards the wall[1], the combination of equations (1.19), (1.20) and (1.21) ensures that the contribution of the wall shear stress to the momentum balance for the wall-adjacent cell is correct.

[1] For the values of z^+ considered here.

Surface: Non-equilibrium conditions

The previous set of surface conditions explicitly assumes that the turbulence production and dissipation rates are always equal in the near-wall cell, regardless of local conditions or flow history. Although in some cases this is a convenient choice, and perfectly appropriate for the present case, it is usually not a necessary assumption.

The original proposal by Richards and Hoxey calls for the source terms in the discretized k transport equation for the near-wall cell to be modified such that $G_k = \varepsilon$ when k_P satisfies equation (1.16). Assuming a locally logarithmic velocity profile, the near-wall cell-averaged production rate is

$$\overline{G_{k,P}} = \frac{u_g^{*3}}{2\kappa(z_P - z_0)} \ln\left(\frac{2z_P - z_0}{z_0}\right). \tag{1.22}$$

Richards and Hoxey suggest the average dissipation rate be calculated with

$$\overline{\varepsilon_P} = \frac{\sqrt{C_\mu} k_P u_g^*}{2\kappa(z_P - z_0)} \ln\left(\frac{2z_P - z_0}{z_0}\right) \tag{1.23}$$

and its cell-centre value for the wall-adjacent cell fixed as

$$\varepsilon_P = \frac{\sqrt{C_\mu} k_P u_g^*}{\kappa z_P}. \tag{1.24}$$

The wall shear stress is now modeled with[2]

$$\tau_w' = C_\mu^{1/4} k_P^{1/2} u_g^*. \tag{1.25}$$

[2]Reconsidering the turbulence production rate, if the shear stress is taken as uniform over the height of the first cell and the velocity profile is again assumed locally logarithmic, it can be argued that $\overline{G_{k,P}}$ should be

$$\overline{G_{k,P}} = \frac{\tau_w' u_g^*}{2\kappa(z_P - z_0)} \ln\left(\frac{2z_P - z_0}{z_0}\right)$$

which is slightly different from equation (1.22).

Substituting equation (1.24) into (1.4) yields

$$\nu_{t,P} = \frac{\sqrt{C_\mu} k_P}{u_g^*} \kappa z_P \tag{1.26}$$

and the wall velocity becomes

$$U_w = U_P - \frac{u_g^{*2}}{\kappa C_\mu^{1/4} k_P^{1/2}} \frac{(z_P - z_0)}{z_P}. \tag{1.27}$$

When k_P satisfies equation (1.16), equations (1.24), (1.26) and (1.27) simplify to (1.17), (1.20) and (1.21), respectively.

Top boundary

The inlet profiles should be maintained entirely through a balance between the driving shear stress at the upper boundary and the retarding shear stress at the surface. Following the RH recommendations, a constant kinematic shear stress $\tau_t' = u_{sl}^{*2}$ is applied. The upper boundary velocity is thus specified using

$$U_t = U_{NT} + \frac{u_{sl}^{*2}}{\nu_{t,t}} (z_t - z_{NT}) \tag{1.28}$$

where

$$u_{sl}^* = \frac{\kappa U_{ref}}{\ln(z_{ref}/z_0)}.$$

To minimize the influence of the upper boundary on the resolved magnitudes of k and ε, gradient conditions are imposed. For k, a zero gradient condition is prescribed while the gradient of ε is fixed using

$$\frac{\partial \varepsilon}{\partial z} = -\frac{u_{sl}^{*3}}{\kappa z_t^2}. \tag{1.29}$$

1.5 Analysis and correction of discretization errors

1.5.1 Solution using standard FVM schemes

To illustrate the problem encountered near solid boundaries, figure 1.2 compares the outlet distributions of velocity, turbulent kinetic energy, and turbulence dissipation and production rates with those prescribed at the inlet for the lowest 10 m of the boundary layer. Here, equations (1.1), (1.2), (1.5) and (1.6) have been discretized using upwind differencing for all convection terms and central-differencing for all diffusion terms. The SIMPLE method has been employed to handle pressure-velocity coupling. The solution is considered converged when the normalized residuals for all variables become stable; this corresponds to an absolute tolerance less than 10^{-6}.[3]

It is evident that although the velocity profile is fairly well maintained, the k and ε distributions do not respect their analytical solutions near the wall. Hargreaves and Wright (2007) note that the ESDU experimental data (ESDU, 1985) support a non-uniform k distribution with a near-ground maximum. However, this is a separate modelling problem requiring a separate set of k and ε (and possibly velocity) boundary conditions to be specified; Yang *et al.* (2009) and Gorlé *et al.* (2009) have recently made efforts to derive such a set. In the present context, the non-uniformity in the resolved k profile is unintended.

Clearly, there exists an imbalance between calculated production and dissipation rates of k in the first few cells near the wall and, furthermore, both are overestimated. Compared to the Fluent^{TM}simulations of Hargreaves and Wright, the maximum relative error in k and ε at the outlet is considerably smaller. Nonetheless, the resolved near-wall velocity profile is quite similar.

As the inlet profiles represent an exact solution of the governing equations with the RH boundary conditions, the errors observed in figure 1.2 must be entirely numerical in nature. Figure 1.3 shows the relative error of each variable with respect to its inlet value as a function of downstream position in the second near-wall cell. The rapid variation in k and ε in the first few

[3] All simulations have been carried out using OpenFOAM 1.6.x (OpenCFD, 2009b).

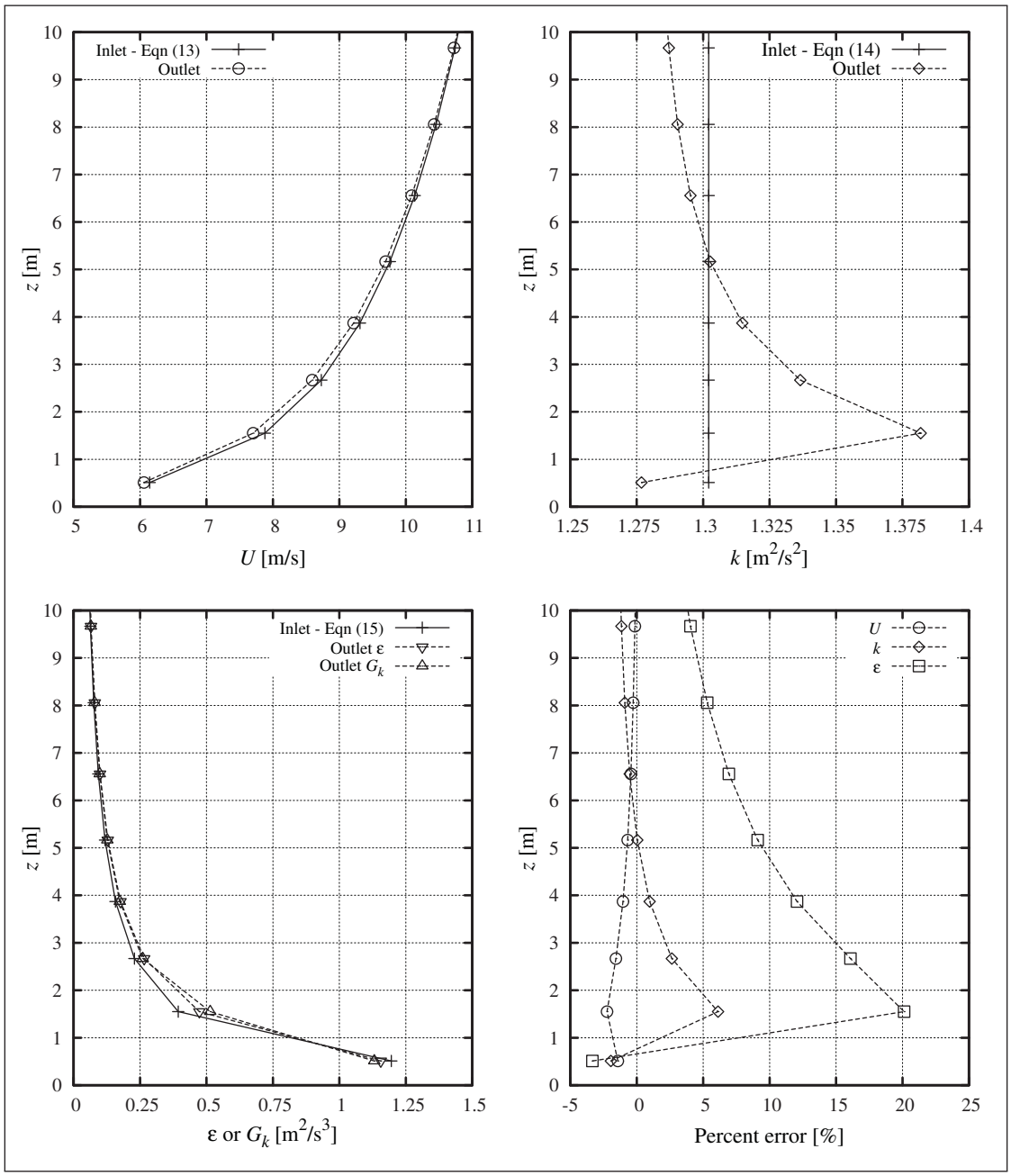

Figure 1.2 Comparison of resolved surface layer properties at outlet with inflow using the Richards and Hoxey boundary conditions

downstream cells suggests the inflow is adapting to the effects of discretization after which it stabilizes. Richards and Norris (2011) have similarly concluded that the near-wall overestimation of k stems directly from discretization error.

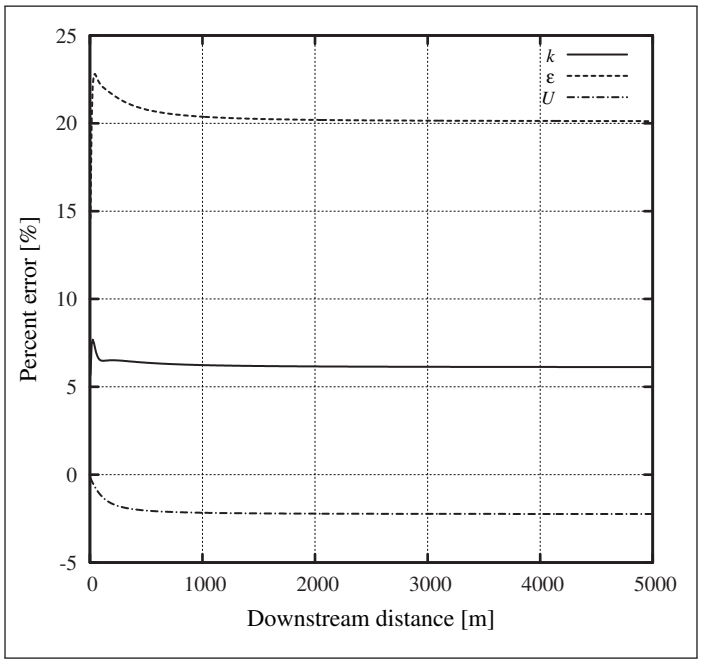

Figure 1.3 Relative error in flow properties with respect to inlet values at second near-wall cell

1.5.2 Grid sensitivity analysis

Figure 1.4 presents the near-wall k distribution using 50, 100 and 200 cells to discretize the vertical direction (the height of the wall-adjacent cell and the grid expansion factor are roughly halved with each refinement). A peak in k is always present in the second cell. If the overestimation of k stems from numerical errors, it is expected that sufficient grid refinement would eventually result in a uniform distribution. The work of Gorlé *et al.* (2009) has shown this to be true: in their analysis of atmospheric dispersion in a wind tunnel, a z^+ of approximately 30 yielded perfect horizontal homogeneity. For the current grid, $z^+ \approx 2 \times 10^4$. As noted by others, this level of refinement will not be practical for many ABL flows, especially for large domains in which obstacles are present. The solution proposed herein is thus to adapt the numerical method. In the following section, the FVM schemes used to discretize the governing equations are reviewed and revised such that the inflow will be preserved on relatively coarse grids.

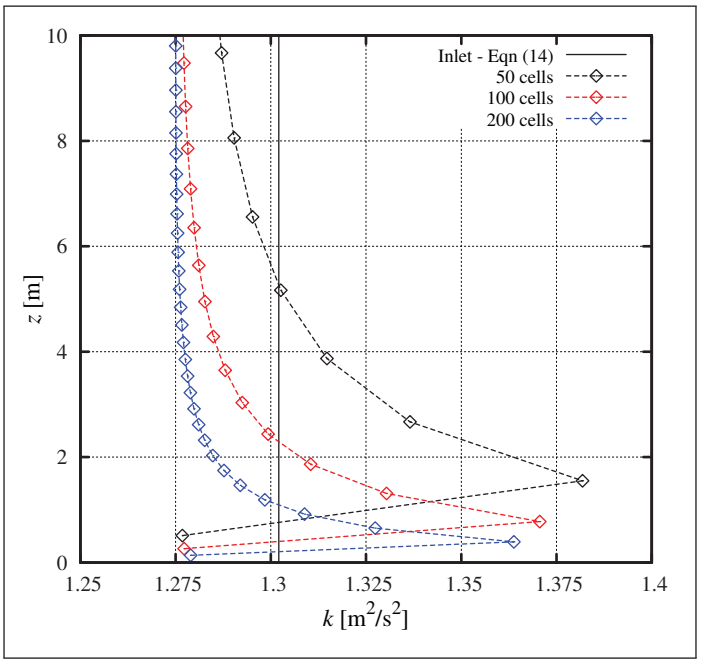

Figure 1.4 Near-wall k distribution using successively finer grids

1.5.3 Derivation of corrections to standard FVM schemes

For the case under consideration, the solution of equations (1.1), (1.2), (1.5) and (1.6) does not yield equations (1.13)–(1.15) as the approximations introduced in the discretization process result in some non-negligible error. However, by revising the FVM schemes in light of the known analytical solution, it should be possible to eliminate this effect. Corrections to standard discretization schemes are thus developed by comparing exact expressions with those found by introducing the analytical solution into the discretized form of the governing equations. A typical control volume (CV) and its upper and lower neighbours are illustrated in figure 1.5.

1.5.3.1 $k-\varepsilon$ equations

Evaluation of convection terms

For the present case, all convections terms integrate to zero as required, regardless of the convection scheme.

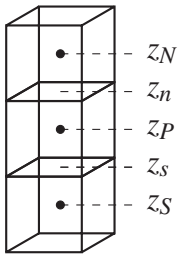

Figure 1.5 Arbitrary control volume P and its neighbours

Evaluation of source terms

Source terms are generally treated explicitly and evaluated as

$$\int_{CV} S dV = \overline{S}\Delta V \approx S_P \Delta V \tag{1.30}$$

the underlying assumption being that $S_P \to \overline{S}$ for sufficiently small ΔV. In the case of the $k-\varepsilon$ source terms, it is proposed to apply wall-damping-style functions such that $f \cdot S_P = \overline{S}$. Considering the production rate, the volume average is calculated analytically as

$$\begin{aligned} \overline{G_k} &= \frac{1}{\Delta V}\int_{CV} \nu_t \left(\frac{\partial U}{\partial z}\right)^2 dV \\ &= \frac{1}{\Delta z}\frac{u^{*3}}{\kappa}\ln\left(\frac{z_n}{z_s}\right) \end{aligned} \tag{1.31}$$

while the finite-volume approximation of this quantity is

$$G_{k,P} = \nu_{t,P}\left(\overline{\frac{\partial U}{\partial z}}\right)^2. \tag{1.32}$$

The average gradient of U will be correctly calculated using the scheme presented in section 1.5.3.2. The discretization error here stems from the inequality

$$\left(\overline{\frac{\partial U}{\partial z}}\right)^2 \neq \overline{\left(\frac{\partial U}{\partial z}\right)^2}.$$

The correction is thus

$$f_G = \frac{\overline{G_k}}{G_{k,P}} = \frac{\Delta z}{z_P \ln\left(\frac{z_n}{z_s}\right)}. \tag{1.33}$$

Interestingly, applying a similar analysis to the dissipation rate yields

$$f_\varepsilon = \frac{1}{f_G}.$$

The source term corrections for the ε equation are

$$f_{G\varepsilon} = \frac{\Delta z^2}{z_n z_s \ln\left(\frac{z_n}{z_s}\right)^2}, \tag{1.34}$$

$$f_{\varepsilon^2} = \frac{z_P^2}{z_n z_s}. \tag{1.35}$$

Evaluation of diffusion terms

Laplacian terms are evaluated as follows (Jasak, 1996; OpenCFD, 2009b)

$$\begin{aligned} \int_{CV} \nabla \cdot (\gamma \nabla \phi) dV &= \oint_S (\gamma \nabla \phi) \cdot \hat{n} dS \\ &\approx \sum_f \gamma_f (\nabla \phi)_f \cdot \vec{s}_f \end{aligned} \tag{1.36}$$

where $\hat{n}$ is the local surface normal and dS an elemental surface area. $\vec{s}_f$ is the finite face area vector. It is necessary to specify a scheme for calculating the surface normal gradient of the general scalar ϕ and its diffusion coefficient; assuming piecewise linear distributions is the most common approach. For the present case, treating the coefficient γ in this way is appropriate as $\nu_t \propto z$ within the idealized surface layer (see equation (1.20)). This scheme is also appropriate for the gradient of k. However, the surface normal gradient for ε is poorly estimated through central-differencing.

Given that ε is inversely proportional to the normal wall distance, the surface normal gradient at a horizontal face should be

$$\left.\frac{\partial \varepsilon}{\partial z}\right|_f \propto -\frac{1}{z_f^2}$$

whereas central-differencing yields

$$\left.\frac{\partial \varepsilon}{\partial z}\right|_n \approx \frac{\Delta \varepsilon}{\Delta z} \propto -\frac{1}{z_N z_P} \tag{1.37}$$

and the required correction is

$$f_{\nabla \varepsilon} = \frac{z_N z_P}{z_n^2}. \tag{1.38}$$

$f_{\nabla \varepsilon}$ is set to unity for vertical faces. The Laplacian term is evaluated as

$$\int_{CV} \nabla \cdot \left(\frac{\nu_t}{\sigma_\varepsilon} \nabla \varepsilon \right) dV \approx \sum_f \frac{\nu_{t,f}}{\sigma_\varepsilon} f_{\nabla \varepsilon} (\nabla \varepsilon)_f \cdot \vec{s}_f. \tag{1.39}$$

Finally, the steady $k-\varepsilon$ transport equations become

$$\nabla \cdot k\vec{U} = \nabla \cdot \left(\frac{\nu_t}{\sigma_k} \nabla k \right) + \frac{G_k}{f_\varepsilon} - f_\varepsilon \varepsilon, \tag{1.40}$$

$$\nabla \cdot \varepsilon \vec{U} = \nabla \cdot \left(\frac{\nu_t}{\sigma_\varepsilon} \nabla \varepsilon \right) + C_{\varepsilon 1} f_{G\varepsilon} G_k \frac{\varepsilon}{k} - C_{\varepsilon 2} f_{\varepsilon^2} \frac{\varepsilon^2}{k}. \tag{1.41}$$

1.5.3.2 The momentum equation

Evaluation of convection and pressure terms

Integration of the discretized analytical solution causes these terms to go to zero regardless of the chosen convection scheme.

Evaluation of Reynolds stresses

Calculation of the Reynolds stresses is divided into implicit and explicit components

$$\nabla \cdot \boldsymbol{\tau}' = \underbrace{\nabla \cdot \left(\nu_t \nabla \vec{U} \right)}_{\text{implicit}} + \underbrace{\nabla \cdot \left(\nu_t \left(\nabla \vec{U}^{\mathsf{T}} - \frac{1}{3} (\nabla \cdot \vec{U}) \mathbf{I} \right) \right)}_{\text{explicit}}.$$

Treating the explicit component first, the average gradient of a field quantity within a control volume is evaluated through Gauss's Theorem as

$$\int_{CV} \nabla \phi dV = \oint_S \phi \hat{n} dS. \tag{1.42}$$

The FVM approximates this quantity as a discrete sum over all control volume faces (Ferziger and Perić, 2002)

$$\oint_S \phi \hat{n} dS \approx \sum_f \phi_f \vec{s}_f. \tag{1.43}$$

As such, an interpolation scheme is required to estimate face values from cell-centre values. The usual scheme is linear interpolation. However, when the variable of interest varies in a highly non-linear manner, it may be more appropriate to adopt different weighting schemes. For U, it is proposed to evaluate its face value using

$$U_n = \alpha U_P + (1 - \alpha) U_N \tag{1.44}$$

where

$$\alpha = \frac{\ln(z_N / z_n)}{\ln(z_N / z_P)}. \tag{1.45}$$

By virtue of continuity, the second explicit term must go to zero.[4]

[4] In fact, it can be shown that the entire explicit term is zero for the present case; the correction factor is included here as it is needed in the calculation of the turbulence production rate and it may have application for non-homogeneous flows. For such cases, however, some care is required when evaluating the stress divergence as the use of a non-zero wall velocity boundary condition could result in a significant error in the explicit part. The simplest solution is to reformulate the shear stress boundary condition using

$$\nu_{t,w} = \frac{\kappa C_\mu^{1/4} k_P^{1/2} (z_P - z_0)}{\ln(z_P / z_0)}$$

Concerning the implicit term, evaluation of the Laplacian will be markedly improved by using an alternate scheme for the surface normal gradient of U. Analytically, the gradient of U at horizontal cell faces is

$$\left.\frac{\partial U}{\partial z}\right|_n = \frac{u^*}{\kappa z_n} = \frac{U_N - U_P}{z_n \ln\left(\frac{z_N}{z_P}\right)}. \tag{1.46}$$

Central-differencing yields

$$\left.\frac{\partial U}{\partial z}\right|_n \approx \frac{U_N - U_P}{z_N - z_P} \tag{1.47}$$

and the required correction is

$$f_{\nabla U} = \frac{z_N - z_P}{z_n \ln\left(\frac{z_N}{z_P}\right)}. \tag{1.48}$$

$f_{\nabla U}$ is set to unity for vertical faces. The Laplacian term is evaluated as

$$\int_{CV} \nabla \cdot (\nu_t \nabla \vec{U}) dV \approx \sum_f \nu_{t,f} f_{\nabla U} (\nabla \vec{U})_f \cdot \vec{s}_f. \tag{1.49}$$

1.5.4 Solution using corrected FVM schemes

Figure 1.6 presents the outlet distributions of velocity and turbulence properties using the proposed corrections. With respect to the previous results using standard FVM schemes, the profiles here are decidedly improved. Indeed, the calculated distributions of U, k and ε at the outlet lie directly on their inlet distributions. G_k is still overestimated but the f_ε factor neatly corrects for it. The maximum errors in flow properties are now shifted to the upper boundary, but in all cases remain less than one-tenth of one percent.

The fact that inlet profiles have been maintained is not a surprising result as, in essence, the correction factors force the numerical method to yield the analytical solution. Of course, to know the flow solution *a priori* is rare and such corrections cannot be derived for every case. But, as shown in figure 1.7, the proposed corrections rapidly go to unity away from the wall and are likely unnecessary for the majority of the domain. The largest corrections occur at the first internal face and concern the gradient calculations of ε and U. This is followed by the volume

with $U_w = 0$.

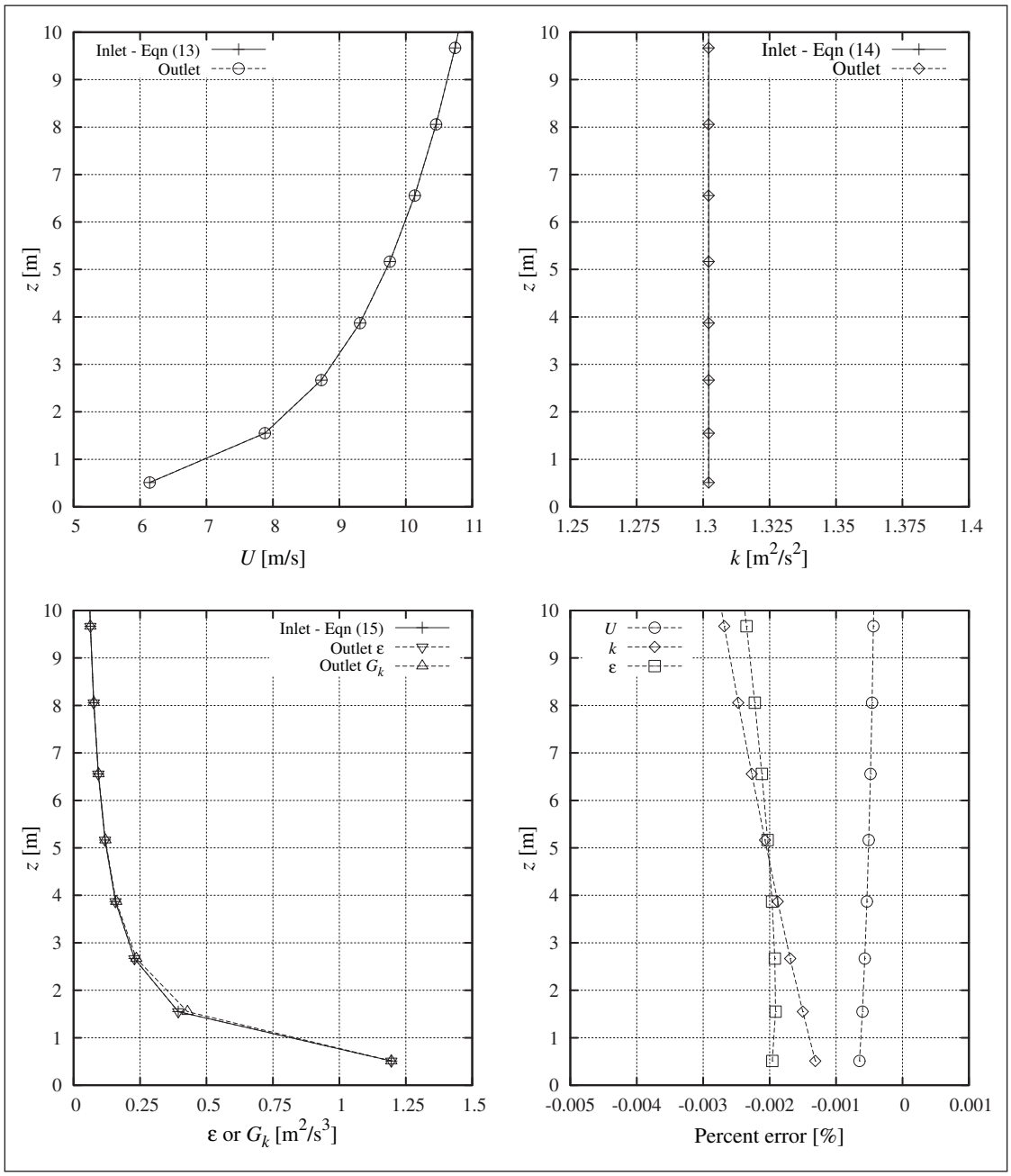

Figure 1.6 Comparison of resolved surface layer properties at outlet with inflow using the Richards and Hoxey boundary conditions and proposed corrections to discretization schemes

integral corrections for $k-\varepsilon$ source terms in the second near-wall cell (note that $f_{G\varepsilon} \approx f_\varepsilon$). Beyond the second internal face, the corrections are only on the order of a few percent. This suggests that it may be possible to use $f = 1$ beyond the second cell and incorporate f as part

of the wall treatment in the first two near-wall cells. This would have the distinct advantage of facilitating the generalization of this approach to complex geometries as close to the surface a wall-normal direction can be defined and used to replace z in equations (1.33)–(1.35), (1.38), (1.45), (1.48).

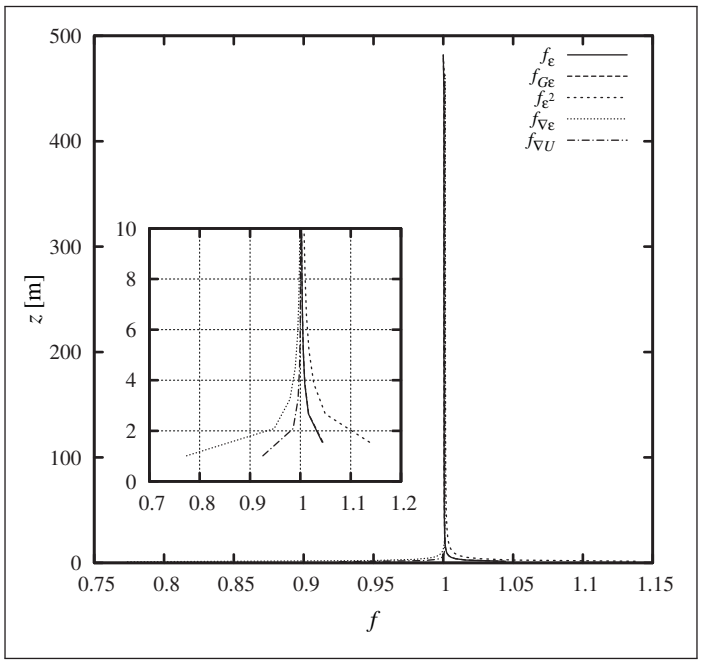

Figure 1.7 Wall functions used to correct discretization errors

1.5.5 Implementation as part of wall treatment

In the context of high *Re* flows, it is normal to make some assumptions about near-wall flow properties to avoid integrating to the wall. This entails use of a law-of-the-wall for velocity with prescriptions for turbulence properties in the wall-adjacent cell. Here, an extended wall treatment is proposed wherein the usual RH conditions are applied in the first cell while the corrected discretization schemes developed in the preceding sections are applied in the first and second cells, *i.e.*

$$f = \begin{cases} f & z_{n,1} \leq z \leq z_{n,2} \\ 1 & z > z_{n,2} \end{cases}$$

where $z_{n,i}$ denotes the location of the upper face of the i^{th} near-wall cell. α is treated similarly.

Unlike in the wall-adjacent cell, no variables are explicitly prescribed in the second cell. As per usual, they are all determined as part of the flow solution. Rather, the construction of the discretized equations for the first three cells is modified through f and α[5]. Essentially, it is proposed to use a different set of discretization schemes in the near-wall region adapted to ABL flow.

This approach is similar to that of Kalitzin *et al.* (2005) where numerical errors involved with standard wall functions and various RANS turbulence models were reduced through the use of lookup tables to specify the proper momentum flux at the first internal face. Of course, the definition of a "coarse" grid in their work is quite different from the present. The above proposal is also comparable to those recently presented by Richards and Norris (2011) and Parente *et al.* (2011) whereby the spike in k is reported to be removed by modifying the calculation of the turbulence production rate. In the case of Richards and Norris, they have demonstrated with a 1D simulation that a perfectly uniform k distribution can be attained by discretizing G_k using the shear stress evaluated at cell faces (as opposed to cell centres). Parente *et al.* have proposed modifying the Richards and Hoxey wall functions such that a) G_k and ε are based on cell-centre values (as opposed to cell-averaged ones) and b) the velocity in the wall-adjacent cell is specified (as opposed to solved). Using a nearly identical test case, they have shown that this treatment removes the peak in k and limits the maximum error to around five percent.

Figure 1.8 presents the flow solution with the proposed wall treatment. This approach appears to be sufficient to maintain the velocity profile as its inlet and outlet profiles are difficult to distinguish. The turbulent kinetic energy profile is not quite uniform, however it varies from its analytical value by less than one percent. With respect to the uncorrected results (see figure 1.2), the maximum percent error in all variables has decreased by roughly an order of magnitude. As a point of interest, the outlet profiles for k with wall treatments extending to the third and fourth near-wall cells are also shown. The profile slowly tends to uniform as more cells are incorporated into the wall treatment. This highlights the sensitivity of k to its source terms and hints at why maintaining inlet distributions has been somewhat elusive.

[5]The third near-wall cell shares a face with the second cell and so its discretized equations are also affected.

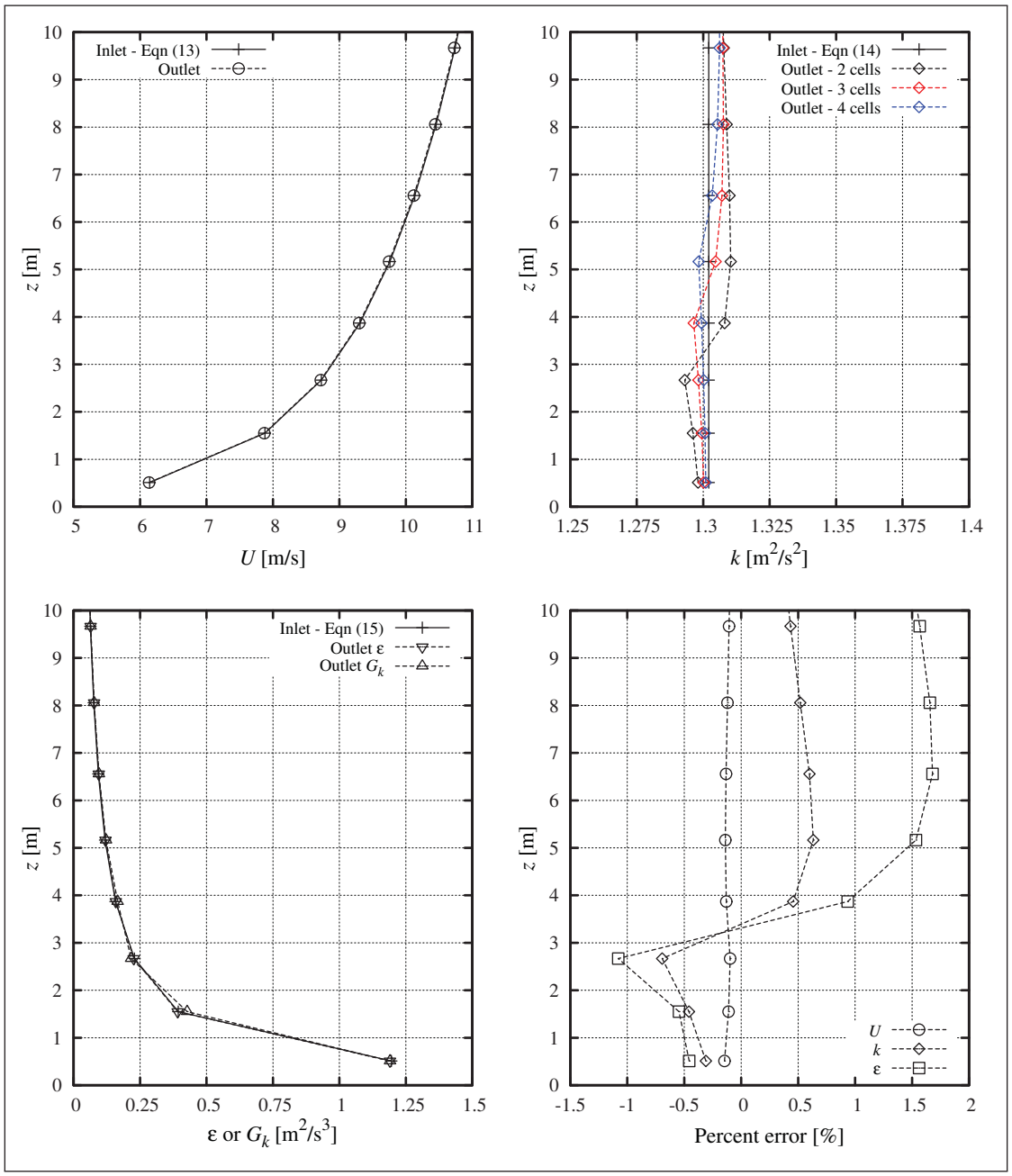

Figure 1.8 Comparison of resolved surface layer properties at outlet with inflow using the Richards and Hoxey boundary conditions and corrected discretization schemes in first two cells only. The resolved k profile at the outlet with corrected discretization schemes extended to the first three and four cells is also shown

Figure 1.9 expands on the above analysis by presenting the maximum error in k for three different values of z_0 (spanning four orders of magnitude) and seven different grids. For these

simulations, the shear stress from the reference case has been maintained (*i.e.* $u^* = 0.625$ m/s) and the grid has been refined as in section 3.4: the expansion factor and near-wall cell height are roughly halved at each refinement (see table 1.3). Although z^+ is usually considered the appropriate non-dimensional wall-normal distance, in the present case the molecular viscosity is taken as null and, strictly speaking, z^+ is undefined; $(z - z_0)/z_0$ is however a useful substitute and plotting the error against this parameter yields a smooth distribution.

Most importantly, the error in k is limited to less than one percent for all cases considered. When cell heights are large with respect to z_0, the error is essentially independent of grid size. This is likely due to the fact that the underlying discretization problem is essentially unchanged with refinement; as shown in figure 1.4, the peak in k is not much diminished as the number of cells is doubled. But continued grid refinement must eventually lead to an exact solution as discretization errors become negligible. Indeed, for normalized first cell heights less than one, a rapid and monotonic decrease in the maximum error is observed.

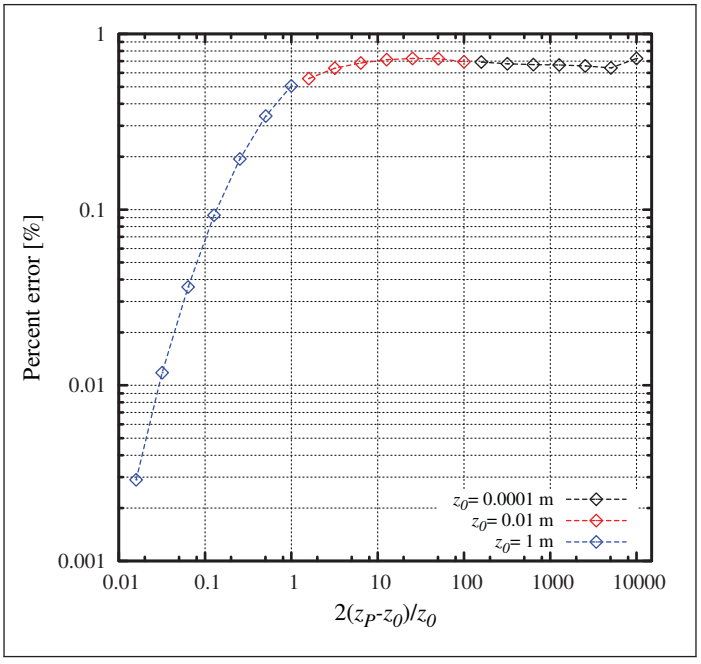

Figure 1.9 Maximum relative error in k at outlet as a function of normalized first cell height. The maximum error is located at the third cell for all cases except $2(z_P - z_0)/z_0 \approx 10000$, where it is at the fifth cell

Although figure 1.9 suggests that non-uniform surface roughness should pose no special problems, some care must be exercised in the use of this wall treatment for flow over surfaces with variable orography. The near-wall grid must be constructed by extruding the surface mesh normal to the wall such that

$$\frac{1}{\Delta V}\int_{CV}\phi dV \approx \frac{1}{\Delta n}\int_{s}^{n}\phi dn$$

as the derivation of equations (1.33)–(1.35) assumes constant cross-sectional area in the wall-normal direction.

Table 1.3 Sensitivity analysis parameters

Grid	1	2	3	4	5	6	7
Aerodynamic roughness length, z_0 [m]	$\{10^{-4}, 10^{-2}, 10^{0}\}$						
Cells in wall-normal direction [$\times 10^2$]	2^{-1}	2^{0}	2^{1}	2^{2}	2^{3}	2^{4}	2^{5}
Approximate first cell height [m]	2^{0}	2^{-1}	2^{-2}	2^{-3}	2^{-4}	2^{-5}	2^{-6}

1.6 Conclusions

Numerically reproducing neutral equilibrium surface layer flow is a subject that has recently received a fair amount of attention in the computational wind engineering community. Herein, it has been shown that maintaining inlet profiles of velocity, turbulent kinetic energy and its dissipation rate on practical grids is possible if a) the full RH conditions are implemented, and b) discretization errors are corrected. These appear to be the necessary and sufficient conditions.

In addition, an extended wall treatment has been proposed in which corrected discretization schemes are applied in the first two near-wall cells. For the cases considered, this approach acceptably maintains the inlet velocity profile while limiting the error in turbulent kinetic energy to less than one percent. This treatment may also be useful for other closure schemes and inflow conditions, but this remains to be evaluated. Future work is also required to test the proposed wall treatment under non-homogeneous flow conditions.

CHAPTER 2

THE APSLEY AND CASTRO LIMITED-LENGTH-SCALE $k-\varepsilon$ MODEL REVISITED FOR IMPROVED PERFORMANCE IN THE ATMOSPHERIC SURFACE LAYER

Jonathon Sumner[1] and Christian Masson[1],

[1]Département de Génie Mécanique, École de Technologie Supérieure, 1100 Notre-Dame Ouest, Montreal, Quebec, Canada H3C 1K3

Article published May 2012 by Springer in *Boundary-Layer Meteorology*, vol. 144, no. 2, p. 199–215, DOI: 10.1007/s10546-012-9724-7.

Foreword

With boundary conditions and discretization issues related to the simulation of (neutral) surface-layer flows addressed, the attention in this chapter turns to questions of physical modelling. Concerning near-surface atmospheric flows, the standard implementation of the $k-\varepsilon$ model is strictly only valid for neutral thermal stratification where, under equilibrium conditions, the mixing length increases linearly with height above ground and model predictions match theory. However, the physical reality is that the mixing length does not increase indefinitely: it is generally limited by some physical process to a finite maximum.

Detering and Etling (1985) recognized this weakness with $k-\varepsilon$-type closures and adjustments to the standard $k-\varepsilon$ model have since been proposed. Of greatest interest here is the work of Apsley and Castro (1997), who have modified the ε equation to impose an upper bound on the mixing length for atmospheric boundary layer simulations. However, in the context of surface-layer simulations, it is found that this modified closure is not entirely in agreement with theory. In this chapter, the framework proposed by Apsley and Castro to modify the ε equation is refined and the boundary conditions of Richards and Hoxey are generalized such that the mathematical model can be calibrated to exactly yield an arbitrary desired mixing length distribution for surface layer simulations.

Abstract

The limited-length-scale $k-\varepsilon$ model proposed by Apsley and Castro for the atmospheric boundary layer (Boundary-Layer Meteorology, 1997, Vol. 83, 75–98) is revisited with special attention given to its predictions in the constant-stress surface layer. The original model proposes a modification to the length-scale-governing ε equation that ensures consistency with surface-layer scaling in the limit of small ℓ_m/ℓ_{max} (where ℓ_m is the mixing length and ℓ_{max} its maximum) and yet imposes a limit on ℓ_m as ℓ_m/ℓ_{max} approaches one. However, within the equilibrium surface layer and for moderate values of z/ℓ_{max}, the predicted profiles of velocity, mixing length, and dissipation rate using the Apsley and Castro model do not coincide with analytical solutions. In view of this, a general ε transport equation is derived herein in terms of an arbitrary desired mixing-length expression that ensures exact agreement with corresponding analytical solutions for both neutral and stable stability. From this result, a new expression for $C_{\varepsilon 3}$ can be inferred that shows this coefficient tends to a constant only for limiting values of z/L; and, furthermore, that the values of $C_{\varepsilon 3}$ for $z/L \to 0$ and $z/L \to \infty$ differ by a factor of exactly two.

2.1 Introduction

We begin by restating the primary motivation for the Apsley and Castro (1997) model that "in many flows of interest, there is some *maximum* size of turbulent eddy - a scale defined, for example, by boundary-layer depth or imposed by stratification." From this observation naturally arises the question of how such a limit on the mixing length might be imposed using two-equation turbulence closure, especially since the standard $k-\varepsilon$ model implies a mixing length that increases roughly linearly and without limit away from the ground (Detering and Etling, 1985). The Apsley and Castro solution consists of an additional source term in the ε transport equation multiplied by a weighting function that serves to cancel net production of ε as the mixing length ℓ_m approaches some limiting value ℓ_{max} and thus limit its growth. Furthermore, the weighting function ensures that the model reduces to the standard $k-\varepsilon$ equations for $\ell_m \ll \ell_{max}$, so as to be consistent with surface-layer scaling.

In the original paper, a simple weighting function ℓ_m/ℓ_{max} was proposed. In this work, we look at the performance of the original model in the surface layer and ask what exact form the weighting function should take. The objective is to modify the Apsley and Castro model such that it is not only consistent with surface-layer scaling in the limit of small ℓ_m/ℓ_{max} but in fact yields the exact similarity profiles when only the surface layer is considered.

The following section briefly reviews a model of the equilibrium, incompressible, constant-stress surface layer, as well as the Apsley and Castro limited-length-scale model. The derivation of an exact form for the standard ε transport equation, for an arbitrary desired mixing-length expression, is given in section 3. Supposing ℓ_m to be half the harmonic mean between the Prandtl mixing length and some established maximum, one-dimensional numerical simulations of the surface layer using the Apsley and Castro ε equation, the derived ε equation, and an empirical fit follow in section 4 for both neutral and stable conditions. A discussion regarding $C_{\varepsilon 3}$ is presented in section 5 followed by a brief conclusion. For consistency, the same notation as the original Apsley and Castro paper has been used throughout.

2.2 The equilibrium surface layer

2.2.1 Governing equations

For the discussion that follows, the Apsley and Castro model for equilibrium atmospheric boundary-layer flow is simplified for the idealized surface layer by ignoring Coriolis effects and pressure gradients, and assuming a constant heat flux. By defining U in the direction of the mean flow, the velocity field is just $\vec{U} = (U(z), 0, 0)$ and, assuming viscous effects are negligible, the steady incompressible Reynolds-Averaged Navier–Stokes equations reduce to

$$\frac{d}{dz}(-\overline{u'w'}) = 0. \tag{2.1}$$

The eddy viscosity concept is used to relate the Reynolds stresses to mean flow properties via

$$-\overline{u'w'} = \nu_t \frac{dU}{dz} \tag{2.2}$$

where the turbulent viscosity ν_t is modelled with standard $k-\varepsilon$ closure (Jones and Launder, 1972), viz.

$$\nu_t \propto \sqrt{k}\ell, \tag{2.3}$$

$$\ell \propto \frac{k^{3/2}}{\varepsilon}, \tag{2.4}$$

and the conservation of momentum is thus expressed as

$$\frac{d}{dz}\left(\nu_t \frac{dU}{dz}\right) = 0. \tag{2.5}$$

The transport equations for turbulent kinetic energy (TKE) k and its dissipation rate ε corresponding to equilibrium surface-layer flow are

$$\frac{d}{dz}\left(\nu_t \frac{dk}{dz}\right) + \Pi_k - \varepsilon = 0, \tag{2.6}$$

$$\frac{d}{dz}\left(\frac{\nu_t}{\sigma_\varepsilon}\frac{d\varepsilon}{dz}\right) + P_\varepsilon - C_{\varepsilon 2}\frac{\varepsilon^2}{k} = 0, \tag{2.7}$$

where

$$P_\varepsilon = \Pi_k C_{\varepsilon 1}\frac{\varepsilon}{k} \tag{2.8}$$

and Π_k is the total turbulence production rate from both mechanical shear (P_k) and thermal effects (G_k), where

$$P_k \equiv -\overline{u'w'}\frac{dU}{dz} = \nu_t\left(\frac{dU}{dz}\right)^2, \tag{2.9}$$

$$G_k \equiv \alpha g\overline{\theta'w'} = -\alpha g\frac{\nu_t}{\sigma_\theta}\frac{d\Theta}{dz}. \tag{2.10}$$

Here, α is the coefficient of thermal expansion, g is the gravitational field strength, and σ_θ is the turbulent Prandtl number.

For a constant heat flux, the transport equation for mean potential temperature Θ is simply

$$\frac{d}{dz}\left(\frac{\nu_t}{\sigma_\theta}\frac{d\Theta}{dz}\right) = 0. \tag{2.11}$$

2.2.2 A comment on $k-\varepsilon$ closure for stably-stratified surface-layer flow

As in the Apsley and Castro model, the velocity scale implied in equation (2.3) is often taken as $u_0 = C_\mu^{1/4} k^{1/2}$. Using the definition of TKE and assuming equilibrium conditions (*i.e.* $u_0 = u_*$), C_μ can thus be calibrated using statistical data from surface-layer field experiments with

$$\frac{1}{\sqrt{C_\mu}} = \frac{1}{2}\left[\left(\frac{\sigma_u}{u_*}\right)^2 + \left(\frac{\sigma_v}{u_*}\right)^2 + \left(\frac{\sigma_w}{u_*}\right)^2\right] \tag{2.12}$$

where the right-hand side of equation (2.12) is the inverse of the structure function. Pahlow *et al.* (2001) have used least-squares regression to fit velocity variance data from several sources and found that all components follow Monin-Obukhov scaling and increase rapidly as $z/L \gtrsim 0.1$. This suggests that the coefficient of proportionality between k and u_*^2 also depends on the stability condition and thus $C_\mu = f(z/L)$.

Be that as it may, for the present work we nonetheless follow the Apsley and Castro model and take C_μ as a constant and equal to its neutral value. One consequence of this assumption is that for surface-layer simulations, with the aforementioned velocity scale, k will be modelled as invariant with height and stability

$$k = \frac{u_*^2}{\sqrt{C_\mu}}. \tag{2.13}$$

A second consequence is related to the TKE budget. For the surface layer, this can be written in terms of length scales as (Panofsky and Dutton, 1984)

$$\frac{1}{\ell_t} + \frac{1}{\ell_m} - \frac{1}{\kappa L} - \frac{1}{\ell_\varepsilon} + I = 0. \tag{2.14}$$

In the stable surface layer, it is generally assumed that $\ell_m \approx \ell_\varepsilon$ and turbulent transport is negligible, which implies that the pressure imbalance I cancels with buoyant production (Kaimal and Finnigan, 1994)[1]. By taking C_μ as a constant in equation (2.13), we ensure infinite ℓ_t. However, in the $k-\varepsilon$ model, the pressure contribution is not explicitly modelled; thus we cannot respect $\ell_m \approx \ell_\varepsilon$ and, to balance the modelled TKE budget, we enforce local equilibrium

$$\frac{1}{\ell_\varepsilon} = \frac{1}{\ell_m} - \frac{1}{\kappa L}, \tag{2.15}$$

which likely overestimates the importance of buoyancy effects (Frenzen and Vogel (2001) have however plotted the left-hand and right-hand sides of the above equation based on their own measurements and found the residual to be tolerably small for stable conditions). Also implicit to this simplified budget equation is the assumption that, for neutral conditions, turbulent production is exactly balanced by dissipation, which is not universally accepted (Frenzen and Vogel, 2001; Pahlow *et al.*, 2001; Hartogensis and Bruin, 2005). Clearly, two-equation closure can only approximate the observed turbulence structure in the surface layer. Nevertheless, the primary objective is to predict the turbulent viscosity (or, moreover, the mixing length) and, with the following caveat, this model does so exactly.

The turbulent viscosity is defined by the relationship between shear stresses and mean velocity gradients. Taking $\ell_m = \kappa z/\phi_m$, similarity theory requires $\nu_t = u_* \ell_m$ whereas equation (2.3) and equation (2.4) yield $\nu_t = u_* \ell_\varepsilon$. Of course, these are equivalent for neutral flow. However, for non-neutral flows, a correction is required for buoyancy effects. Assuming local equilibrium, Apsley and Castro reason that

$$\nu_t = \frac{\tau'^2}{\varepsilon}(1 - R_f) \tag{2.16}$$

where the flux Richardson number $R_f \equiv -G_k/P_k$. If we take equation (2.13) with C_μ constant, by virtue of the simplified TKE budget, $(1-R_f)$ is exactly equal to the ratio of length scales.

[1] An analysis by Cuxart *et al.* (2002) casts some doubt on this accounting of the energy distribution by suggesting that turbulent transport may, in fact, be an important process in the stable nocturnal boundary layer while the pressure imbalance is often of similar order as the other terms and the buoyancy contribution is negligible.

The turbulent viscosity is then consistent with similarity theory if calculated as

$$\nu_t = C_\mu \frac{k^2}{\varepsilon}(1 - R_f) \tag{2.17}$$

where C_μ is effectively reduced by $(1 - R_f)$.

This approach represents but one of several possibilities for modelling stable flow with the $k - \varepsilon$ model. In general, though, either the assumption of local equilibrium is exactly satisfied (by ensuring the transport term is zero) and the turbulent viscosity consequently modified to account for $\ell_\varepsilon \neq \ell_m$ or the standard equation for ν_t is maintained (by changing the velocity scale to $u_0 = C_\mu^{1/4} k^{1/2} (1 - R_f)^{-1/4}$) and small violations of the local equilibrium assumption accepted. Here, we aim to derive a model for which, among other things, Monin-Obukhov similarity theory is an exact solution to the model equations and have thus adopted the former approach. In the context of stably-stratified atmospheric flow, Alinot and Masson (2005) have investigated use of the latter. The Level-2.5 model of Freedman and Jacobson (2003) also follows the latter approach but, in addition, takes C_μ as a function of R_f.

2.2.3 The mixing length

By default, equations (2.6) and (2.7) only agree with similarity theory for purely neutral conditions where the mixing length is unbounded and given by $\ell_m = \kappa z$. Apsley and Castro have proposed a modified $k - \varepsilon$ closure to model an atmospheric boundary layer where the mixing length is limited through stable stratification or some other physical process. For example, the mixing length may be prescribed as (Blackadar, 1962)

$$\ell_m = \frac{\kappa z}{1 + \kappa z / \ell_{max}} \tag{2.18}$$

where ℓ_{max} is given by $\kappa L / \beta$ for stable conditions or can be determined from observations for neutral conditions (Apsley and Castro, 1997). Under the assumption of constant shear stress and heat flux, and taking σ_θ as independent of stability, the corresponding surface-layer

distributions of velocity, potential temperature and turbulence properties are given by

$$U(z) = u_* \int_{z_0}^{z} \frac{1}{\ell_m} dz', \tag{2.19}$$

$$\Delta\Theta(z) = \sigma_\theta \theta_* \int_{z_0}^{z} \frac{1}{\ell_m} dz', \tag{2.20}$$

$$k(z) = \frac{u_*^2}{\sqrt{C_\mu}}, \tag{2.21}$$

$$\varepsilon(z) = \frac{u_*^3}{\ell_\varepsilon} \tag{2.22}$$

where z_0 corresponds to the aerodynamic roughness length and $z \geq z_0$.

2.2.4 Imposing a mixing-length limit

The turbulence transport equations must be modified to yield the desired mixing-length expression such that equations (2.19)-(2.22) represent a solution to the system of differential equations governing fluid flow. In the context of a general atmospheric boundary layer, Apsley and Castro propose the following modification to the ε equation. If ℓ_{max} can be specified *a priori*, they suggest

$$P_\varepsilon = \left[C_{\varepsilon 1} + (C_{\varepsilon 2} - C_{\varepsilon 1}) \frac{\ell_m}{\ell_{max}} \right] \frac{\Pi_k \varepsilon}{k} \tag{2.23}$$

with $\ell_m = u_0^3/\varepsilon$. For stable conditions, where ℓ_{max} might be determined from local flow properties, they propose

$$P_\varepsilon = C_{\varepsilon 1}(1 + C_{\varepsilon 3} R_f') \frac{\Pi_k \varepsilon}{k} \tag{2.24a}$$

$$= \left[C_{\varepsilon 1} + (C_{\varepsilon 2} - C_{\varepsilon 1}) \beta \left(1 - \frac{\ell_m}{\ell_\varepsilon} \right) \right] \frac{\Pi_k \varepsilon}{k} \tag{2.24b}$$

where $R_f' \equiv -G_k/\Pi_k$.

As $\ell_m \to \ell_{max}$ in the first case or $\ell_m/\ell_\varepsilon \to (\beta - 1)/\beta$ in the second, the source terms in the ε equation cancel and ε (and consequently the mixing length) becomes constant. Furthermore, for $\ell_m \ll \ell_{max}$ or $\ell_m \approx \ell_\varepsilon$, equations (2.23) and (2.24a) reduce to equation (2.8). Clearly, both approaches have the desired behaviour for limiting values of ℓ_m. They do not, however, guar-

antee that the resolved ε distribution will match its analytical solution given by equation (2.22). Apsley and Castro acknowledge that equations (2.23) and (2.24a) are but the simplest way to achieve the desired length-limiting action; the question of the exact form required to reproduce a desired surface layer is addressed in the next section.

2.3 Revised limited-length-scale model

2.3.1 Definition of a weighting function

Incorporating the destruction of ε into the Apsley and Castro production term and recalling that $\Pi_k = \varepsilon$ for an equilibrium boundary layer, one can write

$$\frac{d}{dz}\left(\frac{\nu_t}{\sigma_\varepsilon}\frac{d\varepsilon}{dz}\right) + (C_{\varepsilon 2} - C_{\varepsilon 1})\frac{\varepsilon^2}{k}\left(\frac{\ell_m}{\ell_{max}} - 1\right) = 0, \tag{2.25a}$$

which can be further generalized as

$$\frac{d}{dz}\left(\frac{\nu_t}{\sigma_\varepsilon}\frac{d\varepsilon}{dz}\right) + F(C_{\varepsilon 2} - C_{\varepsilon 1})\frac{\varepsilon^2}{k} = 0 \tag{2.25b}$$

where F is a weighting function that corrects the net production of ε such that the model equations yield the desired mixing-length expression.

2.3.2 Derivation of an exact weighting function

The exact weighting function for a desired mixing-length expression can be derived by substituting the corresponding analytical solution into equation (2.25b) and solving for F. Here, we consider the general case of $\ell_\varepsilon \neq \ell_m$. Recalling that $\nu_t = u_* \ell_m$ and $\varepsilon = u_*^3/\ell_\varepsilon$, the first term simplifies to

$$\frac{d}{dz}\left(\nu_t \frac{d\varepsilon}{dz}\right) = \frac{u_*^4}{\ell_\varepsilon^2}\left[2\frac{\ell_m}{\ell_\varepsilon}\left(\frac{d\ell_\varepsilon}{dz}\right)^2 - \frac{d\ell_m}{dz}\frac{d\ell_\varepsilon}{dz} - \ell_m \frac{d^2\ell_\varepsilon}{dz^2}\right]. \tag{2.26}$$

Substituting equation (2.26) into equation (2.25b) with the surface-layer distributions for k and ε yields

$$2\frac{\ell_m}{\ell_\varepsilon}\left(\frac{d\ell_\varepsilon}{dz}\right)^2 - \frac{d\ell_m}{dz}\frac{d\ell_\varepsilon}{dz} - \ell_m\frac{d^2\ell_\varepsilon}{dz^2} + F\sigma_\varepsilon(C_{\varepsilon 2} - C_{\varepsilon 1})\sqrt{C_\mu} = 0. \tag{2.27}$$

For atmospheric flows, the $k-\varepsilon$ model should be calibrated such that the combination of coefficients appearing in the last term is simply κ^2 (Detering and Etling, 1985). Thus,

$$F = \frac{1}{\kappa^2}\left[\frac{d\ell_m}{dz}\frac{d\ell_\varepsilon}{dz} + \ell_m\frac{d^2\ell_\varepsilon}{dz^2} - 2\frac{\ell_m}{\ell_\varepsilon}\left(\frac{d\ell_\varepsilon}{dz}\right)^2\right]. \tag{2.28}$$

Now, reverting to the original equation (2.7) for ε and redefining P_ε as

$$P_\varepsilon = \Big[C_{\varepsilon 1} + (F+1)(C_{\varepsilon 2} - C_{\varepsilon 1})\Big]\frac{\Pi_k \varepsilon}{k} \tag{2.29}$$

the above weighting function ensures the system of equations (2.19)-(2.22) is an exact solution of the model equations for a desired mixing-length expression. Note that, while ℓ_m may be arbitrarily chosen, the expression for ℓ_ε is fixed by the TKE budget.

2.3.2.1 Stable conditions

Here we take $\ell_m = \kappa z/\phi_m$ (and similarly $\ell_\varepsilon = \kappa z/\phi_\varepsilon$) that is consistent with equation (2.18) if ϕ_m is assumed to be a linear function of z/L equal to unity for neutral conditions, viz.

$$\phi_m = 1 + \beta\left(\frac{z}{L}\right). \tag{2.30}$$

Although more advanced fits for ϕ_m have been proposed that cover the full stability range (see Cheng and Brutsaert, 2005), this form has the advantage of simplifying the resulting expression for F. However, in strictest terms, its valid range is limited by some critical value of z/L. In

terms of ϕ, equation (2.28) becomes[2]

$$F = \frac{1-2\phi_m}{(\phi_m\phi_\varepsilon)^2}, \tag{2.31}$$

which can be written in terms of length scales by inverting the mixing-length expression for z and replacing $\kappa L/\beta$ with ℓ_{max},

$$F = -\left(1+R_f'\right)^2\left(\frac{\ell_m}{\ell_{max}}+1\right)\left(1-\frac{\ell_m}{\ell_{max}}\right)^3 \tag{2.32}$$

where $\ell_m = u_0^3/P_k$. It can be completely expressed in terms of local flow properties by substituting $\ell_m/\ell_{max} = \beta R_f$. Using equation (2.32) in the ε transport equation results in a form very similar to that of Freedman and Jacobson (2003) except that, in their case, the $(1-R_f)$ appearing in the equation (2.17) has been effectively subsumed into the expression for k, reducing F by $(1+R_f')^{1/2}$.

2.3.2.2 Neutral conditions

For neutral conditions, equation (2.28) shortens to

$$F = \frac{1}{\kappa^2}\left[\ell_m\frac{d^2\ell_m}{dz^2} - \left(\frac{d\ell_m}{dz}\right)^2\right]. \tag{2.33}$$

In the simplest case where $\ell_m = \kappa z$, $F = -1$, which reduces equation (2.29) to equation (2.8). If ℓ_m is given by equation (2.18),

$$F = -\left(\frac{\ell_m}{\ell_{max}}+1\right)\left(1-\frac{\ell_m}{\ell_{max}}\right)^3. \tag{2.34}$$

If ℓ_{max} is taken as infinite, equation (2.29) again reduces to equation (2.8) and the standard $k-\varepsilon$ model is recovered.

Comparison of equations (2.32) and (2.34) shows that there are two distinct parts to the weighting function: one that is concerned with the magnitude of ℓ_{max} and a second accounting for the

[2] An expanded derivation is provided in Appendix 3.

source of the limiting action. The necessity of the stability-dependent term can be understood by considering that, for a given ℓ_{max}, the shear production rate is the same but the net turbulence production must always be zero. Any contribution from G_k to the overall budget then must be compensated by a decrease in ε. The role of the $(1+R'_f)$ factor is to dampen the length-limiting action thereby ensuring $P_k + G_k - \varepsilon = 0$.

2.3.2.3 Exact expression in the Apsley and Castro form

A good approximation to equation (2.34) is given by

$$(F+1) = \left(\frac{\ell_m}{\ell_{max}}\right)^{\gamma} \tag{2.35}$$

where

$$\gamma = 10^{-\ell_m/\ell_{max}}. \tag{2.36}$$

Using the relationship between equations (2.34) and (2.32), this can be further generalized to

$$(F+1) = (1+R'_f)^2 \left[\left(\frac{\ell_m}{\ell_{max}}\right)^{\gamma} - 1\right] + 1. \tag{2.37}$$

In this light, the Apsley and Castro weighting function can be considered a special case where $\gamma = 1$ and stability effects are ignored. Figure 2.1 shows a plot of the Apsley and Castro (*i.e.* ℓ_m/ℓ_{max}), exact (equation (2.34)), and "empirical" (equation (2.35)) weighting functions as a function of the non-dimensional height $\zeta = z/\ell_{max}$ for the mixing-length expression given by equation (2.18) and neutral conditions. Both the Apsley and Castro and empirical weighting functions have large errors for small ζ but, as $F+1$ is quite small, this is not critical. More significant is the large difference between the Apsley and Castro and exact weighting functions for moderate values of ζ (say, $0.1-10$) where the limiting action of the Apsley and Castro approach is less aggressive. As will be shown, this leads to an overestimation of the mixing length and consequently an underestimation of velocity in the surface layer.

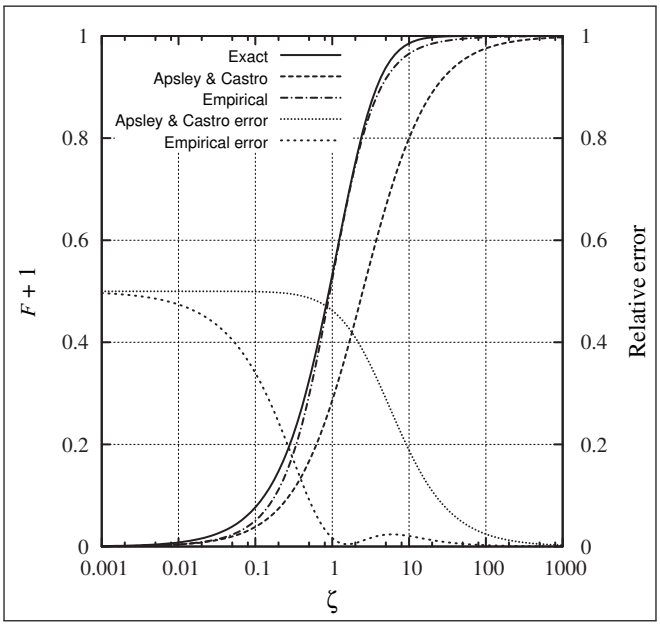

Figure 2.1 Comparison of weighting functions for a neutral length-limited surface layer

2.4 One-dimensional simulations

2.4.1 Grid, boundary conditions, and numerics

The Apsley and Castro model was not intended to resolve surface-layer flow uniquely. While its ε equation ensures $\ell_m < \ell_{max}$ is everywhere respected, the corollary is that for simulations of the idealized surface layer in a domain where $\kappa z_{max} > \ell_{max}$, $\ell_m \approx \ell_{max}$ will be implicitly imposed at the upper boundary. This could lead to problems for surface-layer simulations if the domain height is insufficient. To illustrate, similarity theory requires the ratio of ℓ_m/ℓ_{max} at $\zeta = 10$ to be roughly 0.8 whereas the Apsley and Castro closure would predict unity if the upper boundary was located at this level. The problem is easily sidestepped by extending the domain to $\zeta = 250$ (where $\ell_m/\ell_{max} > 0.99$). This is well beyond physical heights for which Coriolis effects can be safely neglected, but is a simple expedient by which the appropriate *numerical* conditions are ensured.

The lower and upper limits of the domain are thus placed at $\zeta = z_0/\ell_{max}$ and $\zeta = 250$, respectively, and the grid is discretized using 1116 cells for the neutral simulation and 880 cells for

the stable one. Such a high density of cells serves to ensure discretization errors are entirely negligible. For both grids, the near-wall cell centre has a non-dimensional height ($= zu_*/\nu$) of 30 that is sufficient to properly resolve the strong vertical gradients near the ground (Gorlé *et al.*, 2009). The grids are geometrically expanded using a ratio of 1.01.

The boundary conditions are essentially those of Richards and Hoxey (1993) generalized for an arbitrary mixing-length expression. For the momentum equations, horizontal kinematic shear stresses of $-u_{0w}u_{*w}$ and u_{*sl}^2 are exerted at the lower and upper boundaries, respectively, while the vertical velocity component is set to zero. The local wall friction velocity u_{*w} is calculated from the flow solution in the wall-adjacent cell using

$$u_{*w} = \frac{U_P}{\int_{z_0}^{z_P} \frac{1}{\ell_m} dz'}, \tag{2.38a}$$

which for equation (2.18) becomes

$$u_{*w} = \frac{\kappa U_P}{\ln(z_P/z_0) + \kappa(z_P - z_0)/\ell_{max}}. \tag{2.38b}$$

u_{*sl} is the surface layer friction velocity (specified *a priori*) related to the shear stress that, under these idealized conditions, drives the flow.

Wall functions are used to specify turbulence properties at the lower boundary. The near-wall cell centre ε is specified with

$$\varepsilon_P = \frac{\sqrt{C_\mu} k u_{*w}}{\ell_\varepsilon}, \tag{2.39}$$

where ℓ_ε is related to the mixing length via equation (2.15). The source terms for the k equation in the wall-adjacent cell are set using:

$$\begin{aligned}\overline{\Pi}_{k,P} &= \frac{u_{*w}^3}{\Delta z}\int_{z_0}^{2z_P-z_0}\left(\frac{1}{\ell_m}-\frac{1}{\kappa L}\right)dz' \\ &= u_{*w}^3\left[\frac{1}{2\kappa(z_P-z_0)}\ln\left(\frac{2z_p-z_0}{z_0}\right)+\frac{1}{\ell_{max}}-\frac{1}{\kappa L}\right], \qquad (2.40)\end{aligned}$$

$$\overline{\varepsilon_P} = \frac{\sqrt{C_\mu}k}{u_{*w}^2}\overline{\Pi}_{k,P}. \qquad (2.41)$$

The gradient of k at the wall is taken as zero. To avoid biasing the solution, turbulence properties at the upper boundary are specified through Neumann conditions: the gradient of k again being taken as zero and that of ε derived from

$$\begin{aligned}\frac{d\varepsilon}{dz} &= \frac{d}{dz}\left(\frac{u_{*sl}^3}{\ell_\varepsilon}\right) \\ &= -\frac{u_{*sl}^3}{\kappa z^2}. \qquad (2.42)\end{aligned}$$

The surface sensible heat flux is constant in the surface layer and is used to formulate the condition for mean potential temperature at both boundaries

$$\frac{d\Theta}{dz} = -\frac{Q_H}{\rho c_p}\frac{\sigma_\theta}{\nu_t}. \qquad (2.43)$$

Using equation (2.17) to calculate the eddy viscosity, equations (2.5)–(2.7) and (2.11) are resolved with OpenFOAM 1.6.x (OpenCFD, 2009a). The same $k-\varepsilon$ model coefficients and constants as in the Apsley and Castro simulations are used:

$$C_\mu = 0.09,\ C_{\varepsilon 1} = 1.44,\ C_{\varepsilon 2} = 1.92,\ \sigma_k = 1.0,\ \sigma_\varepsilon = 1.111,\ \sigma_\theta = 0.9.$$

Given the absence of pressure gradients and momentum sources, the resolved kinematic shear-stress distribution must be uniform at convergence (*i.e.* $\tau'(z) = u_{*sl}^2$), regardless of the weighting function. Furthermore, at equilibrium, the velocity scale and the friction velocity are iden-

tical (*i.e.* $u_0 = u_*$). Thus, a convenient measure of convergence is the normalized residual $\mathbb{R} = \max|u_0(z) - u_{*sl}|/u_{*sl}$. All fields are initialized with an approximate solution such that $u_0 \neq u_{*sl}$ and the solution is considered converged (to the accuracy provided by the numerical discretization) when further iteration provides negligible improvement in $\mathbb{R}$; generally, $\mathbb{R}_{final} \sim 10^{-5}$. As the residual is essentially the maximum relative error in $\sqrt{k}$, its magnitude is also a measure of the extent to which the local equilibrium condition is respected.

2.4.2 Neutral length-limited surface layer

Figure 2.2 compares the predicted normalized velocity and mixing length distributions with analytical solutions for a neutral atmosphere defined by $z_0 = 0.3$ m, $u_{*sl} = 0.65$ m s^{-1} and $\ell_{max} = 36$ m (these are the fitted parameters used by Apsley and Castro for the Leipzig data). All profiles overlap in the near-wall region and are not shown. Clearly, the resolved velocity distributions are dependent on the method by which the length scale is limited in the ε equation: the profile generated using the exact weighting function (equation (2.34)) coincides with the analytical solution whereas the error in predicted velocity associated with the other functions depends on how closely the resolved mixing length matches the desired distribution. As expected, the Apsley and Castro weighting function does not limit the mixing length quickly enough (*i.e.* $F + 1$ is too small for all ζ) and, at $\zeta = 10$, the velocity deficit using the Apsley and Castro model is greater than 12%. As the empirical F is in fairly close agreement with the exact function, the resolved mixing length is much closer to the analytical solution and the error in predicted velocity considerably less.

2.4.3 Stable surface layer simulation

To simulate stable flow, the original Apsley and Castro model would, in fact, use $\ell_\varepsilon/\ell_{max}$ as it supposes a single turbulent length scale. As here we distinguish between ℓ_ε and ℓ_m (most notably in the calculation of the eddy viscosity) and as the intent of the model is to limit the latter quantity, simulations are carried out using ℓ_m/ℓ_{max}.

With that in mind, figure 2.3 presents the resolved normalized profiles of mean velocity, mean potential temperature difference, mixing length and TKE budget using the three weighting

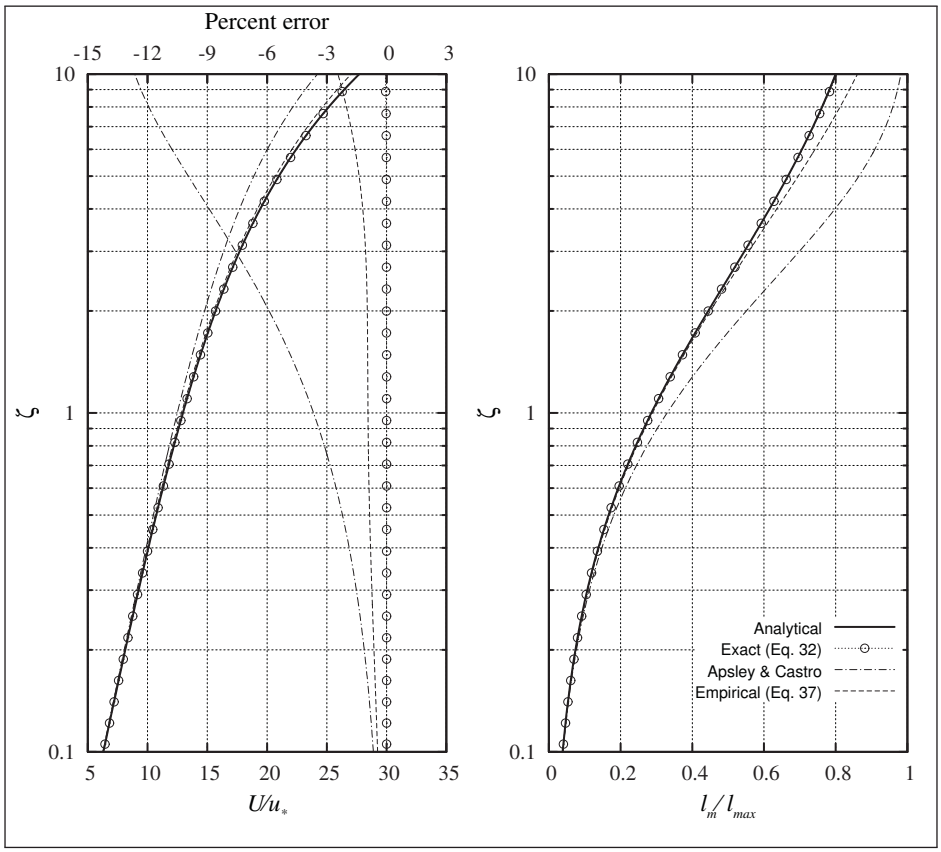

Figure 2.2 Resolved normalized profiles of mean velocity (with associated error) and mixing length for neutral length-limited atmospheric conditions using the Apsley and Castro, exact, and empirical weighting functions

functions and compares them with similarity theory (*i.e.* equations (2.19) and (2.20)). Stable atmospheric conditions are defined by $z_0 = 0.3$ m, $L = 100$ m, $Q_H = -20$ W m^{-2} (with $Q_H/(\rho c_p) = -1.625 \times 10^{-2}$ m K s^{-1}) and $u_{*sl} = 0.28$ m s^{-1}. The corresponding mixing-length limit is $\ell_{max} = 8$ m.

The resolved normalized mixing length profiles are quite similar to the neutral case as are the errors in predicted velocity. Of course, the TKE budget is quite different. The exact weighting function (equation (2.32)) properly reproduces all budget terms whereas the (modified) Apsley and Castro approach only predicts the buoyant production correctly; the other components are underestimated. Although not shown, the empirical weighting function again provides a better approximation.

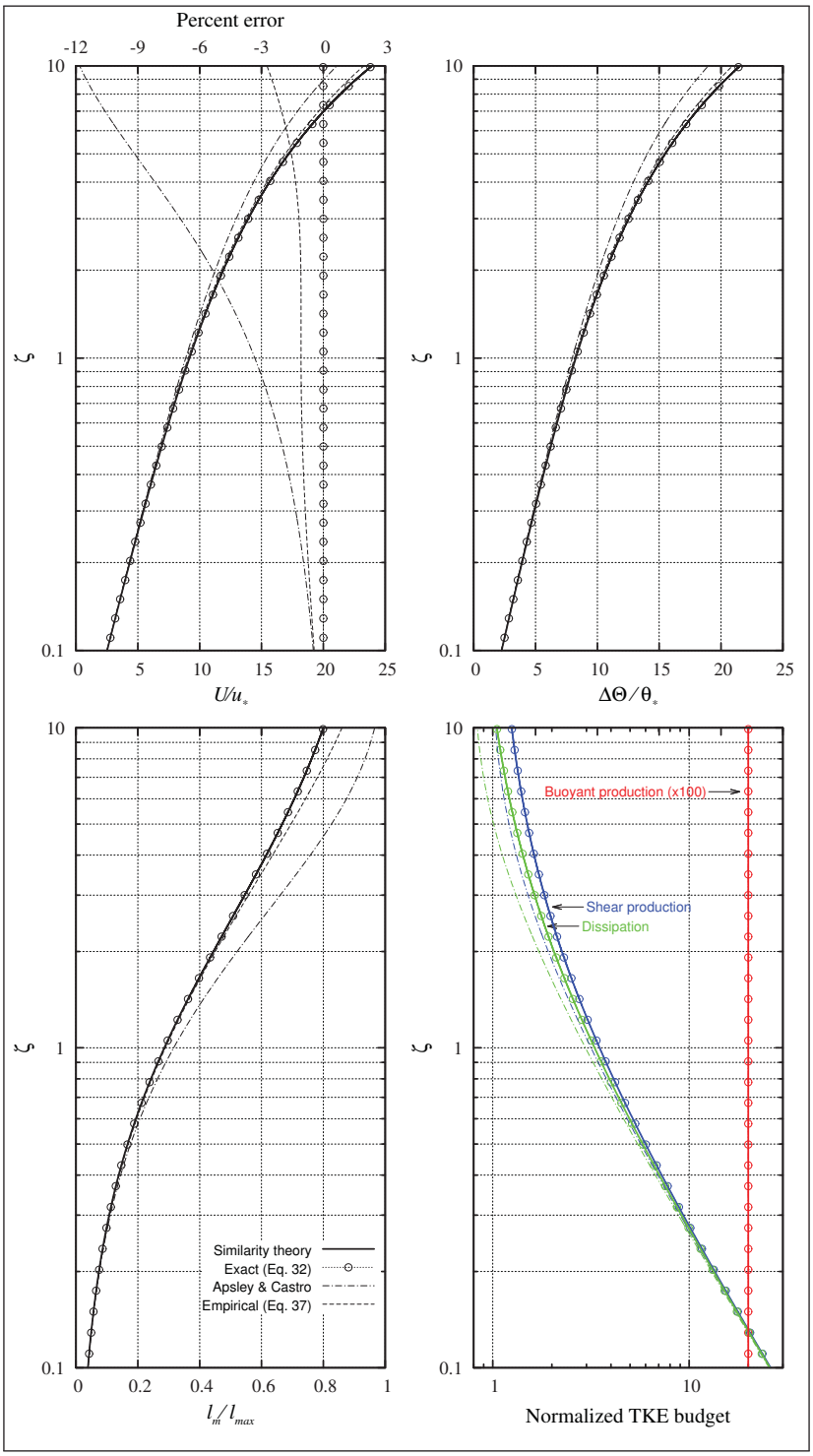

Figure 2.3 Resolved normalized profiles of mean velocity (with associated error), mean potential temperature difference, mixing length, and turbulent kinetic energy budget for stably-stratified atmospheric conditions using the Apsley and Castro, exact, and empirical weighting functions. The turbulence budget predictions using the empirical weighting function have been omitted for clarity

2.5 Regarding $C_{\varepsilon 3}$

As the ε equation is now exact for equilibrium stably-stratified surface-layer flow (at least in the context of section 2.2.2), we can comment briefly on the $C_{\varepsilon 3}$ coefficient. Taking equation (2.24a) for the production term, the preceding derivation of the exact weighting function can be recast as an expression for $C_{\varepsilon 3}$

$$C_{\varepsilon 3} = \frac{(C_{\varepsilon 2} - C_{\varepsilon 1})}{C_{\varepsilon 1}} \left[1 - (1 + R'_f)^2 \left(\frac{\ell_m}{\ell_{max}} + 1 \right) \left(1 - \frac{\ell_m}{\ell_{max}} \right)^3 \right] \frac{1}{R'_f}. \tag{2.44}$$

This may be somewhat unexpected form as the trailing $1/R'_f$ cancels its counterpart in equation (2.24a) and the so-called buoyancy term is no longer simply a coefficient multiplied by the buoyant production rate. Rather $C_{\varepsilon 3}$ is itself a function of R'_f and is now a multiplier of the total production rate, effectively making $C_{\varepsilon 1}$ variable as in Freedman and Jacobson (2003). Unlike in their work, the $C_{\varepsilon 3} R'_f$ term is non-zero for $z/L = 0$, if ℓ_{max} is not large, as equation (2.44) is valid for stable and neutral length-limited conditions.

Several authors have simulated stable surface-layer flow using $k - \varepsilon$ closure and various proposals regarding $C_{\varepsilon 3}$ can be found in the literature. However, the ε equation varies among them: many calculate P_ε using equation (2.24a) while

$$P_\varepsilon = C_{\varepsilon 1} P_k \frac{\varepsilon}{k} + C_{\varepsilon 1} C^\star_{\varepsilon 3} G_k \frac{\varepsilon}{k} \tag{2.45}$$

is also common. The two expressions are equivalent if $C^\star_{\varepsilon 3} = 1 - C_{\varepsilon 3}$.

Figure 2.4 compares some of these proposals for the stable atmosphere considered in section 2.4.3. As not all models use the same set of coefficients, direct comparisons are difficult and a more just portrait is hoped to be achieved by plotting $C_{\varepsilon 3} C_{\varepsilon 1} / (C_{\varepsilon 2} - C_{\varepsilon 1})$. Historically, $C_{\varepsilon 3}$ has generally been considered a constant. Based on experiments involving stably-stratified shear flows, Rodi (1987) suggested that $0.8 \leq C_{\varepsilon 3} \leq 1$. In applying Rodi's model to atmospheric flows, Kitada (1987) assumed unity whereas the Apsley and Castro model predicts $C_{\varepsilon 3}$ to be 1.67. Based on the Kansas surface-layer experiments of Businger *et al.* (1971), Betts and

Haroutunian (1983) found 2.15 through numerical optimization but additionally suggested $C_{\varepsilon 3}$ should be a continuous function of z/L. Using data from FLEX'76 (Brockmann *et al.*, 1984), Burchard and Baumert (1995) have argued $C_{\varepsilon 3}$ could be as high as 2.4. A summary of other proposals for constant $C^{\star}_{\varepsilon 3}$ can be found in Baumert and Peters (2000).

Freedman and Jacobson (2003) have conclusively shown, however, that constant coefficients are inconsistent with similarity theory for non-neutral flow. Their expression for $C_{\varepsilon 3}$ is plotted assuming constant C_{μ} which, as mentioned, differs from equation (2.44) only by a factor of $(1+R'_f)^{1/2}$. Alinot and Masson (2005) have opted for an approximate solution by fitting a fifth-order polynomial based on similarity theory. All the variable $C_{\varepsilon 3}$ expressions are in good agreement for $z/L > 0.1$ while their differences likely have little effect for a weakly-stratified flow.

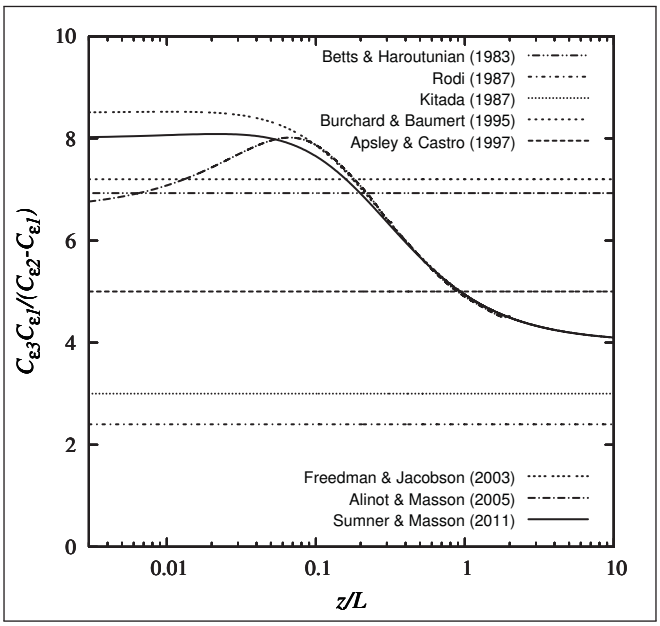

Figure 2.4 Comparison of various proposals for $C_{\varepsilon 3}$ for a stable atmosphere defined by $z_0 = 0.3$ m and $L = 100$ m. The Alinot and Masson polynomial is plotted for $z_0/L \leq z/L \leq 2$

Whereas the Apsley and Castro model anticipates the coefficient of $(C_{\varepsilon 2} - C_{\varepsilon 1})/C_{\varepsilon 1}$ to be β, the expression derived here finds it to vary by a factor of exactly two between $(\beta - 1)$ and $2(\beta - 1)$. The optimized value of Betts and Haroutunian is based on simulations for $0.1 < z/L < 1$

and, perhaps unsurprisingly, transects the exact expressions over this range. Interestingly, the constant value proposed by Rodi and used by Kitada does not lie within the predicted limits of $C_{\varepsilon 3}$. It is suggested that, if a constant value must be used, it should at least satisfy the requirement

$$(\beta - 1) \leq \frac{C_{\varepsilon 1} C_{\varepsilon 3}}{(C_{\varepsilon 2} - C_{\varepsilon 1})} \leq 2(\beta - 1).$$

But, as the buoyancy term is unimportant for near-neutral conditions, it is preferable to take the constant value closer to its lower limit. In this light, the Apsley and Castro proposal of β seems reasonable.

2.6 Conclusions

The original limited-length-scale $k - \varepsilon$ model proposed by Apsley and Castro has been previously shown to be effective at reproducing observations in both the neutral and stable atmospheric boundary layers while being quite elegant in its simplicity. Here, the performance of this model specifically in the constant-stress surface layer, where Coriolis forces and pressure gradients can be neglected, has been evaluated. For the mixing-length expression considered, simulations indicate that the original model is slow in limiting the growth of ℓ_m, which leads to non-negligible errors in predicted velocity.

Given this, a general ε transport equation and the boundary conditions required to exactly reproduce surface-layer profiles of velocity, potential temperature, and turbulence properties corresponding to an arbitrary desired mixing-length expression have been derived based on the framework of the original model. Taking $\ell_m = (1/\kappa z + 1/\ell_{max})^{-1}$, a single exact formulation of the $k - \varepsilon$ model covering both stable and length-limited neutral conditions results. The performance of this closure for general boundary-layer simulations and under non-homogeneous conditions remains to be evaluated.

Fitting an empirical equation, of similar form as the original model, to this exact formulation shows that, in terms of velocity predictions, the Apsley and Castro weighting function is generally too small (*i.e.* γ should always be ≤ 1) and, in terms of resolved turbulence properties,

explicit correction for the flux Richardson number is needed to distinguish between length scales.

Considering stably-stratified flow, the derived ε equation has been recast to yield a new expression for $C_{\varepsilon 3}$. It is very similar to that of Freedman and Jacobson (2003) (with constant C_μ), however differences in the modelling of the TKE lead to a reduction by $(1+R'_f)^{1/2}$ in the stability-dependent term. Also, whereas Freedman and Jacobson (2003) derive a consistency condition between all $k-\varepsilon$ model coefficients, here the standard coefficients are calibrated to neutral conditions and $C_{\varepsilon 3}$ is related to them by satisfying the simplified TKE budget.

To close, a comment on the treatment of TKE as independent of stability might be warranted. Although this proves beneficial by ensuring that local equilibrium is always satisfied, it would be fair to say that we may be sacrificing some of the flow physics for the sake of mathematical consistency. As for other possibilities, the TKE could be modelled as non-uniform by assuming a different velocity scale or by taking C_μ as a function of stability (or both). It is quite common to take C_μ as a constant in $k-\varepsilon$ models so, considering the former option, it is worth noting that the reduction in TKE in the surface layer associated with the use of a stability-dependent expression for k is, at most, $1-\sqrt{1-1/\beta}$, or roughly 10%. Thus, for stable surface-layer simulations, taking k constant is not an altogether unreasonable approximation within the context of *this* model. Similarly, for atmospheric boundary-layer simulations, the assumption of invariant TKE in the derivation of the ε equation also appears to be reasonable since differences in the derived $C_{\varepsilon 3}$ expressions are small and only noticeable for $z/L \lesssim 0.1$ where buoyancy effects assume less importance.

CHAPTER 3

EVALUATION OF RANS MODELLING OF WIND TURBINE WAKE FLOW USING WIND TUNNEL MEASUREMENTS

Jonathon Sumner[1], Guillaume Espana[2], Christian Masson[1], Sandrine Aubrun[2],
[1]Département de Génie Mécanique, École de Technologie Supérieure, 1100 Notre-Dame Ouest, Montreal, Quebec, Canada H3C 1K3
[2]PRISME - Polytech'Orléans, 8 rue Léonardo de Vinci, 45072 - Orléans Cedex 2, France
Article submitted June 2012 for publication in a special issue of the *International Journal of Engineering Systems Modelling and Simulation* dedicated to the proceedings of the *47th Symposium of Applied Aerodynamics* organized by the 3AF. The version presented here includes revisions based on the comments of the Board of Examiners.

Foreword

The previous chapters have explored two aspects of modelling the homogeneous surface-layer within a RANS/$k-\varepsilon$ context. At some point, however, the presence of a rotor and the energy extraction process also needs to be taken into account. While modelling the system of vortices shed from an operating rotor in a turbulent flow would likely provide the most accurate description of wake properties, this level of detail is generally unnecessary for analyses at the scale of wind farms. Of primary interest is modelling the so-called *far wake*.

Unfortunately, the $k-\varepsilon$ model is notorious for its poor wake predictions. This flaw stems from weaknesses in the eddy-viscosity concept that are exacerbated by actuator disk modelling of the rotor (Réthoré, 2009). What is attempted here is a validation of various turbulence closures, including a newly proposed one, based on wind tunnel measurements downstream of a porous disk. While these case studies prove ill-suited to the task, as all models perform well, the necessary wind tunnel conditions are deduced from the discussion. Likely, the most important contributions of this work are the method by which flow and rotor properties are deduced from wake measurements and the discussion on similitude.

Abstract

Wake modelling plays a central role in the planning of a wind farm during the evaluation of losses, prediction of the energy yield, and estimation of turbine loads. These models must be reasonably accurate – to minimize financial risk – and yet economical so that many configurations can be tested within reasonable time. While many such models have been proposed, an especially attractive approach is based on the solution of the Reynolds-Averaged Navier–Stokes equations with two-equation turbulence closure and an actuator disk representation of the rotor. The validity of this approach and its inherent limitations however remains to be fully understood. To this end, detailed wind tunnel measurements in the wake of a porous disk (with similar aerodynamic properties as a turbine rotor) immersed in a uniform flow are compared with the predictions of several closures. Agreement with measurements is found to be excellent for all models. This unexpected result seems to derive from a fundamental difference in the turbulent nature of the homogeneous wind tunnel flow and that of the atmospheric boundary layer.

3.1 Introduction

All wind energy technology is based on the conversion of some fraction of the kinetic energy of moving air into useful mechanical energy through aerodynamic interaction with a rotor. Consequently, wind speeds downstream of a well-designed wind turbine are considerably lower than those upstream. This region of reduced wind speed and increased turbulence intensity is the so-called wake. Clearly, a wind turbine operating in the wake of another will extract less energy and experience larger fatigue loads than its upstream neighbour. Yet, for economic reasons, large-scale exploitation of the wind resource typically involves installing turbines in a densely packed arrangement with the majority of machines operating under wake conditions. The ability to accurately quantify and minimize wake effects is thus essential for the commercial success of most industrial-scale wind energy projects.

While various methods have been developed to model the wake of horizontal-axis turbines (see *e.g.* Crespo *et al.* (1999); Vermeer *et al.* (2003); Sanderse *et al.* (2011)), one of the most

promising approaches for wind farm analysis is based on the solution of the Reynolds-Averaged Navier–Stokes (RANS) equations wherein the rotor is represented by a pressure discontinuity derived from the turbine thrust curve (Ammara *et al.*, 2002). The appeal lies in the physical realism of predictions: conservation of mass and momentum is always respected and the inherently non-linear nature of fluid flow is retained. The main disadvantages of this approach are that *i*) the blade geometry and near-wake flow characteristics are not resolved and *ii*) the turbulence is entirely modelled. However, if the primary interest lies in the prediction of flow properties far downstream, where the rotor influence on the flow is more or less axisymmetric due to diffusive processes, the relative economy of this method makes it especially attractive.

Of course, the accuracy of predictions will largely depend on the relative importance of turbulent processes in the flow and how well they are modelled. In this regard, it is hoped that the comparison of flow solutions with highly detailed wind tunnel measurements will help identify weaknesses and lead to improvements. Herein, solutions from a RANS-based generalized actuator-disk method, with various turbulence models, will be validated against experiments involving the wake of a porous disk. The perfect analogy between a numerical actuator disk and a physical porous disk makes these comparisons particularly relevant: differences between predictions and measurements should be attributable primarily to the choice of governing equations and turbulence closure. The following popular two-equation turbulence models will be considered: standard $k-\varepsilon$ (Jones and Launder, 1972), RNG $k-\varepsilon$ (Yakhot and Orszag, 1986; Yakhot and Smith, 1992), and rotor-corrected $k-\varepsilon$ (El Kasmi and Masson, 2008). In addition, a modified $k-\varepsilon$ closure wherein the eddy-viscosity assumption is partially dropped for the near-rotor region will also be investigated.

Model rotors immersed in both a uniform flow and in a modelled atmospheric boundary layer have previously been studied at the PRISME Laboratory of the University of Orléans (Espana, 2009). In these experiments, laser Doppler anemometry was employed to obtain a detailed description of the wake flow. Herein, numerical predictions for homogeneous conditions are compared with these measurements.

3.2 Wind tunnel experiments

3.2.1 Reduction of scale

Physical modelling of atmospheric flows in wind tunnels is a powerful tool. It has already been used for several decades in environmental research and extensive guidelines have been published by Snyder (1981) and the German Engineering Association VDI (VDI, 2000). The typical strategy is to reduce all length scales (*i.e.* building and vegetation dimensions, boundary layer thickness, *etc.*) while maintaining the dimensionless parameters describing the fluid, flow and thermal properties, that is the Prandtl (Pr), Eckert (Ec), Reynolds (Re), Rossby (Ro), and Richardson (Ri) numbers. The turbulence intensity level is also maintained.

Since the fluid in both cases is air and the flow velocity is relatively low, Pr and Ec will always be similar. The Rossby criterion, which represents the influence of the Coriolis force on the flow, does not need to be respected if the longest dimension of the modelled area is smaller than approximately 5 km. No thermal effects are taken into account ($Ri = 0$) which corresponds to neutral stability conditions at full scale. It is not necessary to respect Reynolds number similarity (where Re is based on the rotor diameter: $Re_D = 10^5$ at model scale and $Re_D = 10^8$ at full scale) if Reynolds number independence can be demonstrated. This is generally the case for very turbulent approach flows over rough surfaces and sharp-edged obstacles, and at a geometric scale larger than 1:1000. In such cases, model velocities can be on the same order as at full scale, usually < 20 m/s. In this work, Reynolds number independence has been systematically checked, repeating measurements of flow properties over the range of velocities available in the wind tunnel. Modelling the wind turbine rotor with a porous disk made from a metallic mesh contributes to fulfilling these conditions since the flow through a grid is found to be Reynolds number independent (Comte-Bellot and Corrsin, 1966).

3.2.2 Porous disk and actuator disk theory

The simplified theory of an actuator disk enables consideration of the energy extraction process without reference to any specific rotor design. Its physical equivalent is a porous disk:

simulation of flow through an actuator disk will resemble the observed flow passing through a porous disk.

The axial induction factor, a, is defined as the ratio of the induced velocity at the disk to the freestream velocity, U_∞. If the disk is divided into annular elements, a unique induction factor can be calculated for each element based on the streamtube which contains it. Global thrust and power coefficients are related to the disk-averaged induction by

$$C_T \equiv \frac{T}{\frac{1}{2}\rho A_{disk} U_\infty^2} = 4\overline{a}(1-\overline{a}), \tag{3.1}$$

$$C_P \equiv \frac{P}{\frac{1}{2}\rho A_{disk} U_\infty^3} = 4\overline{a}(1-\overline{a})^2 \tag{3.2}$$

where T denotes the force on the disk caused by the pressure drop across the rotor plane, P is the power extracted from the air, ρ is the air density, and A_{disk} is the disk/rotor area. According to equations (3.1) and (3.2), one induction factor corresponds to a unique operating point of the modelled wind turbine. In the present study, the porous disk had a diameter $D = 0.10$ m. Two different types of disks made from metallic mesh were used: one with a mesh size of 3.2 mm and a wire diameter of 1 mm and another with a mesh size of 5.6 mm and a wire diameter of 1.4 mm. They were fixed in place via a 5-mm-diameter mast. The disk solidities were 45% and 35%. Table 3.1 provides a summary of the disk properties.

Table 3.1 Summary of porous disk properties

Disk	Mesh size [mm]	Wire diameter [mm]	Solidity [%]
1	5.6	1.4	35
2	3.2	1	45

3.2.3 Flow conditions

Wake measurements were carried out under homogeneous conditions at the Eiffel-type wind tunnel at the PRISME Laboratory. The test section has a width and height of 0.5 m, and a length of 2 m. Two different turbulence-generating grids were fixed at the entrance of the test section

to augment the turbulence intensity. The model wind turbines were placed 0.5 m downstream of the grids. Grid characteristics are listed in table I-3.

Table 3.2 Dimensions of grids used to generate upstream turbulence. The streamwise turbulence intensity, I_U, is given near the disk location

Grid	I_U [%]	Mesh size [mm^2]	Lattice type
1	3	22.5×22.5	Circular bars $\varnothing$2.5 mm
2	12	40×40	Square bars 20×20 mm^2

3.2.4 Deducing disk thrust from wake data

Similarity between the wind tunnel experiments and the numerical simulations is achieved by maintaining three non-dimensional parameters: the disk thrust coefficient, the turbulence intensity, and the turbulent Reynolds number based on the disk diameter and the turbulent eddy viscosity,

$$Re_t = \frac{DU_\infty}{\nu_t}. \tag{3.3}$$

While a method for characterizing the thrust (and power) coefficient of the porous disks has been previously presented by Aubrun *et al.* (2007), the approach is revisited here to account for possible wind tunnel blockage effects.

The challenge in determining the aerodynamic properties of the disk lies in the fact that the thrust has not been directly measured. Rather, it must be deduced from the measured velocity deficit in the wake through a control volume analysis. As shown in figure 3.1, the control volume is taken coincident with the wind tunnel where the inflow is defined by flow conditions in absence of a disk and the outflow location is defined by the various wake measurements. Considering the tunnel cross section (0.5×0.5 m^2) and relative size of the disks, the work of

Mikkelsen (2003) suggests that tunnel blockage effects should be taken into account. They are nonetheless expected to be small (average blockage is 1.3%).

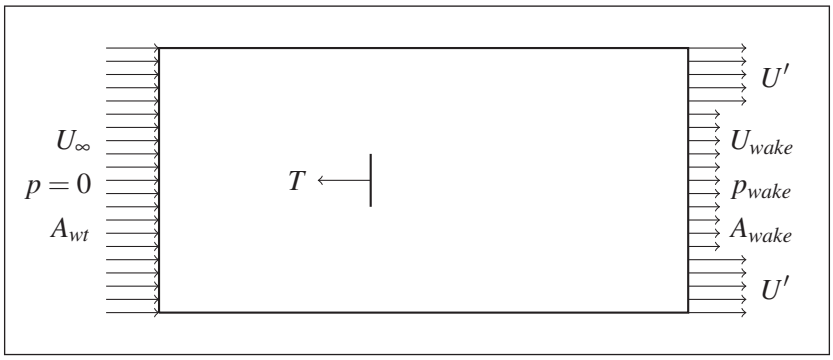

Figure 3.1 Control volume analysis of wind tunnel

The total number of unknowns is four: the freestream velocity U_∞, the velocity field between the measurement region and the wall $U'(r)$, the wake pressure p_{wake}, and the disk thrust T. If a smoothness condition is applied to the velocity distribution in the radial direction and the unmeasured velocity is assumed to be uniform (*i.e.*, $U' = U_{wake}(r = R_{wake})$), the freestream velocity can be determined directly from continuity:

$$U_\infty = \frac{1}{A_{wt}} \left[U' \left(A_{wt} - A_{wake} \right) + \iint_{A_{wake}} U_{wake} dA \right] \tag{3.4}$$

where the integral in the wake is evaluated numerically from measurements assuming axisymmetric conditions. As U_∞ may vary slightly for each of set of wake measurements, a separate value is deduced for each control volume.

The thrust coefficient and wake pressure can be estimated by considering conservation of momentum and energy. For the low turbulence case, any contribution from wall shear stress to the overall momentum balance is likely negligible and the wall can be modelled with a full-slip condition. The momentum balance yields:

$$-T - \iint_{A_{wake}} p_{wake} dA = -\rho U_\infty^2 A_{wt} + \iint_{A_{wake}} \rho U_{wake}^2 dA + \rho U'^2 \left(A_{wt} - A_{wake} \right). \tag{3.5}$$

Normalizing by $-1/2\rho U_\infty^2 A_{disk}$, equation (3.5) can be solved for the disk thrust coefficient.

As p_{wake} cannot be neglected *a priori*, the Bernoulli equation is applied from the inflow to the disk and from the disk to the outflow along the axis of symmetry. After some algebra,

$$C_T = 1 - \frac{2}{U_\infty^2}\left[\frac{p_{wake}}{\rho} + \frac{1}{2}U_{wake}^2(r=0)\right]. \tag{3.6}$$

If $p_{wake} = 0$, the familiar expression $C_T = 4\overline{a}(1-\overline{a})$ results. By combining the normalized form of equation (3.5) with equation (3.6), estimates of both C_T and p_{wake}/ρ can be determined from each set of wake measurements.

Figure 3.2 presents the results of such an analysis for each disk with low ambient turbulence. In both cases, the scatter in the predicted thrust coefficient is quite low; the average thrust coefficients are 0.61 and 0.43. Interestingly, the velocity outside the wake is found to be roughly 2-2.5% greater than U_∞, supporting the assertion that blockage effects may be small but noticeable.

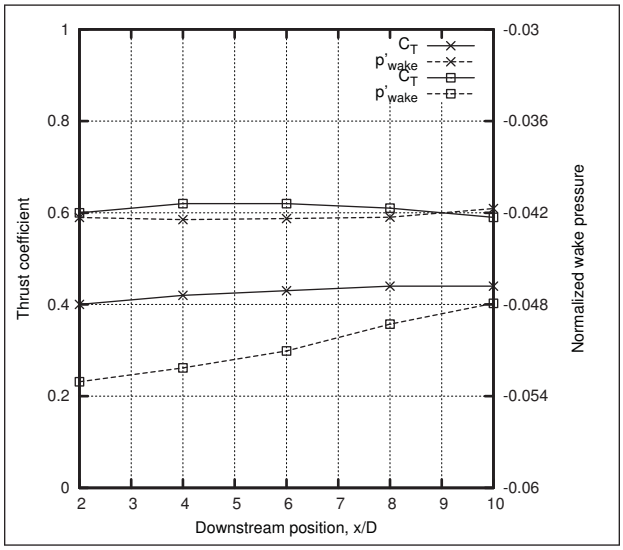

Figure 3.2 Thrust coefficient and wake pressure normalized with dynamic pressure deduced from wake measurements at various downstream positions with low ambient turbulence. Symbols: $\times$ low-induction disk; $\square$ high-induction disk

Figure 3.3 presents an identical analysis for the more turbulent inflow. Clearly, the analysis is invalid as the predicted disk thrust varies greatly for different control volumes. Likely, the assumption of frictionless flow in the Bernoulli equation proves inaccurate as wake velocity

recovery is not entirely due to a decrease in pressure but rather through diffusion of momentum from outside the wake. The best estimate of the thrust coefficient is obtained from the nearest wake measurements where turbulence effects might be expected to have least influence. Values of 0.56 and 0.73 are used for the low- and high-solidity disks, respectively. This result implies that the aerodynamic properties of the porous disks are dependent on flow properties and further emphasizes the need for Re_t and I similarity.

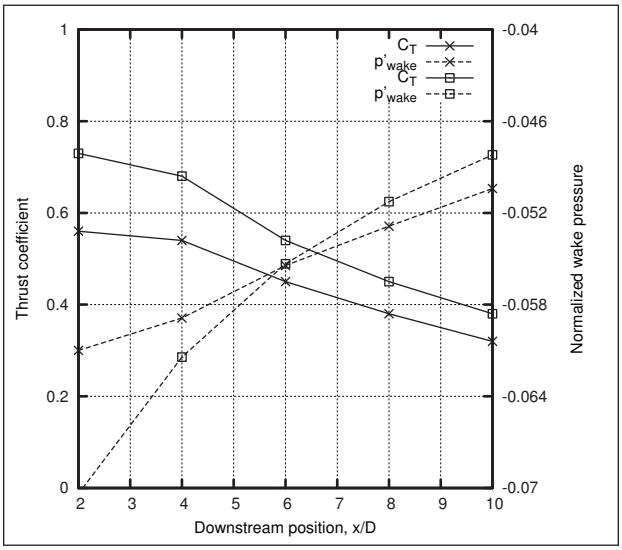

Figure 3.3 Thrust coefficient and wake pressure normalized with dynamic pressure deduced from wake measurements at various downstream positions with high ambient turbulence. Symbols: $\times$ low-induction disk; $\square$ high-induction disk

3.3 Mathematical models

3.3.1 RANS equations

The mathematical model is based on the finite-volume solution of the steady RANS equations with two-equation turbulence closure. Conservation of mass and momentum are expressed in differential form as

$$\nabla \cdot \vec{U} = 0, \tag{3.7}$$

$$\nabla \cdot \vec{U}\vec{U} = -\frac{1}{\rho}\nabla p + \nabla \cdot \boldsymbol{\tau}' \tag{3.8}$$

where $\vec{U}$ represents the mean velocity vector, ρ is the fluid density, and p is the modified mean pressure (Pope, 2000). $\boldsymbol{\tau}'$ is the deviatoric component of the kinematic stresses where, to close the equations, the eddy-viscosity concept is used to relate turbulent stresses to the mean strain rate tensor, $\mathbf{S}$, in analogy with viscous stresses in a Newtonian fluid:

$$\boldsymbol{\tau}' = 2(\nu + \nu_t)\mathbf{S} \tag{3.9}$$

where ν is the molecular viscosity and ν_t must be modelled. In general, the turbulent viscosity is derived from the transport of two turbulent quantities: the turbulent kinetic energy, k, and its dissipation rate, ε, viz.

$$\nu_t = C_\mu \frac{k^2}{\varepsilon}. \tag{3.10}$$

3.3.2 Turbulence

The most common RANS closures are based on the eddy-viscosity assumption and a two-equation parameterization of turbulent effects. While two-equation closure has proven to be remarkably accurate for many common engineering flows, it has several well-known weaknesses (see Wilcox (1998) for an overview). Combining these models with an actuator disk representation of the rotor only compounds these problems: the eddy-viscosity assumption ties turbulence production to velocity gradients leading to an erroneous increase in k across the actuator surface (Réthoré, 2009).

Some remedies have been proposed. The model of El Kasmi and Masson (2008) aims to treat this problem specifically: the dissipation equation is augmented with a term tied to the local strain rate but is only applied in the immediate vicinity of the rotor (*i.e.* in a cylinder formed by projecting the rotor a distance of $\pm 0.25D$ in the disk-normal direction). In this regard, the RNG model is quite similar in that it also proposes an additional term in the dissipation equation although it is applied over the entire domain.

In light of the work of Réthoré (2009), one might expect any closure based on the eddy viscosity assumption used in conjunction with an actuator disk to be at best approximate. This simple fact provides considerable impetus to further develop stress transport models. However, the popularity and relative economy of two-equation closures continues to make them attractive. A tempting work-around to the eddy-viscosity/actuator disk problem is to simply drop source terms in the $k-\varepsilon$ model in the near-disk region. This sidesteps the original over-production problem and also avoids unphysical increases in dissipation that may be used to compensate. To investigate the possible advantages of such a scheme (referred to here as 'Sumner & Masson'), simulations will be carried out wherein the $k-\varepsilon$ source terms are neglected in the El Kasmi & Masson correction volume.

For all closures, the steady transport equation for turbulent kinetic energy is

$$\nabla \cdot k\vec{U} = \nabla \cdot \left(\frac{\nu_t}{\sigma_k} \nabla k \right) + P_k - \varepsilon \tag{3.11}$$

where the turbulent production rate is given by

$$P_k = 2\nu_t \mathbf{S} : \mathbf{S}. \tag{3.12}$$

The steady transport equation for dissipation rate for the standard model is implemented as

$$\nabla \cdot \varepsilon\vec{U} = \nabla \cdot \left(\frac{\nu_t}{\sigma_\varepsilon} \nabla \varepsilon \right) + \chi_1 \left(C_{\varepsilon 1} P_k \frac{\varepsilon}{k} - C_{\varepsilon 2} \frac{\varepsilon^2}{k} + \chi_2 C_{\varepsilon 4} \frac{P_k^2}{k} \right). \tag{3.13}$$

Here χ_1 and χ_2 are step functions taking values of zero or one depending on the desired model behaviour and region of space. The El Kasmi & Masson model sets χ_2 to unity in a small volume around the rotor; otherwise it is null. The Sumner & Masson proposal is to set $\chi_1 = 0$ in this same region of "non-equilibrium turbulence"; otherwise it is unity. For the standard $k-\varepsilon$ model, $\chi_1 = 1$ and $\chi_2 = 0$ throughout the domain.

The RNG ε equation takes a slightly different form:

$$\nabla \cdot \varepsilon \vec{U} = \nabla \cdot \left(\frac{\nu_t}{\sigma_\varepsilon} \nabla \varepsilon \right) + (C_{\varepsilon 1} - R) P_k \frac{\varepsilon}{k} - C_{\varepsilon 2} \frac{\varepsilon^2}{k} \tag{3.14}$$

with the additional term a function of the strain rate tensor

$$\eta = \sqrt{2\mathbf{S} : \mathbf{S}} \frac{k}{\varepsilon}, \tag{3.15}$$

$$R = \frac{\eta \left(1 - \eta/\eta_0\right)}{1 + \beta \eta^3}. \tag{3.16}$$

C_μ, $C_{\varepsilon 1}$, $C_{\varepsilon 2}$, $C_{\varepsilon 4}$, σ_ε, σ_k, η_0 and β are closure coefficients; standard values are used for all models.

3.3.3 Computational domain and grid generation

Although the wind tunnel geometry is square, the simulations assume axisymmetric conditions. Thus, a wedge-shaped domain is dimensioned and discretized based on the recommendations of Leclerc (1998). The disk is uniformly divided into 36 cells while geometric expansion is used to decrease the cell density away from the disk. The grid is smooth and at no point does the cell aspect ratio exceed 25. A schematic is illustrated in figure 3.4.

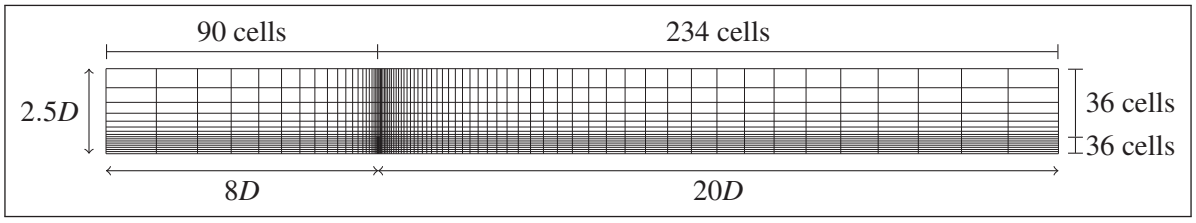

Figure 3.4 Schematic representation of computational grid

3.3.4 Boundary conditions

At the inflow boundary, uniform distributions of velocity, turbulent kinetic energy and its dissipation rate are specified. To ensure Re_t similarity, the dissipation rate is set as follows:

$$\varepsilon_0 = C_\mu k_0^2 \frac{Re_t}{DU_0} \tag{3.17}$$

where $k_0 = \overline{k}$, the spatial average value of turbulent kinetic energy measured near the disk location without the disk present, and U_0 is the inflow wind speed (which corresponds roughly to the calculated U_∞). D is the equivalent full-scale rotor diameter. Re_t is determined from wind tunnel conditions using equation (3.3) where D is the diameter of the porous disk and the turbulent eddy viscosity is estimated from

$$\nu_t = C_\mu \frac{\overline{k}^2}{\overline{\varepsilon}}. \tag{3.18}$$

The *in situ* dissipation rate is assumed to be related to the maximize size of the opening in the grid used to generate turbulence via (Wilcox, 1998)

$$\overline{\varepsilon} = C_\mu \frac{\overline{k}^{3/2}}{0.07L}. \tag{3.19}$$

The turbulence properties are maintained from the inlet to the location where $\overline{k}$ has been measured (at or just upstream of the disk position) by means of additional source terms in the turbulence transport equations (Leclerc, 1998)

$$S_k^{axi} = \varepsilon_0, \tag{3.20}$$

$$S_\varepsilon^{axi} = C_{\varepsilon 2} \frac{\varepsilon_0^2}{k_0}. \tag{3.21}$$

Turbulence freely dissipates downstream of this position.

The radial boundary is treated with a full-slip condition. The outflow assumes fully developed flow while the outlet pressure is fixed to zero.

The actuator disk is treated as a discrete pressure jump across a set of cell faces. Two separate implementations have been tested: one based on a constant thrust coefficient and the freestream velocity,

$$\Delta p(r,\theta) = \frac{1}{2}\rho U_{\infty}^{2} C_T \tag{3.22}$$

and the other on a constant drag coefficient and the local velocities at the disk,

$$\Delta p(r,\theta) = \frac{1}{2}\rho U(r,\theta)^{2} C_D. \tag{3.23}$$

The model predictions are nearly identical and the constant thrust coefficient representation has been retained for the following simulations.

3.3.5 Computational considerations

All simulations are carried out using OpenFOAM 1.6.x (OpenCFD, 2009b). The RANS and turbulent transport equations are discretized using the QUICK scheme (Leonard, 1979) for convection terms. To ensure boundedness, the interpolated face value of the convected quantity is limited between upwind and downwind values. Other terms are discretized with standard central differencing. The SIMPLE (Patankar, 1980) algorithm is used to handle pressure-velocity coupling and the systems of linear equations are solved with a geometric-algebraic multigrid algorithm. The inflow is used to define the initial conditions and iterations are carried out until the normalized equation residuals have decreased several orders of magnitude and stabilize.

3.4 Results

3.4.1 Velocity defect

Figures 3.5 and 3.6 compare the predicted radial distributions of the normalized axial velocity at several downstream positions with wind tunnel measurements for the low- and high- solidity disks, respectively. In both cases, the calculated velocity defect along the symmetry axis is in excellent agreement with measurements. Furthermore, and particularly for the higher solidity

disk, the relatively small effect of tunnel blockage can be discerned from the fact that the normalized velocity outside the wake is consistently greater than unity. Again, the agreement here between simulations and observations is quite good.

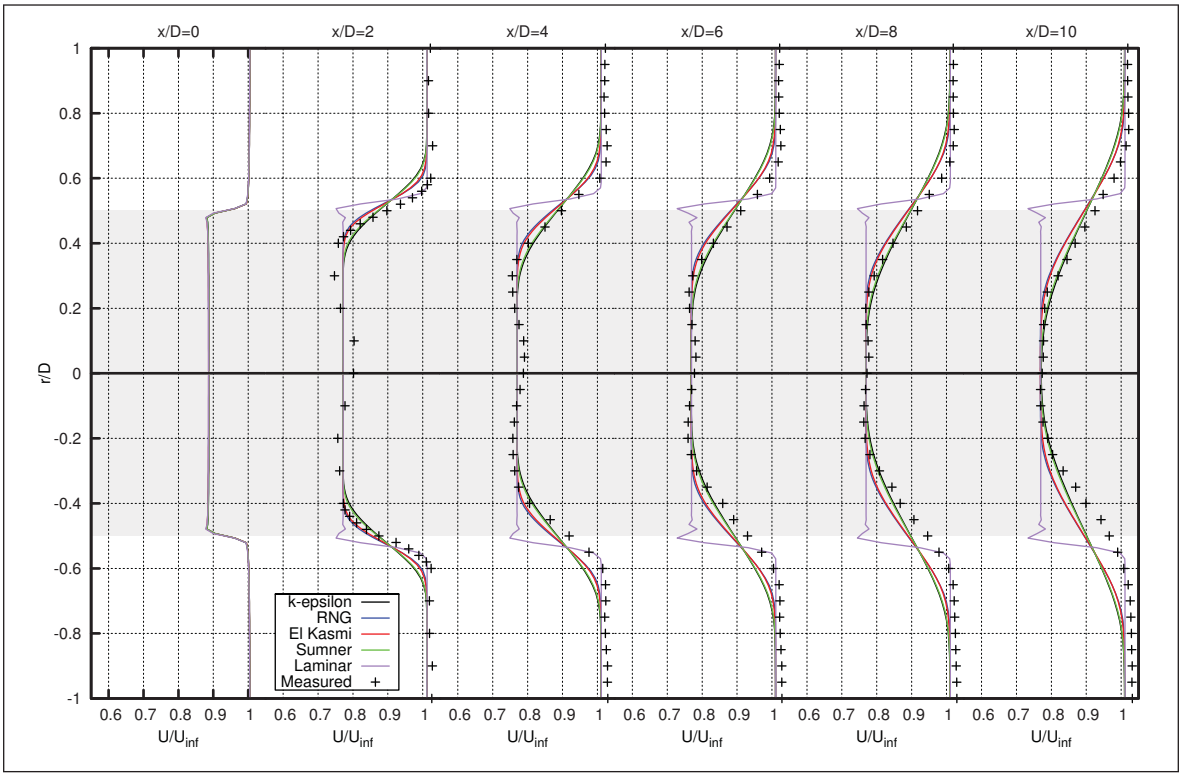

Figure 3.5 Comparison of predicted and measured velocity defect downstream of a porous disk with thrust coefficient of $C_T = 0.43$ at 3% turbulence intensity

The largest differences are found in the shear layer at the disk edge. In general, it appears that the ε–correcting models perform slightly better in the very near wake while standard $k-\varepsilon$ (with or without the source-term correction at the rotor) performs marginally better within the rotor shadow in the far wake.

Figures 3.7 and 3.8 compare predicted wake velocity distributions with measurements for an ambient streamwise turbulence intensity of 12%. In this case, there is remarkably little difference between the various closure schemes. Again, the predicted centreline velocity defect coincides very closely with the wind tunnel observations. Considering the radial velocity distribution, some asymmetry in the measurements is noted with simulations mimicking the ob-

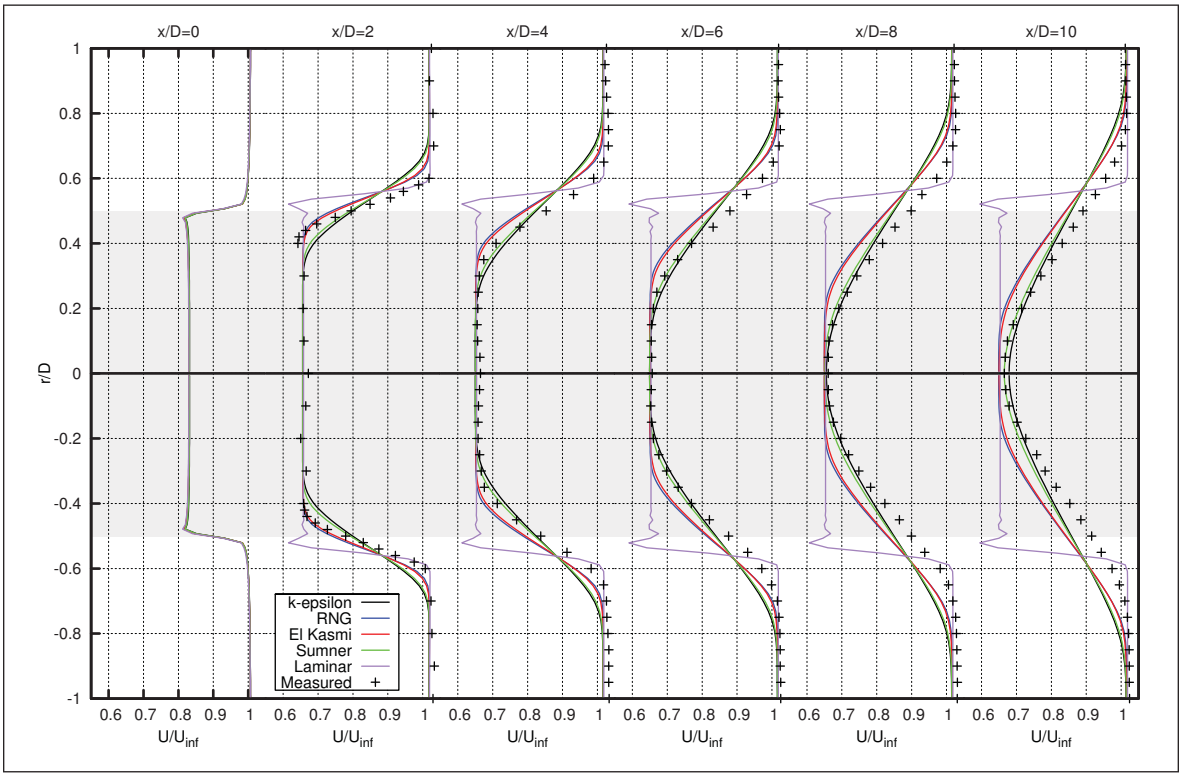

Figure 3.6 Comparison of predicted and measured velocity defect downstream of a porous disk with thrust coefficient of $C_T = 0.61$ at 3% turbulence intensity

servations very closely only for the 'upper' half. With respect to the low turbulence case, increased diffusion leads to a much less distinct wake region and smoother velocity profiles. The ability of the models to capture wake recovery is demonstrated by the excellent agreement at $10D$.

3.4.2 Turbulent kinetic energy

Figure 3.9 presents the turbulent kinetic energy in the wake (normalized by U_∞^2) of the two disks at low turbulence intensity. Only the half wake has been shown for brevity. The numerical results are largely in agreement with observations. It can be seen, however, that while the simulations predict the maximum for turbulent kinetic energy to be located at, or very near, the disk edge, the measurements suggest that it migrates towards the wake centre with downstream distance.

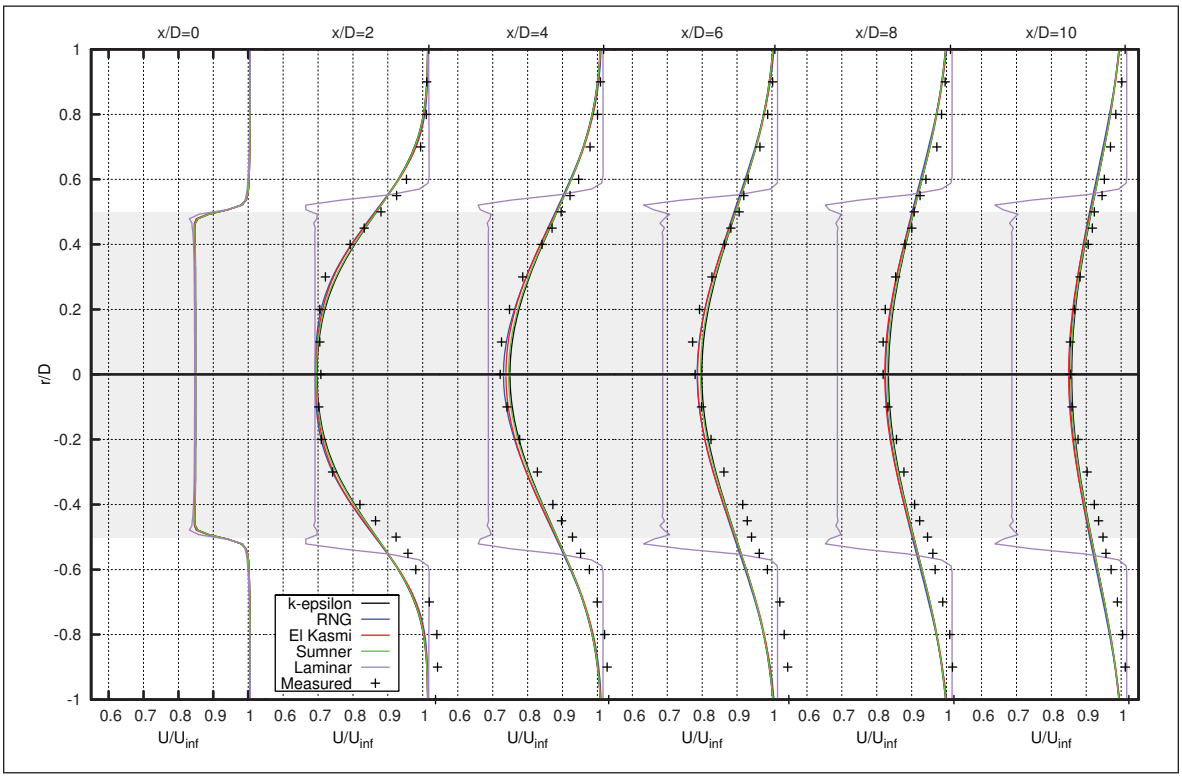

Figure 3.7 Comparison of predicted and measured velocity defect downstream of a porous disk with thrust coefficient of $C_T = 0.56$ at 12% turbulence intensity

The results for the higher turbulence level are quite similar (see figure 3.10). As might be expected, neglecting the source terms in the turbulence transport equations in the volume immediately surrounding the rotor serves to decrease k somewhat in this region. However, this does not appear to have an important effect downstream.

3.5 Discussion

Overall, predictions are in very good agreement with measurements and all models perform exceedingly well. This is, however, entirely unexpected and appears to contradict the works of several other authors who have applied these closures to the analysis of wind turbine wakes. A case in point is the work of El Kasmi and Masson (2008) where the standard $k-\varepsilon$ model has been applied to study the MOD-0A, Nibe B and Danwin turbines and has been shown to greatly overpredict wake recovery. They further demonstrate that their proposed correction yields significant improvement for single-wake simulations.

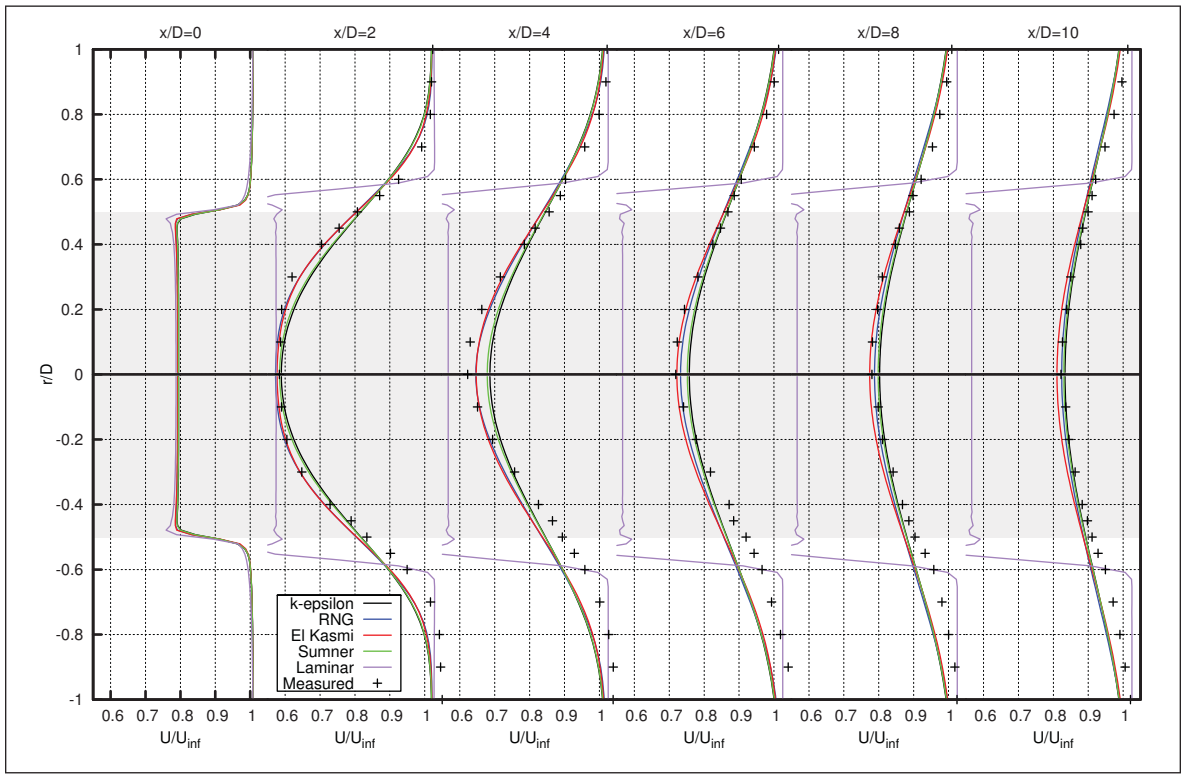

Figure 3.8 Comparison of predicted and measured velocity defect downstream of a porous disk with thrust coefficient of $C_T = 0.73$ at 12% turbulence intensity

This gives rise to two questions. First, why are the solutions so nearly independent of closure, even for the highly turbulent case? Second, why is the performance of the $k-\varepsilon$ model so much improved?

3.5.1 The ε equation

Logic dictates that if the predictions of all models are essentially identical, the models themselves must be as well. This is indeed the case, at both low and high turbulence intensity, although for unique reasons. To illustrate, figure 3.11 presents the distribution of terms in the ε equation (normalized by the local dissipation rate, $C_{\varepsilon 2}\varepsilon^2/k$), downstream of the disk at 95% radius for the low-turbulence, low-C_T case. In the very near wake, the terms indeed vary between closures which explains the differences in wake turbulence predictions. However, at roughly $2D$, it can be seen that the normalized production for all models is near unity which indicates that the source terms in fact cancel: the models are essentially identical and the (turbulence)

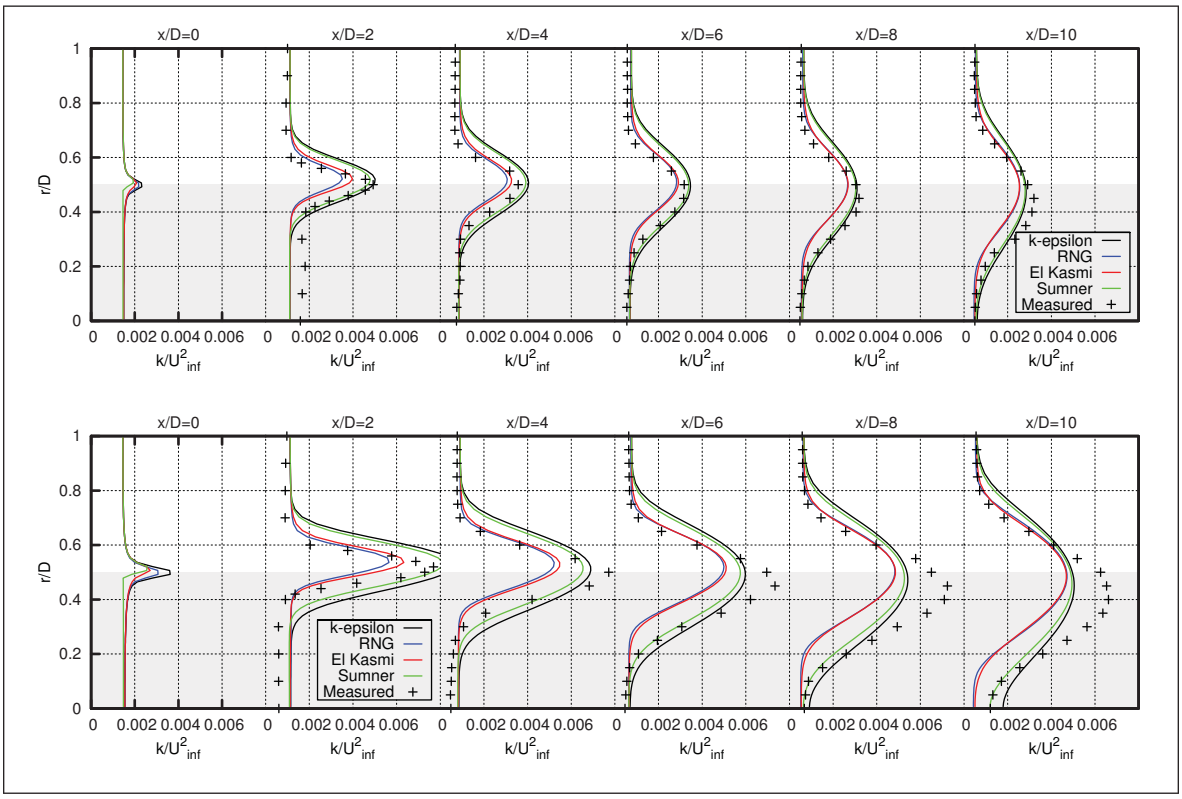

Figure 3.9 Comparison of predicted and measured turbulent kinetic energy (half wake only) downstream of a porous disk with thrust coefficient of $C_T = 0.43$ (top) and $C_T = 0.61$ (bottom) at 3% turbulence intensity

problem is reduced to one of convection-diffusion type. The similarity of solutions for velocity defect is further assured by the fact that the influence of eddy viscosity in the momentum equations is relatively small given the low level of turbulence.

Figure 3.12 presents the same analysis but for the high-turbulence, high-C_T case. Of greatest interest here is the production term for $x/D > 1$. This term is what distinguishes the models and it is interesting to note that in the region of highest shear (near the disk edge) the dissipation term is larger than the production term: the problem is reduced to one of turbulence decay. This can be seen in the measurements: the wake turbulence level drops off rapidly as production is insufficient to increase, or even maintain, k. As the production term assumes less importance, the differences between the models is also diminished.

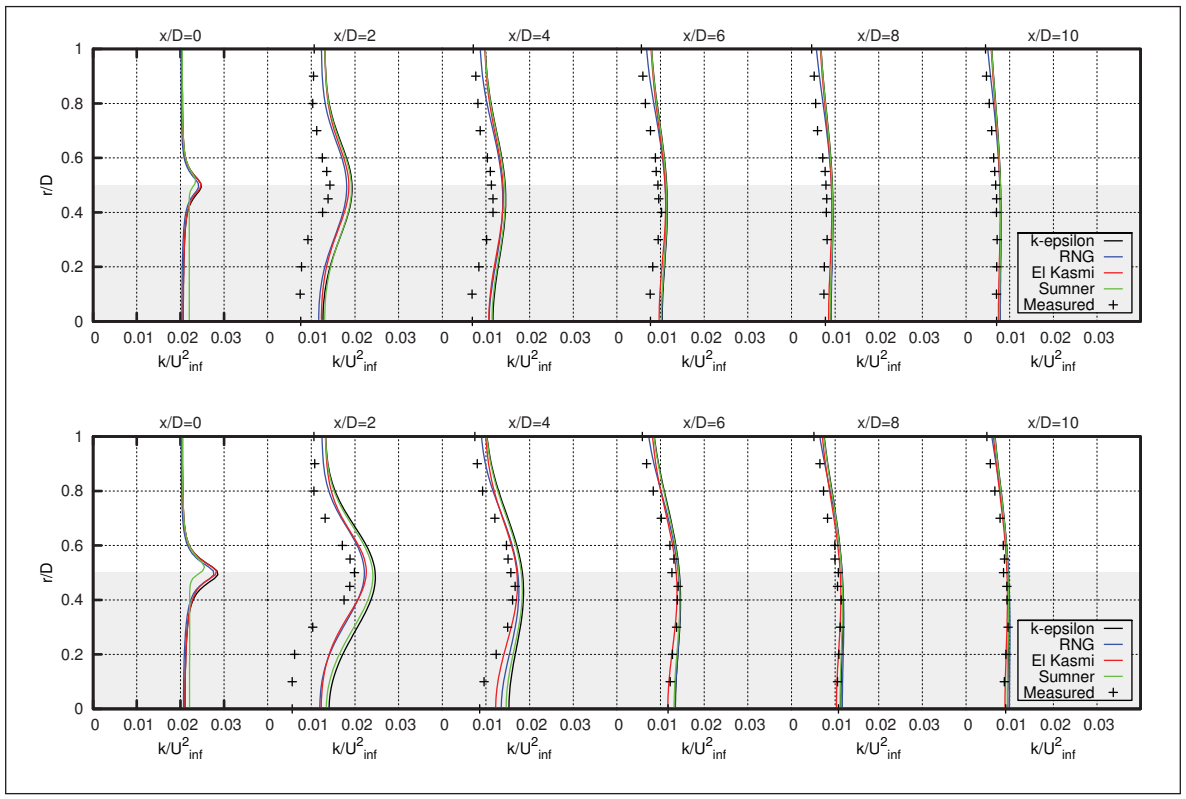

Figure 3.10 Comparison of predicted and measured turbulent kinetic energy (half wake only) downstream of a porous disk with thrust coefficient of $C_T = 0.56$ (top) and $C_T = 0.73$ (bottom) at 12% turbulence intensity

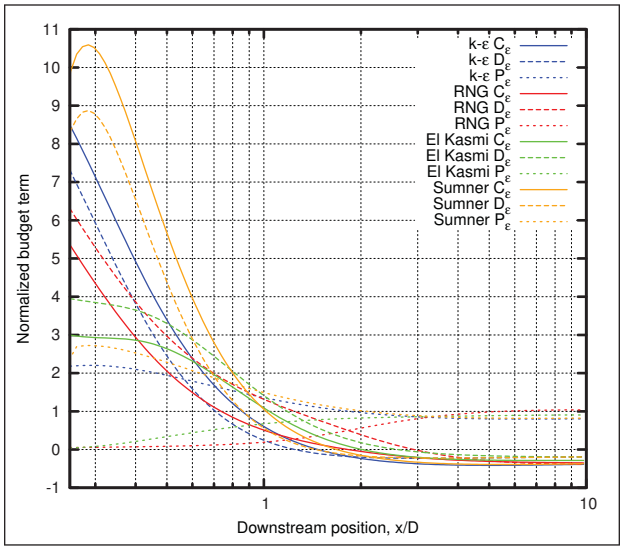

Figure 3.11 Normalized convection (C), diffusion (D) and production (P) terms of the ε transport equation downstream of the disk at 95% radius ($C_T = 0.43$, $I_U = 3\%$)

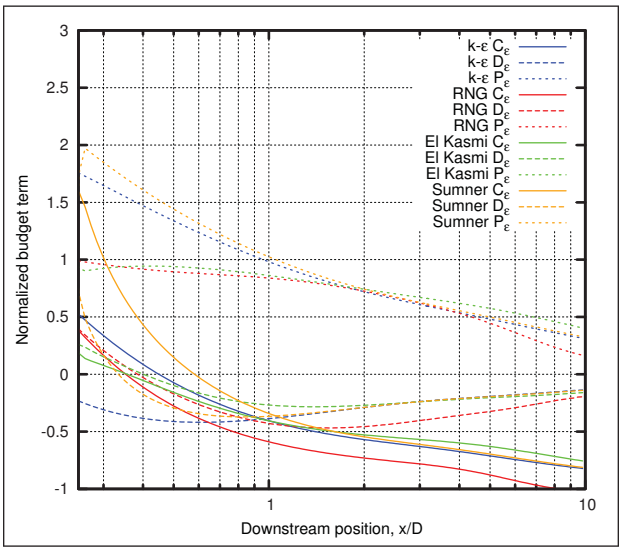

Figure 3.12 Normalized convection (C), diffusion (D) and production (P) terms of the ε transport equation downstream of the disk at 95% radius ($C_T = 0.73$, $I_U = 12\%$)

3.5.2 Similitude

The preceding analysis clarifies why all models yield similar predictions and also hints at why the predictions are so accurate: dependence on the modelling of turbulence production – the greatest source of uncertainty – is minimal. But these results are still at odds with past studies carried out at similar velocity and turbulence intensity levels. Plotting the ambient conditions in a non-dimensional space defined by turbulence intensity and turbulent Reynolds number serves to provide context. As shown in figure 3.13, the conditions from the cited case studies, where the $k-\varepsilon$ model has been shown to perform poorly, all fall within a fairly narrow range of Re_t. This stems from the fact that turbulence intensity in the atmosphere increases rapidly as Re_t decreases. Considering a neutral atmosphere (with $C_\mu = 0.033$ and the von Karman constant taken as 0.4), it can be shown that

$$I_{atm} = \frac{4.79D}{Re_t H}. \tag{3.24}$$

For the range of I_{atm} and D/H generally observed, Re_t varies from just 40 to 60, as indicated by the shaded region.

The wind tunnel conditions numerically reproduced here are well outside this envelope. Moreover, moving towards higher Re_t or lower I has the effect of decreasing the importance of turbulence modelling. These observations suggest that in addition to maintaining the aforementioned dimensionless parameters, another parameter representing the turbulence dissipation should be considered in the design of wind tunnel experiments for the study of wind turbine wake flow. Considering the adimensional form of the RANS equations wherein the eddy-viscosity assumption has been used to model the Reynolds stresses, Re_t is particularly relevant.

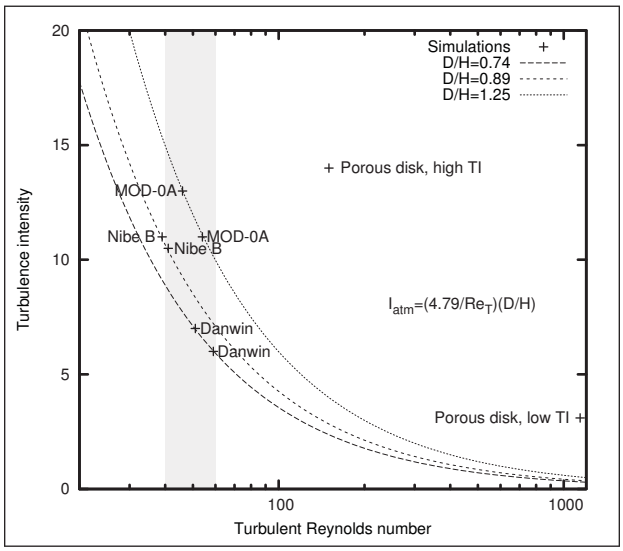

Figure 3.13 Comparison of ambient turbulent flow conditions for various wake studies

3.6 Closing remarks

Turbulent flow through an actuator disk has been simulated and compared with wind tunnel measurements of flow through a porous disk in an effort to evaluate the ability of various two-equation RANS closures to simulate the wake of a wind turbine.

Regarding the numerical representation of wind tunnel conditions, the assumption of axisymmetric conditions for the simulations appears quite reasonable. Furthermore, the quality of agreement with measurements both inside and outside the wake validates the methods by which the thrust coefficient, freestream wind speed and turbulence dissipation have been estimated.

Although some discrepancy between modelled and measured conditions is noted, the distributions of velocity and turbulent kinetic energy in the wake are generally very well predicted. While asymmetry in the measurements explains some of the observed differences, the results at $2D$ suggest that the numerical approach may be too diffusive. This, however, does not appear to adversely affect far-wake predictions.

Significantly, the results are nearly independent of the turbulence closure as the turbulence production term seems to play a relatively minor role. Although the wind tunnel observations have been demonstrated to be Reynolds number independent, they are not necessary representative of full-scale atmospheric conditions despite the fact that the turbulence intensity level is maintained. Specifically, dissipation seems too high. To improve similarity between full-scale and wind-tunnel experiments, at least for the purposes of turbulence model validation, it is suggested to maintain non-dimensional parameters quantifying both turbulent kinetic energy and its dissipation rate. Turbulence intensity and the turbulent Reynolds number are good candidates.

To address the need for representative conditions and to provide a more challenging test of these closures, the present analysis is currently being repeated based on wake measurements behind a single and multiple porous disks in a modelled atmospheric boundary layer.

CONCLUSION

The objective of this research has been to tackle some fundamental issues related to RANS/$k-\varepsilon$ modelling of flows for wind energy assessment purposes. To that end, modest, but conceptually significant, contributions have been made towards the simulation of the atmospheric surface layer. Notably, it has been demonstrated that lingering anomalies in the near-wall distributions of flow properties for such simulations are directly related to linearity assumptions in the finite-volume discretization of the governing equations. Furthermore, an extended wall treatment wherein corrected discretization schemes are applied only in the first two near-wall cells has been shown to limit the error in turbulent kinetic energy (the most difficult case) to less than one percent for the range of conditions likely to arise in a typical wind energy (or wind engineering) simulation.

With respect to physical modelling of the neutral and stable surface layer, a general transport equation for the turbulence dissipation rate and a consistent set of boundary conditions have been derived which, taken together, will exactly reproduce profiles of velocity, potential temperature, and turbulence properties corresponding to a desired mixing length expression. If the typical form based on the harmonic mean between the Prandtl mixing length and some established maximum is selected, a single exact formulation of the $k-\varepsilon$ model results equally applicable to neutral and stable conditions. As a consequence of this last incarnation of the ε equation, a new expression for the historically enigmatic $C_{\varepsilon 3}$ closure coefficient has been derived which is unique, but largely in agreement, with other recently proposed stability-dependent expressions.

Additionally, these two contributions are likely to find useful application in the simulation of both atmospheric boundary-layer flows, where Coriolis effects and pressure gradients are important parameters, and flows over complex terrain. The proposed wall treatment can be generalized in terms of a local wall-normal co-ordinate to permit greater first-cell heights while minimizing the introduction of discretization errors. The proposed ε transport equation is, of course, applicable to arbitrarily complex flows. Any improvements that these proposals may bring to such cases remain to be quantified.

As regards the modelling of wind turbine wakes, a new closure has been proposed wherein the source terms in the turbulence transport equations are dropped in a discrete volume around the actuator disk to avoid the rapid increase in eddy viscosity otherwise observed in this region. Subsequently, the predictions of several two-equation closures for the mean flow properties in the far wake of a porous disk have been compared with detailed wind tunnel measurements. In general, all models are found to perform exceedingly well with the distributions of velocity and turbulent kinetic energy nearly coinciding with observations. The surprising accuracy and apparent independence of the results with respect to the closure appears to be due to the relative insignificance of turbulence production in these experiments. To improve similarity with full-scale conditions, it is suggested that wind tunnel conditions mimic not only the observed turbulence intensity but the turbulent Reynolds number as well.

With an eye to the ultimate goals of improving wind resource assessment and reducing uncertainty in energy yield calculations, two additional case studies have been carried out and are included as annexes. In the first study, wind speed and turbulent kinetic energy predictions of several two-equation turbulence closures for neutrally stratified flow over a small isolated island are compared with measurements. As these simulations have been completed "blindly", *i.e.* based solely on a specified inflow and topographic information, the error analysis is especially pertinent and yields an unbiased measure of accuracy. It is found that, outside of the wake region, RANS modelling generally provides good estimates of wind speed-up factors but fails to attain the same level of accuracy for turbulence predictions. In the second study, the flow through a medium-sized wind farm situated on a plateau has been simulated using both the $k-\varepsilon$ and RNG turbulence models. In light of some of the limitations of two-equation closures, simulations have also been carried out using a stress transport model to investigate possible advantages of a higher-order scheme. In addition, two actuator disk implementations have been considered, their primary difference being the method by which the rotor thrust is determined. While power predictions tend to lie within one standard deviation of observations it is interesting to note that no single combination of actuator disk model and turbulence closure is found to be significantly more accurate than the rest. Although the stress transport model appears to

have some advantage over its two-equation counterparts, the additional computational cost is quite high.

To close, while tangible improvements in the RANS modelling of wind-energy-related flows have been demonstrated in this dissertation – particularly with respect to atmospheric flows – it must be acknowledged that this work barely scratches the surface in the larger context. To reach the greater objectives of improved wind resource assessment and turbine micro-siting, a litany of issues remain to be addressed from the accurate extrapolation of turbulence intensity, to the quantification of limitations on the RANS framework itself. Nonetheless, it is hoped that by considering such fundamental cases as those presented here, this work will serve to solidify the foundation upon which future developments might be based.

ANNEX I

RANS SIMULATIONS OF BOLUND

Jonathon Sumner[1], Bibiana Garcia[2], Mathias Cehlin[3,4], Andreas Bechmann[5], John M. Prospathopoulos[6], Christian Masson[1], Daniel Cabezón[2], Javier Sanz Rodrigo[2], Ylva Odemark[3,7], Niels N. Sørensen[5], Evangelos S. Politis[6], P. K. Chaviaropoulos[6]

[1]Département de Génie Mécanique, École de Technologie Supérieure, Montreal, Canada

[2]Centro nacional de energías renovables (CENER), Wind Energy Department, Spain

[3]Vattenfall Research & Development, Älvkarleby, Sweden

[4]University of Gävle, Faculty of Engineering and Sustainable Development, Gävle, Sweden

[5]Risø DTU, National Laboratory for Sustainable Energy, Roskilde, Denmark

[6]Centre for Renewable Energy Sources and Saving (CRES), Wind Energy Department, Pikermi, Greece

[7]Royal Institute of Technology, Stockholm, Sweden

Article submitted October 2011 for publication in *Wind Energy*. It is presently undergoing first revision.

Foreword

Although the studies considered within the body of the dissertation focus on simple geometries, the goal has been nonetheless to contribute to the development of modelling techniques applicable to the most difficult wind resource and wind energy assessments: those for which empirical and simplified approaches typically struggle. In this annex and the next, attempts are made to advance RANS modelling of such cases in a more direct way.

The following article is a collaborative effort between several participants of the Bolund blind comparison; an exercise that involved simulating neutrally stratified flow over a small coastal island (Bechmann *et al.*, 2011). Here, the predictions of five distinct RANS implementations are summarized and a comparison with measurements reveals some of the strengths and weaknesses of RANS/two-equation modelling of atmospheric flows over variable terrain.

Abstract

In the Bolund blind comparison of flow models organized by Risø DTU, modelers were invited to predict the wind speed and turbulent kinetic energy over a low coastal island of moderate complexity given only the topographic description of the site and upstream conditions. A detailed overview of five RANS-based models which participated in this exercise, as well as their respective predictions for four wind directions, are given herein. Comparisons with available measurements suggest that models based on RANS/two-equation closure can provide reasonably good estimates of the speed-up factor, especially outside the wake region. Despite some differences in model formulation, the agreement between models is impressive and the differences in overall mean error for speed-up factor at 5 m agl (neglecting the wake) is quite small. The results for predicted turbulence are somewhat less encouraging; the model results are less consistent and the error with respect to measurements generally greater. By far, the best resolved case corresponds to an easterly wind where the slope on the windward side of the hill is less steep. For this case, the average error in speed-up factor is less than 3% for all models. While this result is encouraging, further research is clearly needed to improve agreement with measurements and meet the long-term objectives set by the European Wind Energy Technology Platform of 3% uncertainty in predicted lifetime energy production and turbine loading.

1 Introduction

Wind energy is one of the fastest growing energy sectors worldwide, consistently producing annual double-digit increases in installed capacity (Pullen and Sawyer, eds., 2010). However, although the resource itself is inexhaustable, the infrastructure requirements for a wind energy project are non-negligible; that is to say, large-scale wind farms require a considerable amount of space and past developments have occupied most ‘ideal’ sites. The continued high demand for energy from renewable sources (of which on-shore wind energy is, at least currently, the most economically competitive (IEA, 2010b)) coupled with the scarcity of relatively flat, windy, terrestrial sites has naturally led to a surge in developments both offshore and in complex terrain.

Each setting presents unique challenges for wind park modelling and resource assessment. In the case of offshore wind farms, accurate determination of wake effects is likely the most important modelling task and considerable efforts are being made to develop advanced wind farm wake models (see *e.g.* Crespo *et al.* (1999); Vermeer *et al.* (2003); Sanderse *et al.* (2011); Barthelmie *et al.* (2011)). For wind farms located in complex terrain, prediction of topographic effects is probably more important than wake effects (although these too can have an important impact on the production), especially where flow separation may be present, which is famously difficult to properly resolve.

Despite the challenges, the ability to accurately evaluate mean turbulent flow properties (*i.e.* mean wind speed, turbulence intensity, and inclination) is essential to the success of wind power projects. As such, decreasing modelling uncertainties has been formally recognized as an important research goal and is explicitly included as part of the European Wind Energy Technology Platform objectives (TPWind, 2008). Among other things, this manifesto sets the ambitious long-term objective of obtaining 3% uncertainty in lifetime energy production and external loading predictions, regardless of site conditions. Certainly, this level of uncertainty is only attainable with advanced modelling approaches, be they physical (*e.g.* wind tunnel, water flume, *etc.*) or high-order numerical ones (*e.g.* RANS, DES, LES, *etc.*).

The most popular dataset available for the purposes of validating numerical wind flow models in complex terrain is based on the Askervein experiment, which was carried out in 1982–83 (Taylor and Teunissen, 1987; Mickle *et al.*, 1988). Although several similar measurement campaigns were performed around this time (*e.g.* Bradley (1980); Jenkins *et al.* (1981); Mason and King (1985); Salmon *et al.* (1988); Emeis *et al.* (1993)), the Askervein case remains something of a benchmark and has been extensively used by the wind energy and meteorological community for the purposes of validating both RANS and LES models (Raithby *et al.*, 1987; Kim and Patel, 2000; Castro *et al.*, 2003; Eidsvik, 2005; Undheim *et al.*, 2006; Prospathopoulos and Voutsinas, 2006; Silva Lopes *et al.*, 2007; Laporte, 2008; Chow and Street, 2009; Bechmann and Sørensen, 2010). State-of-the-art for its time, the Askervein experiment has certainly advanced flow modelling over the last few decades. However, measurement techniques have

since greatly improved (with, for example, the advent of high-frequency sonic anemometers) as has as the need for more detailed validation datasets.

With this in mind, the Bolund experiment was undertaken by Risø DTU in 2007–08 where the flow over a low coastal island was extensively measured. For the purposes of model validation, the Bolund experiment has many advantages: neutral atmospheric stability, negligible Coriolis effects, a fully developed inflow, and it was heavily instrumented. The blind comparison of flow models based on this dataset (Bechmann *et al.*, 2011) has provided an estimate of the current uncertainty for a range of flow modelling techniques.

The aim of the present work is to demonstrate the state-of-the-art in RANS/two-equation closure for the purposes of wind energy resource assessment over (moderately) complex terrain. Herein, five RANS-based models that participated in the blind comparison and performed well are presented along with their respective predictions[1]. All models are based on a RANS formulation with two-equation turbulence closure. In principle, the boundary conditions are all quite similar, but in practice implementations vary between softwares. Domain extents, grid generation techniques and numerics are all unique.

The following section provides a very brief overview of the Bolund experiment and blind comparison. An outline of the RANS approach and its closure, followed by a detailed look at each of the five models (from ÉTS, CENER, Vattenfall, Risø DTU and CRES) is given in section 3. Calculated horizontal and vertical distributions of speed-up factor and added turbulence are presented in section 5 for four wind directions and compared with measurements. Although it is difficult to directly compare the various models due to differences in domain size and discretization, some general conclusions are offered in section 5.

[1] Some of the results have been revised with respect to the original submissions to reflect software improvements and to ensure full second-order accuracy and iterative convergence.

2 The Bolund blind comparison

The Bolund experiment measured the flow over a 12-m high coastal island during a 3-month period from 2007 to 2008. Ten masts were distributed over two axes corresponding to wind directions of 270 (or 90) and 239 degrees; most measurements are taken with sonic anemometers (for full details regarding the experiment set-up see Berg *et al.* (2011)). The dataset has been filtered for neutral stability and, given the low heights, Coriolis effects are negligible. Furthermore, the approach flow is well developed as uniform conditions are present for a significant upstream distance (for westerly winds).

The Bolund blind comparison was based on the dataset resulting from the Bolund experiment. In this exercise, flow modelers were invited to provide predictions of wind velocity and turbulence properties at 600 discrete points for four wind directions (corresponding to 270, 255, 239 and 90 degrees) based solely on the topographic description of the site and upstream observations (for full details regarding the blind comparison see Bechmann *et al.* (2011)). Risø DTU suggested inflow conditions derived by fitting reference measurements to surface layer similarity theory:

$$s(z) = \frac{u_{\star 0}}{\kappa} \ln\left(\frac{z - z_g}{z_0}\right), \tag{A I-1}$$

$$k(z) = 5.8 u_{\star 0}^2 \tag{A I-2}$$

where s is the mean wind speed, k is the turbulent kinetic energy and the von Karman constant, κ, is taken as 0.40. The ground height, z_g, is assumed to be 0.75 m. The reference friction velocity, $u_{\star 0}$, and roughness length, z_0, depend on the wind direction (see table I-1). Models based on $k-\varepsilon$ closure could then specify the dissipation rate using

$$\varepsilon(z) = \frac{u_{\star 0}^3}{\kappa(z - z_g)} \tag{A I-3}$$

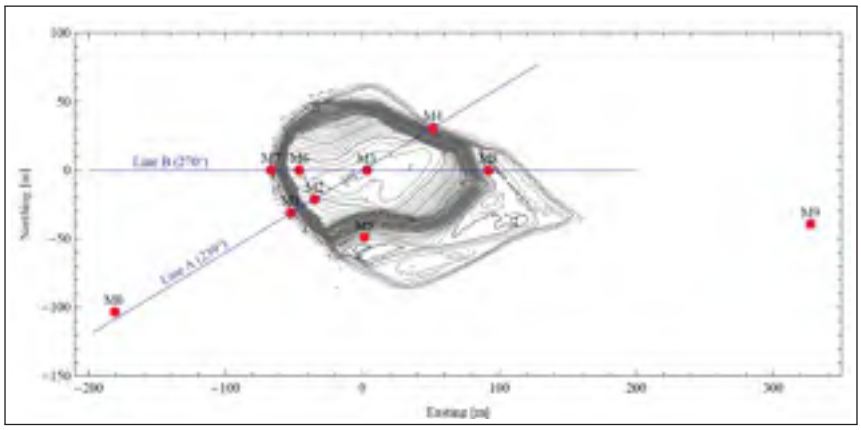

Figure-A I-1 Overview of Bolund and tower installations

Table-A I-1 Reference flow properties for different flow directions

Case	Direction [deg]	z_0 [m]	$u_{\star 0}$ [m/s]
1	270	0.0003	0.40
2	255	0.0003	0.40
3	239	0.0003	0.40
4	90	0.015	0.50

whereas for $k-\omega$ closure the analytical turbulent length scale is based on

$$\omega(z) = 5.8\frac{u_{\star 0}}{(z-z_g)}. \qquad \text{(A I-4)}$$

Modelers were at liberty to define the other boundary conditions. For the simulations presented herein, the equilibrium inflow profiles are also used to define conditions at the upper boundary. Generally, all models assume a fully developed condition (*i.e.* zero gradient in flow properties normal to the boundary) at the outlet. For non-polar (*i.e.* Cartesian) domains, the lateral boundaries are either treated using symmetry (ÉTS) or zero-gradient (CRES) conditions.

3 Mathematical models

All models are based on a finite-volume solution of the Reynolds-Averaged Navier-Stokes (RANS) equations with two-equation turbulence closure. Conservation of mass and momen-

tum can be expressed in differential form as

$$\nabla \cdot \vec{U} = 0, \tag{A I-5}$$

$$\frac{\partial \vec{U}}{\partial t} + \nabla \cdot \vec{U}\vec{U} = -\frac{1}{\rho}\nabla p + \nabla \cdot \boldsymbol{\tau}' + \vec{f} \tag{A I-6}$$

where $\vec{U}$ represents the mean velocity vector ($s = \|\vec{U}\|$), p is the mean pressure and ρ is the fluid density (Pope, 2000). $\vec{f}$ represents a body force (*e.g.* Coriolis, buoyancy, *etc.*) which are neglected here. $\boldsymbol{\tau}'$ is the kinematic Reynolds stress tensor; it appears as part of the averaging process and represents the effect of turbulent transport of momentum, which is generally assumed to dominate viscous terms.

To close the equations, the eddy-viscosity concept is used to relate turbulent shearing stresses, $\boldsymbol{\tau}'$, to the mean strain rate, $\mathbf{S}$:

$$\boldsymbol{\tau}' = 2\nu_t \mathbf{S} \tag{A I-7}$$

where ν_t must be modeled. In general, the turbulent viscosity is derived from the transport of two turbulent quantities: the turbulent kinetic energy and some length-scale governing equation (here either the dissipation rate, ε, or the specific dissipation, ω). The turbulence transport is modeled with either (Jones and Launder, 1972; Wilcox, 1998)

$$\frac{dk}{dt} + \nabla \cdot k\vec{U} = \nabla \cdot \left(\frac{\nu_t}{\sigma_k}\nabla k\right) + P_k - \varepsilon \tag{A I-8}$$

$$\frac{dk}{dt} + \nabla \cdot k\vec{U} = \nabla \cdot (\sigma_\star \nu_t \nabla k) + P_k - \beta_\star k\omega \tag{A I-9}$$

and one of the following

$$\frac{d\varepsilon}{dt} + \nabla \cdot \varepsilon\vec{U} = \nabla \cdot \left(\frac{\nu_t}{\sigma_\varepsilon}\nabla \varepsilon\right) + C_{\varepsilon 1} P_k \frac{\varepsilon}{k} - C_{\varepsilon 2}\frac{\varepsilon^2}{k} \tag{A I-10}$$

$$\frac{d\omega}{dt} + \nabla \cdot \omega\vec{U} = \nabla \cdot (\sigma \nu_t \nabla \omega) + \alpha P_k \frac{\omega}{k} - \beta\omega^2 \tag{A I-11}$$

Table-A I-2 Turbulence model closure coefficients

	A ÉTS OpenFOAM RNG $k-\varepsilon$	B CENER Fluent $k-\varepsilon$	C Vattenfall OpenFOAM $k-\varepsilon$	D Risø DTU EllipSys3D $k-\varepsilon$	E CRES In-house $k-\omega$
κ	0.40	0.4187	0.4187	0.40	0.40
C_μ or $\beta_\star$	0.0297	0.0297	0.033	0.03	0.033
$C_{\varepsilon 1}$	0.403	1.138	1.21	1.21	-
$C_{\varepsilon 2}$	1.68	1.92	1.92	1.92	-
σ_k	1.00	1.00	1.00	1.00	-
σ_ε	1.30	1.30	1.30	1.30	-
η_0	4.38	-	-	-	-
β	0.012	-	-	-	0.0275
α	-	-	-	-	0.3706
σ	-	-	-	-	0.5
$\sigma_\star$	-	-	-	-	0.5

where the turbulence production rate is calculated using

$$P_k = 2\nu_t \mathbf{S} : \mathbf{S} \tag{A I-12}$$

and the turbulent viscosity is modeled with

$$\nu_t = C_\mu \frac{k^2}{\varepsilon} = \frac{k}{\omega}. \tag{A I-13}$$

A summary of model coefficients is provided in table I-2.

The numerical and spatial discretization of these equations is unique to each model, as is the treatment of the rough wall. The salient features of the five models are thus summarized below.

3.1 Model A: ÉTS surface layer model in OpenFOAM 1.6 (ID0053)

Grid generation

A simple in-house code was prepared to generate the grid by a three-step process. First, the native surfer files describing the orography and surface roughness were coarsened (to dimensions of 0.5 m in the flow direction and 2 m in the cross-flow direction) and rotated to be aligned with

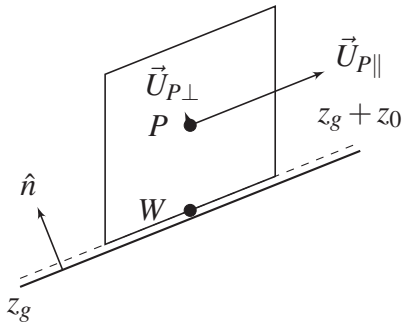

Figure-A I-2 Schematic of near-ground cell

the mean flow direction. Second, the surface grid was horizontally extrapolated to increase the size of the domain. Lastly, the surface grid was projected vertically. This method resulted in excess cells in some areas and some highly skewed cells on the cliff face (see figure I-3a). Despite some non-orthogonality and skewness, the meshes pass OpenFOAM grid quality tests[2]. Mesh properties are summarized in table I-3.

Turbulence modelling

The RNG $k-\varepsilon$ model (Yakhot and Orszag, 1986; Yakhot and Smith, 1992) was used with constants modified for the atmospheric boundary layer (El Kasmi and Masson, 2010).

Wall treatment

Figure I-2 shows an arbitrary cell adjacent to the ground. Here, a kinematic shear stress of $\tau'_w = u_0 u_{\star w}$ was applied based on local conditions:

$$u_0 = C_\mu^{1/4} k^{1/2}, \tag{A I-14}$$

$$u_{\star w} \approx \frac{\kappa U_{P\parallel}}{\ln\left(\dfrac{n_\perp + z_0}{z_0}\right)}, \tag{A I-15}$$

$$n_\perp = (\vec{r}_P - \vec{r}_W) \cdot \hat{n} \tag{A I-16}$$

[2]The standard OpenFOAM utility `checkMesh` was used to evaluate mesh quality.

where $\vec{r}$ is the position vector. The shear stress was imposed by modifying the wall viscosity using

$$\nu_{tw} = \frac{\kappa u_0 n_\perp}{\ln\left(\frac{n_\perp + z_0}{z_0}\right)}. \tag{A I-17}$$

The source terms in the k transport equation are set using:

$$P_k = \frac{u_0 u_{\star w}^2}{2\kappa n_\perp} \ln\left(\frac{2n_\perp + z_0}{z_0}\right), \tag{A I-18}$$

$$\varepsilon = \frac{u_0^2 u_{\star w}}{2\kappa n_\perp} \ln\left(\frac{2n_\perp + z_0}{z_0}\right) \tag{A I-19}$$

while the value of ε at the centre of the wall-adjacent cell is prescribed as

$$\varepsilon_P = \frac{u_0^2 u_{\star w}}{\kappa(n_\perp + z_0)}. \tag{A I-20}$$

Numerics

Convection terms are discretized using second-order linear upwinding while other terms are approximated using central differencing. The SIMPLE method of Patankar (1980) (as implemented in `simpleFoam` (OpenCFD, 2009b)) is used to solve the coupled system of equations. To reduce computing times, the domain is subdivided contiguously for parallel solution. In addition, a geometric-algebraic multigrid solver is used for the pressure equation. The solution is considered converged when further iteration fails to produce decreases in normalized equation residuals.

3.2 Model B: CENER surface layer model in FLUENT 12 (ID0036)

Grid generation

The computational domain consists of a structured cartesian grid with terrain-following coordinates generated through ANSYS ICEM CFD Hexa. A NURBS surface is first created from the

contour lines and then a block topology containing the grid nodes is generated and projected over the surface. For the Bolund simulation, total extents of 1260 m (E-W direction), 1170 m (N-S direction) and 100 m in the vertical direction are considered. Horizontal resolution at the position of the hill is equal to 0.8 m in both directions, decreasing towards the external corners of the grid. The near-wall cell height is 0.30 m. This distribution results in a final domain of approximately 3 million cells.

Turbulence modelling

The standard $k-\varepsilon$ turbulence model was used with coefficients calibrated for surface layer flows (Alinot and Masson, 2005; Sanz Rodrigo *et al.*, 2008).

Wall treatment

The ground is simulated as a wall through the adaptation of the standard wall functions, by establishing a link between the turbulent law-of-the-wall modified for sand-grain roughness and the surface boundary layer log-law based on the roughness length following the method proposed by Blocken *et al.* (2007).

Numerics

A second-order upwind scheme based on a multi-linear reconstruction approach is used for all dependent variables (Barth and Jespersen, 1989).

3.3 Model C: Vattenfall surface layer model in OpenFOAM 1.5 (ID0016)

Grid generation

The domain is discretized using a nine-block structured grid with hexahedral cells, generated with ANSYS ICEM CFD Hexa. The domain shape is cylindrical with a radius of 400 m and a height of 200 m. The fluid domain was rotated for each of the four cases, in order to align the

inner block mesh with the flow direction. The near-wall cell height was 0.30 m, and the total number of cells was approximately 3 million.

Turbulence modelling

The standard $k-\varepsilon$ model was used with constants modified for the atmospheric boundary layer (Panofsky and Dutton, 1984).

Wall treatment

Standard wall functions modified to account for surface roughness were used, as described by Blocken *et al.* (2007) and Cebeci and Bradshaw (1977).

Numerics

The convection terms were discretized using a second order upwind scheme. For pressure and diffusion terms, second-order central differencing was used.

3.4 Model D: Risø EllipSys3D (ID0000)

Grid generation

Since the EllipSys3D code uses terrain-following coordinates it is possible for the lower boundary of the computational mesh to follow the topography. To generate the computational grid, a surface grid is first constructed using an in-house 2D surface grid generator and then the volume grid is generated using the enhanced hyperbolic grid generator HypGrid3D (Sørensen, 1998). As shown in figure I-3d, using a true surface projection when generating the surface grid allows good resolution in areas of steep terrain and avoids highly skewed cells on the cliff face of Bolund.

For the present simulations, a polar computational domain is chosen, which was used for all wind directions. The domain has a radius of 5500 m and a height of 1100 m. The height of the

near-wall grid cells is less than 0.01 m and the horizontal resolution near Bolund is about 1 m. Roughly 13 million grid cells are used to discretize the domain (grid level 1). To assure that the flow is sufficiently resolved, simulation results have been compared on coarser grid levels. The coarse grid levels are constructed by removing every second grid point in all directions. The grid convergence study showed that grid level 3 ($\simeq$ 0.2 mill. cells) and grid level 2 ($\simeq$ 1.6 mill cells) gave near identical results to grid level 1.

Turbulence modelling

The turbulence in the boundary layer is modeled by the $k-\varepsilon$ eddy viscosity model (Launder and Spalding, 1974). The originally proposed model constants were established for industrial flows (with hydraulically smooth walls), while slightly different values have been proposed for atmospheric flows over rough surfaces (*e.g.* Panofsky and Dutton (1984); Zeman and Jensen (1987); Raithby *et al.* (1987); Sogachev and Panferov (2006)). The set presented in table I-2 has been calibrated for neutrally stratified atmospheric flows.

Wall treatment

The logarithmic equilibrium assumptions result in the treatment of the velocities and turbulent quantities at the walls (see Sørensen (1995); Sørensen *et al.* (2007); Hackman (1982) for details). The boundary conditions for the velocities are implemented through the skin friction at the wall. In the EllipSys3D implementation, the first cell is placed on top of the roughness elements, as in figure I-2. The advantages of this procedure is that there are no restrictions on the minimum height of the first cell, which in case of large shifts in roughness height from sea to shore may otherwise pose unwanted restrictions on the computational grid. The skin friction is evaluated at the wall-adjacent cell centre, where the variables are stored, as $\tau_w = \rho u_0 u_{\star w}$.

The boundary condition for the turbulent kinetic energy equation reduces to a balance between the production (P_k) and dissipation (ε) of the quantity itself. In the code, this is implemented with a von Neumann condition on the turbulent kinetic energy, and by replacing the production and dissipation terms in the first cell using equations A I-18 and A I-21, respectively.

The equation for the dissipation of turbulent kinetic energy is abandoned in the wall-adjacent cell; instead the dissipation is specified according to the balance between the production and dissipation obtained for a fully developed flow,

$$\varepsilon = \frac{u_0^3}{\kappa (n_\perp + z_0)}. \qquad \text{(A I-21)}$$

Numerics

The flow solver EllipSys3D was used for all computations. This code has been developed in co-operation between the Department of Mechanical Engineering at the Technical University of Denmark (DTU) and Risø DTU (see Michelsen (1994, 1992); Sørensen (1995)). It is a multi-block, finite-volume discretization of the incompressible Navier-Stokes (NS) equations in general curvilinear coordinates. The code uses a co-located variable arrangement, and Rhie/Chow interpolation (Rhie, 1981) to avoid odd/even pressure decoupling. As the code solves the incompressible flow equations, no equation of state exists for the pressure, and in the present work the SIMPLE algorithm of Patankar and Spalding (1972) is used to enforce the pressure/velocity coupling. The EllipSys3D code is parallelized with MPI for execution on distributed memory machines, using a non-overlapping domain decomposition technique.

In order to accelerate the overall algorithm, a multi-level grid sequence is used in steady-state computations. The convective terms are discretized using a third-order QUICK upwind scheme, implemented using the deferred correction approach first suggested by Khosla and Rubin (1974). Central differences are used for the remaining terms. The three momentum equations are solved decoupled using a red/black Gauss-Seidel point solver and the solution of the Poisson system arising from the pressure correction equation is accelerated using a multi-grid method.

3.5 Model E: CRES surface layer model (ID0017)

Grid generation

The grid was generated using a straightforward in-house procedure. First, a surface grid was obtained from the provided terrain data (without interpolation) by simply keeping one of every four grid points; this resulted in an equidistant mesh in the *xy*-plane with a grid spacing of 1 m. This discretization covered the entire Bolund hill ranging from -98 to +192 m in the *x*-direction and from -132 to +118 m in the *y*-direction. The surface grid was extended outside this region by means of a geometrical progression using ratios of 1.35 and 1.25 in the *x* and *y* directions, respectively. The final range of the *x* and *y* coordinates was (-400, 400) and (-210, 210), respectively, using 320×271 grid points.

In order to generate the 3D mesh, the surface grid is stacked in the normal direction by setting the distance of the first grid point from the ground to 0.15 m and using a geometrical progression of 1.18. The height of the computational domain was set to 1000 m and 45 grid points were distributed in the vertical direction. However, in the case of the Bolund hill, the very steep slopes, especially in the escarpment region, resulted in highly skewed cells, which could reduce the accuracy of predictions. To compensate, the grid in the *xz*-plane was made quasi-orthogonal using an elliptic grid generator, that incorporates appropriate source terms which control the distribution of grid lines, and applies an orthogonality assumption at the ground boundary (see figure I-3e). In the resulting mesh, the minimum distance from the ground remained very close to 0.15 m. A comparison of these two grid generation techniques showed that the steep velocity gradients at regions of high flow acceleration are better predicted using the latter scheme.

Turbulence modelling

The Wilcox $k-\omega$ turbulence model (Wilcox, 1998), suitably modified for atmospheric flows, was used for turbulence closure. The modified coefficients were established using the boundary condition for k at the wall $k = u_*^2/\sqrt{\beta_*}$ and the fact that u_*/k has been measured between 0.17

and 0.18 for a neutral atmosphere. By retaining the turbulence decay ratio value of 1.2 observed by Townsend (1976), the model coefficients can be calibrated and are listed in table I-2.

Boundary conditions

Wall functions were used close to the ground by demanding that the logarithmic velocity profile was maintained at the first grid point above ground. For k and ω, the surface conditions were such that the inflow profiles defined by similarity theory were conserved.

Numerics

The incompressible RANS equations were numerically integrated by means of an implicit pressure correction scheme. A matrix-free algorithm for pressure updating was introduced, which maintained the compatibility of the velocity and pressure field corrections, allowing for practically unlimited large time steps within the time integration process. The basic idea of this method is that there is no need to approximate the pressure correction operator in order to obtain an analytical expression for it; instead the pressure correction equation can be solved using a conjugate gradient solver where the complete term computation is only requested. Since the pressure correction operator is, in general, non-symmetric the restarting GMRES conjugate gradient method was preferred among others because of its smooth convergence behavior. For steady flow (non-time-accurate) computations, as those performed here, the governing equations are not fully converged at each time level. One internal iteration per time step, with a selected dimension of the Krylov subspace of the order 10, is usually enough for final convergence. For the Bolund simulation cases, a time step equal to 0.05 was appropriate to achieve a convergence of more than 4 orders of magnitude after 8000 time steps.

The velocity vector was normalized by a reference value U_∞ and the pressure (or rather the pressure divided by the density) term by U_∞^2, where U_∞ was considered to be the freestream velocity, obtained from the logarithmic law of the input wind speed profile for a height of 1000 m agl. Distances were normalized by the maximum height of the Bolund hill ($\approx$ 12 m), taken as its characteristic length.

Table-A I-3 Grid and domain properties

	A ÉTS OpenFOAM	B CENER Fluent	C Vattenfall OpenFOAM	D Risø DTU EllipSys3D	E CRES In-house
Upstream extension (m)	400	480	400	5500	300
Downstream extension (m)	300	490	400	5500	200
Lateral extensions (m)	200	460	400	5500	100
Domain height (m)	120	100	200	1100	1000
Grid type	Structured	Block structured	Block structured	Block structured	Structured
Grid generation	In-house	ICEM CFD Hexa	ICEM CFD Hexa	In-house	In-house
Cell type	Hexahedral	Hexahedral	Hexahedral	Hexahedral	Hexahedral
Total cell count	7.56×10^6	3.05×10^6	3.1×10^6	13×10^6	4×10^6
Near-wall cell height (m)	< 0.10	0.30	0.30	0.01	0.15

Spatial discretization was performed on a computational domain, resulting from a body-fitted coordinate transformation, using finite-difference/finite-volume techniques. The convection terms in the momentum equations were handled by a second-order upwind scheme bounded through a limiter, while the diffusion terms were discretized using centered second-order schemes. According to a staggering technique, the Cartesian velocity components were stored at grid-nodes, while pressure was computed at mid-cells, thus allowing for pressure field computation without any explicit need of pressure boundary conditions. The velocity-pressure decoupling was prevented through a linear fourth-order dissipation term added to the continuity equation. The turbulence transport equations were linearized and discretized in time following a procedure similar to that of the velocity equations. The two equations were handled in an implicit, but decoupled, way (Prospathopoulos *et al.*, 2011).

4 Results

Results are non-dimensionalized and presented in terms of speed-up factor and added turbulence. The speed-up factor is defined as

$$\Delta S = \frac{s(x,y,z) - s(x_0,y_0,z)}{s(x_0,y_0,z)} \tag{A I-22}$$

while the added turbulence is given by

$$\Delta k = \frac{k(x,y,z) - k(x_0,y_0,z)}{s(x_0,y_0,z)^2} \tag{A I-23}$$

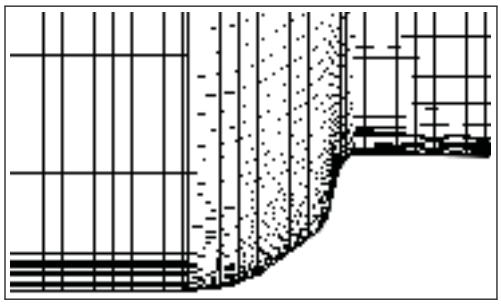

(a) ÉTS

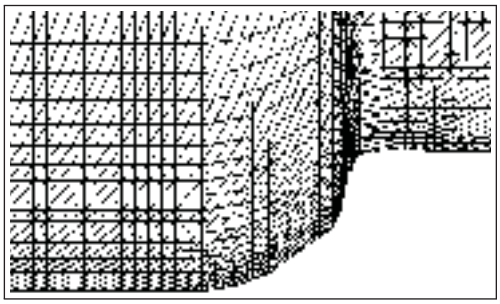

(b) CENER

(c) Vattenfall

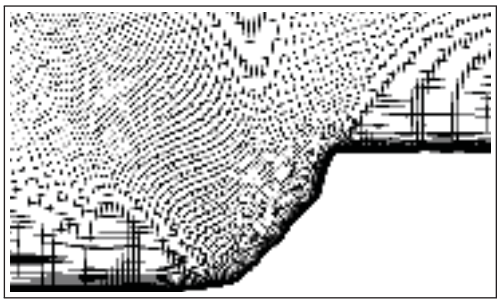

(d) Risø DTU

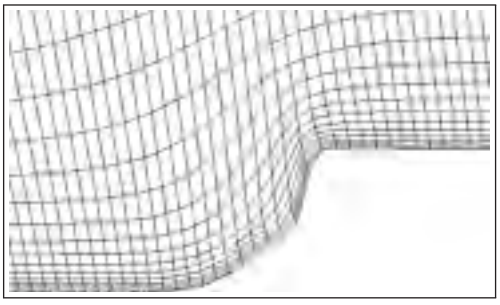

(e) CRES

Figure-A I-3 Discretization at western cliff face: Projection of case 1 meshes onto line (plane) B near mast 7.

and the subscript 0 refers to a reference quantity (for brevity, $s(x_0, y_0, z)$ will be simply denoted as s_0).

Experimental speed-up factors are calculated using a reference logarithmic velocity profile based on the measurement of the 5-m sonic anemometer at the reference mast. The 5-m wind speed measurement is extrapolated to the desired height using

$$\frac{s(z)}{u_{\star 0}} = \frac{s_0(z_{sonic})}{u_{\star 0}} + \frac{1}{\kappa} \ln\left(\frac{z}{z_{sonic}}\right). \qquad \text{(A I-24)}$$

The reference turbulence level is assumed constant with height and thus not corrected. In the following sections, the normalized predictions of all models are compared with measurements (*i.e.* normalized mean value $\pm$ one standard deviation) along principal axes roughly parallel to the inflow as well as at selected masts along these same axes.

4.1 Case 1 – 270 degrees

Case 1 corresponds to a westerly wind with the hill strongly resembling a forward-facing step geometry. The predicted and measured axial distributions of speed-up factor and added turbulence are shown in figure I-4; the simulations have been normalized using the predicted wind speed at (-208 m, 0 m) for axial distributions and (-180.8 m, -103.3 m) for vertical distributions. All measurements are normalized using M0.

Considering first the wind speed at 5 m (all heights are with respect to ground level), all model predictions are in fairly close agreement with measurements. The speed-up over the cliff (near M6) and wake recovery are clearly the most difficult aspects of the flow to accurately predict. The situation is much the same at 2 m, except for a larger spread in the model predictions over the hill with the ÉTS model predicting lower wind speeds. There is somewhat less consensus when turbulence is considered. The large peak in k at 2 m is underestimated, while at 5 m turbulence over the hill is grossly overestimated.

Figure I-5 presents vertical distributions of speed-up factor at masts 3, 6, 7 and 8 as well as added turbulence at masts 6 and 8. Agreement with measurements is very good at masts 7 and 8, while the models do a reasonable job of reproducing the flow acceleration and increase in turbulent kinetic energy over the hill at mast 6. There is some disagreement between models at mast 3 where, as seen in the axial distribution, the ÉTS model recovers more slowly.

4.2 Case 2 – 255 degrees

For this wind direction, the shape of the hill more closely resembles a forward-backward facing step configuration. Considering masts along line A, figure I-6 present vertical distributions of

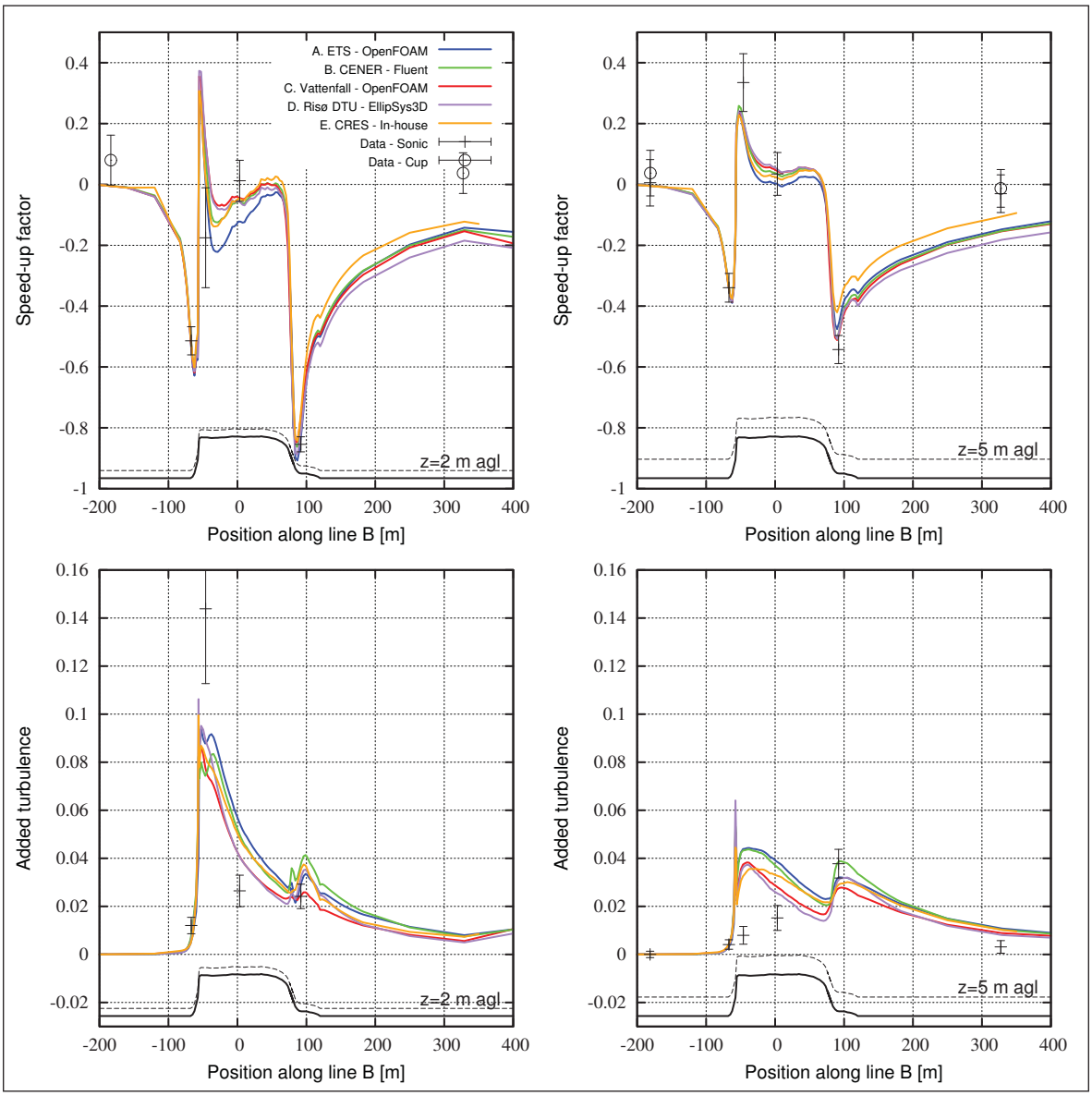

Figure-A I-4 Case 1 – Axial distribution of speed-up factor and added turbulence at 2 and 5 m agl along line B for wind direction of 270°

speed-up factor and added turbulence where all results are normalized using the wind speed at M0. Again, the models accurately predict the slow down in front of the cliff face (at M1) and seem to pass an average line through the measurements at the mast located at the cliff edge (M2). The predictions neatly bound the observations at mast 3 with no model predicting both the 2-m and 5-m speed-up. With the backface being slightly steeper, a stronger recirculation zone is present, which is not as well resolved as the flow at mast 8 for case 1.

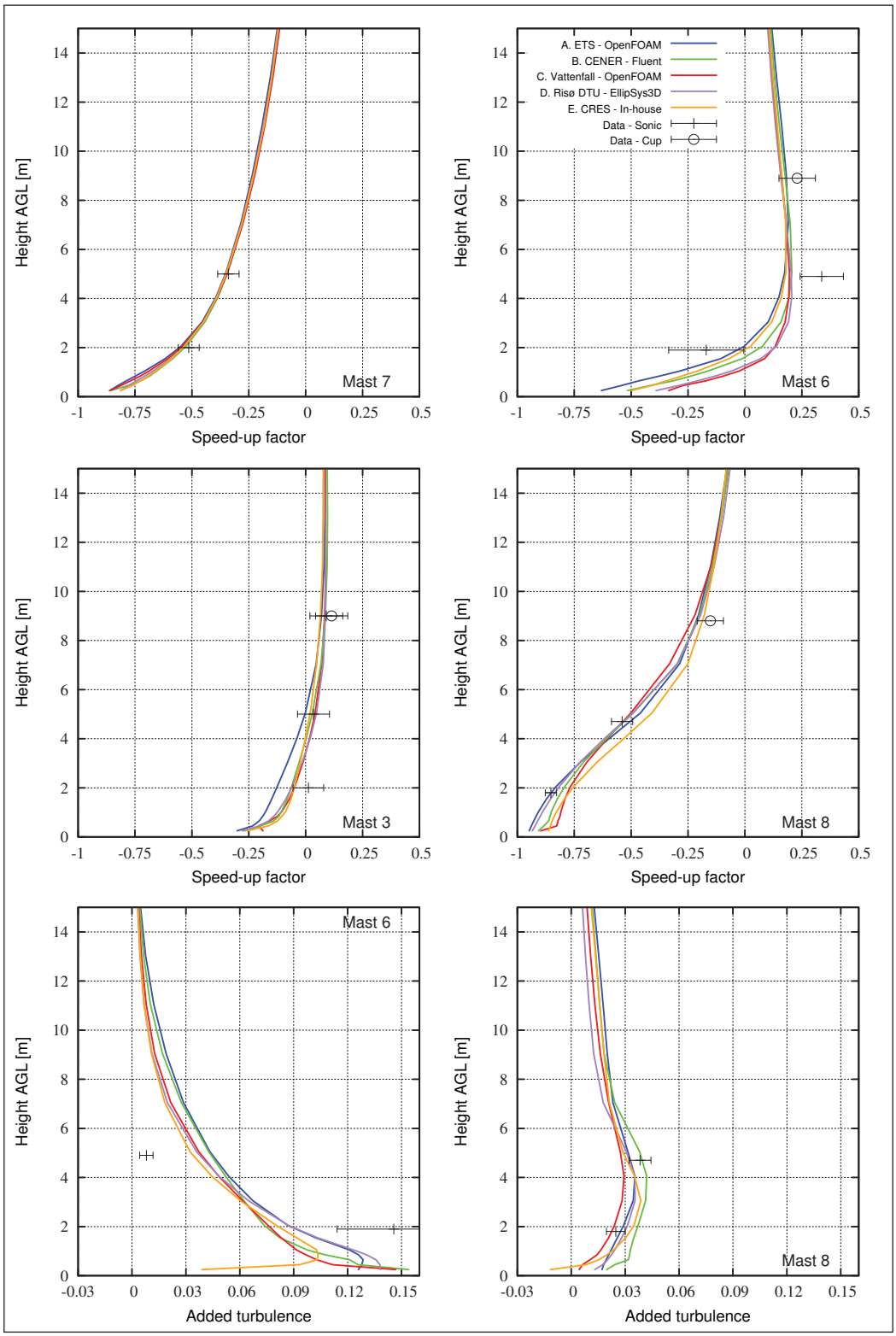

Figure-A I-5 Case 1 – Vertical distribution of speed-up factor at masts 3, 6, 7 and 8 and added turbulence at masts 6 and 8 for wind direction of 270°

4.3 Case 3 – 239 degrees

For this case, the incident wind direction is parallel to line A and the hill geometry is similar to case 2. Distributions of speed-up factor and added turbulence along this axis are presented in figure I-7 where the simulations are normalized using the wind speed at (-178.3 m, -107.1 m) for axial distributions and (-180.8 m, -103.3 m) for vertical distributions. As previously, all measurements are normalized using M0.

The concurrence of model results for this case is certainly encouraging as is the generally good agreement with measurements. The 5-m speed-up at mast 3 clearly overestimated; in fact, the models generally overpredict the velocity at mast 3, as seen in figure I-8. The only significant difference in predicted speed-up factors is at 2 m, just behind the cliff face (at M2), where the ÉTS model again predicts slightly lower wind speeds which, in this case, are supported by measurements.

As for the previous cases, the peak in turbulent kinetic energy at the upstream cliff at 2 m is underestimated while the peak predicted by all models at 5 m is not present in the data.

4.4 Case 4 – 90 degrees

For case 4, the flow approaches from the shore and there are two changes in surface roughness, as opposed to one. Also, the hill geometry on the windward side is much smoother for this configuration. This is reflected in the measured speed-up factor which shows less variation over the hill than the previous cases, as shown in figures I-9 and I-10. Here, the wind speed and turbulent kinetic energy have been normalized using the simulated wind speed at (329.0 m, 0 m) for axial distributions while vertical distributions use (327.3 m, -39.3 m). All measurements are normalized using M9.

Given this, perhaps the excellent agreement between models and measurements is unsurprising. Outside of the wake region, there are only negligible differences in predicted speed-up factor and agreement with measurements is excellent. The differences between models in the wake

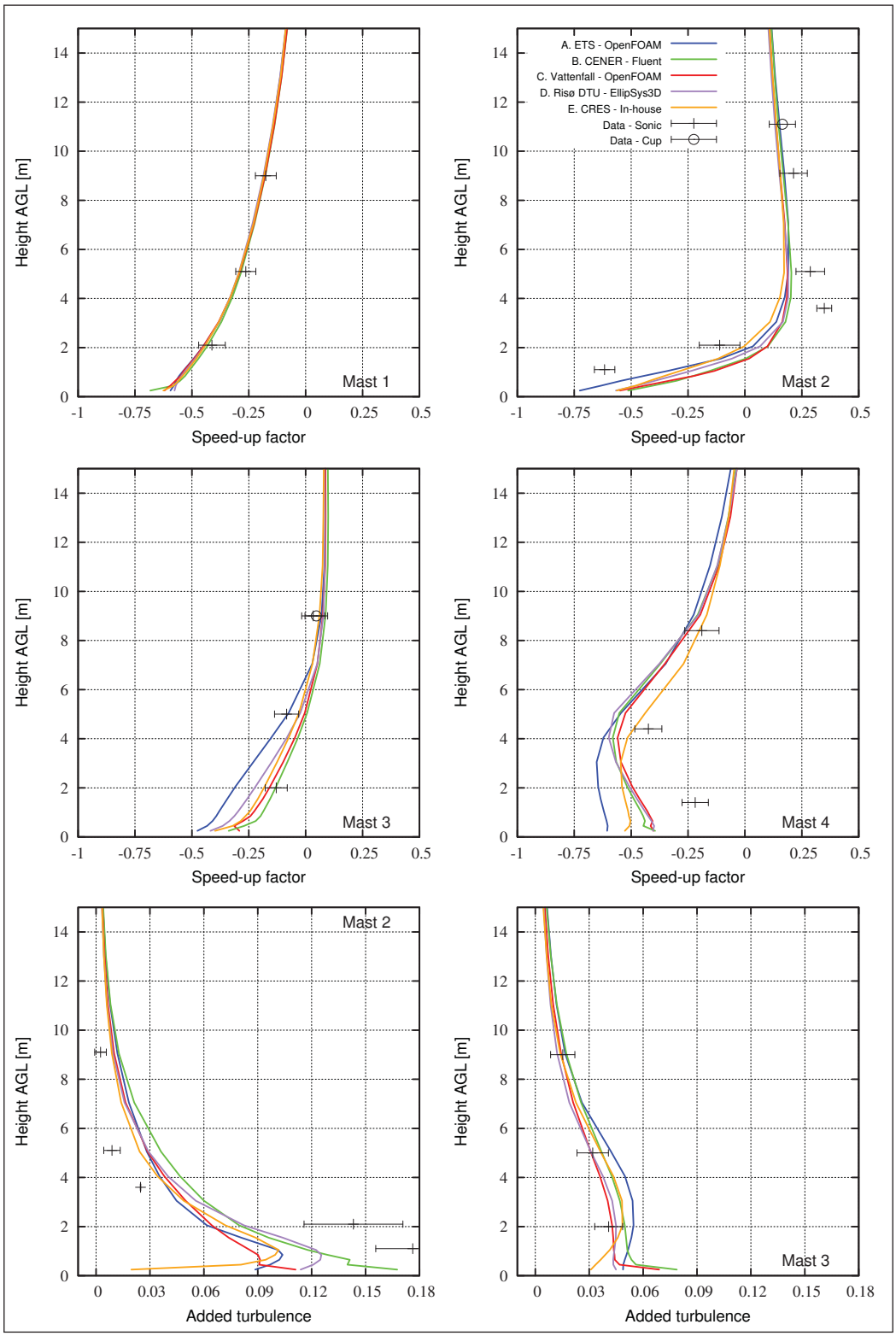

Figure-A I-6 Case 2 – Vertical distribution of speed-up factor at masts 1, 2, 3 and 4 and added turbulence at masts 2 and 3 for wind direction of 255°

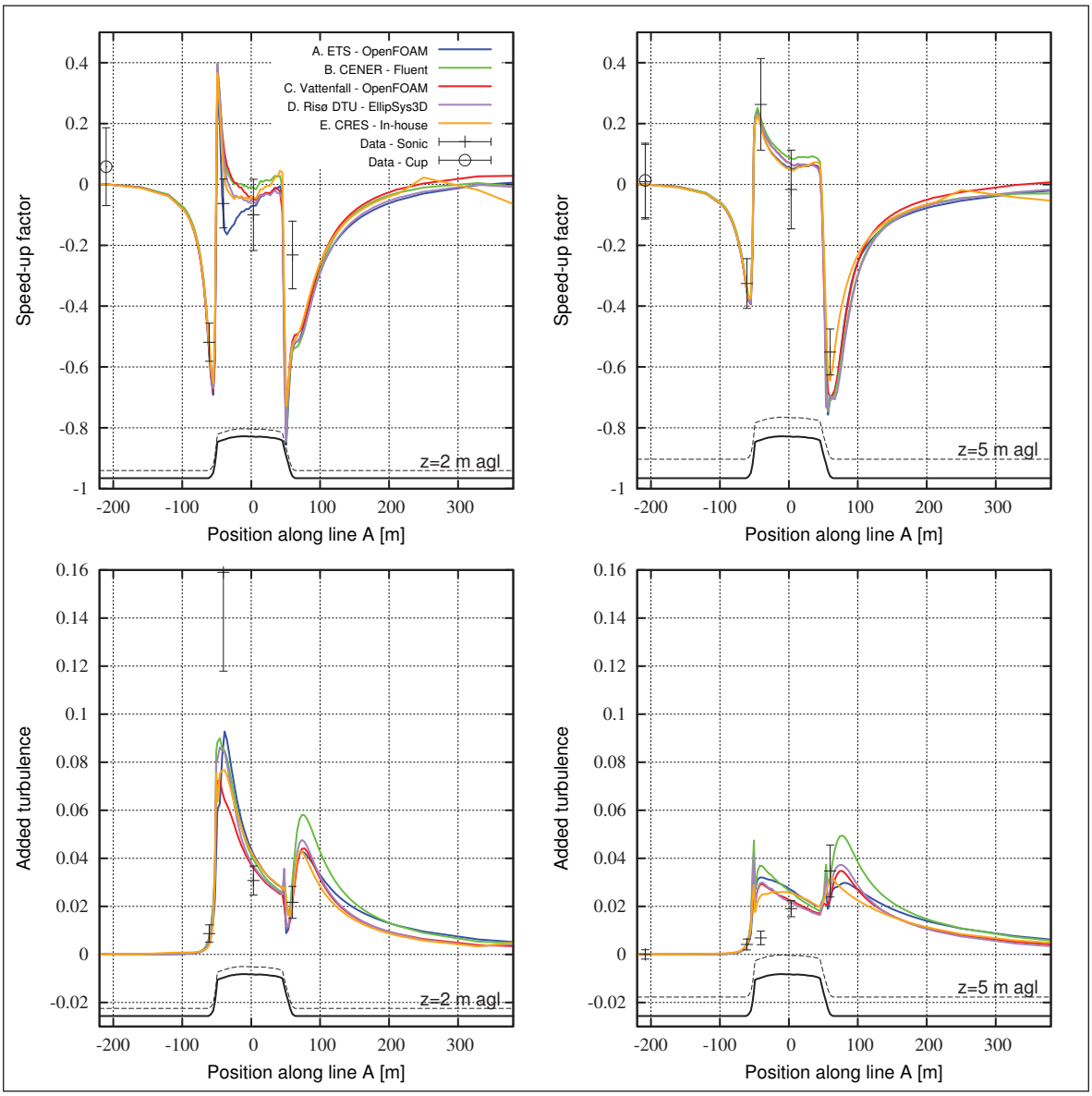

Figure-A I-7 Case 3 – Axial distribution of speed-up factor and added turbulence at 2 and 5 m agl along line A for wind direction of 239°

is, however, much greater than for the westerly cases. The largest discrepancies are for added turbulence where measurements suggest that over the hill there is none (in fact, a small decrease is present) but models expect a small increase. The predicted increase is likely unavoidable given the velocity gradient associated to the change in ground level.

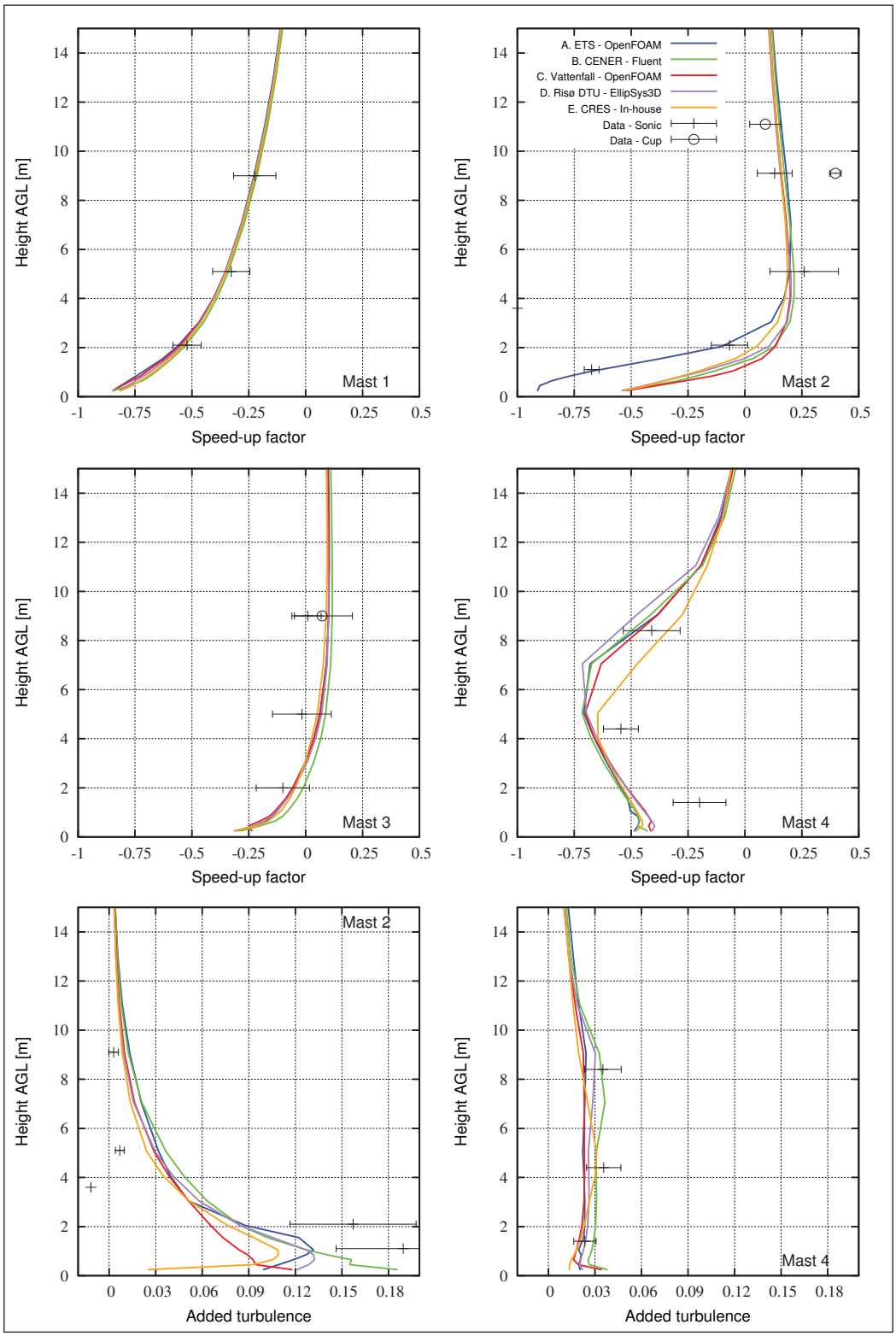

Figure-A I-8 Case 3 – Vertical distribution of speed-up factor at masts 1, 2, 3, and 4 and added turbulence at masts 2 and 4 for wind direction of 239°

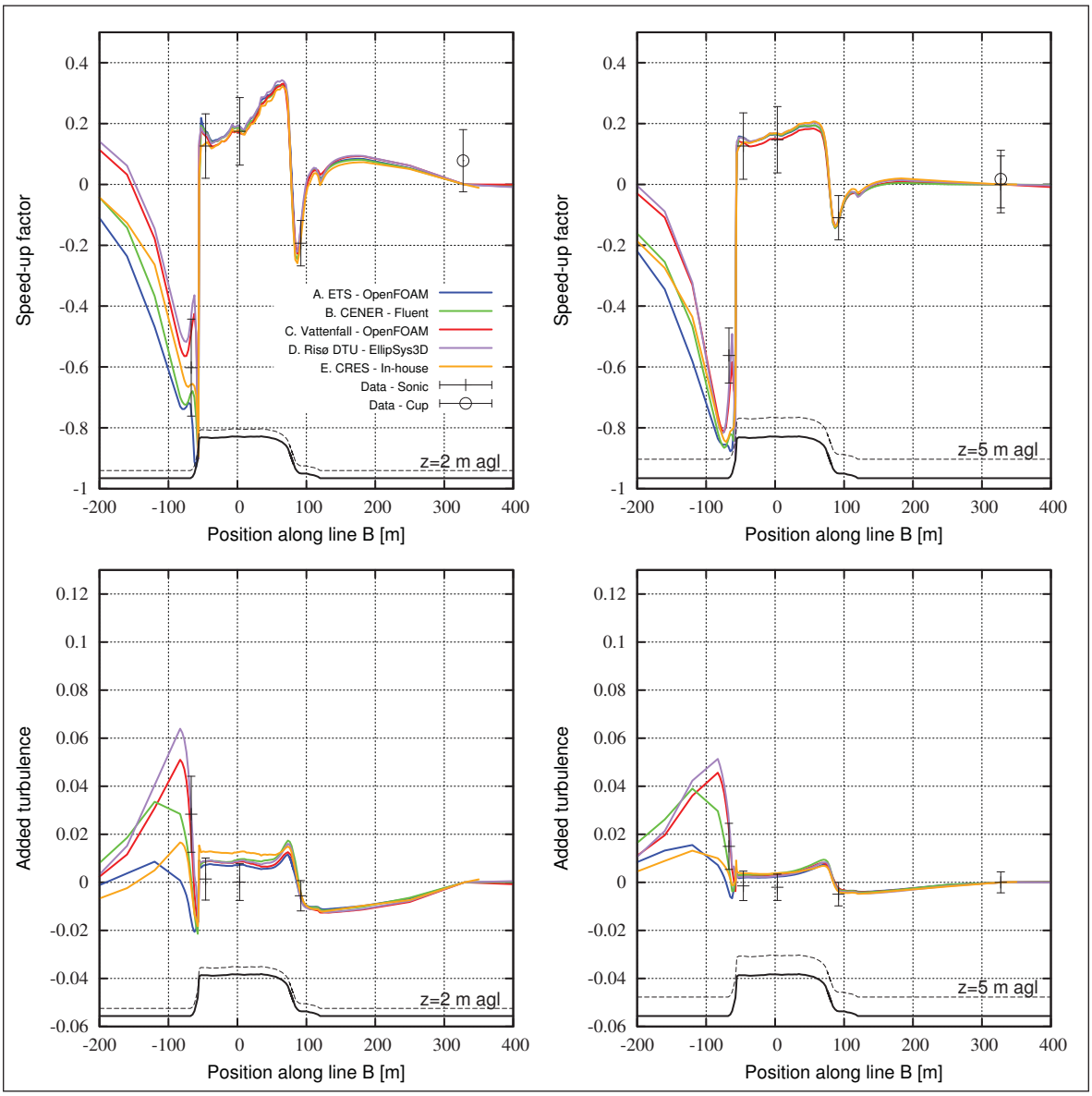

Figure-A I-9 Case 4 – Axial distribution of speed-up factor and added turbulence at 2 and 5 m agl along line B for wind direction of 90°

4.5 Overall results

It is somewhat difficult to attain an objective, non-biased estimate of the accuracy of the models by comparing field predictions with measurements at a few discrete locations. However, as proposed in the recently published analysis of the blind comparison results Bechmann *et al.* (2011), the accuracy of the numerical predictions **at these points** can be quantified by the

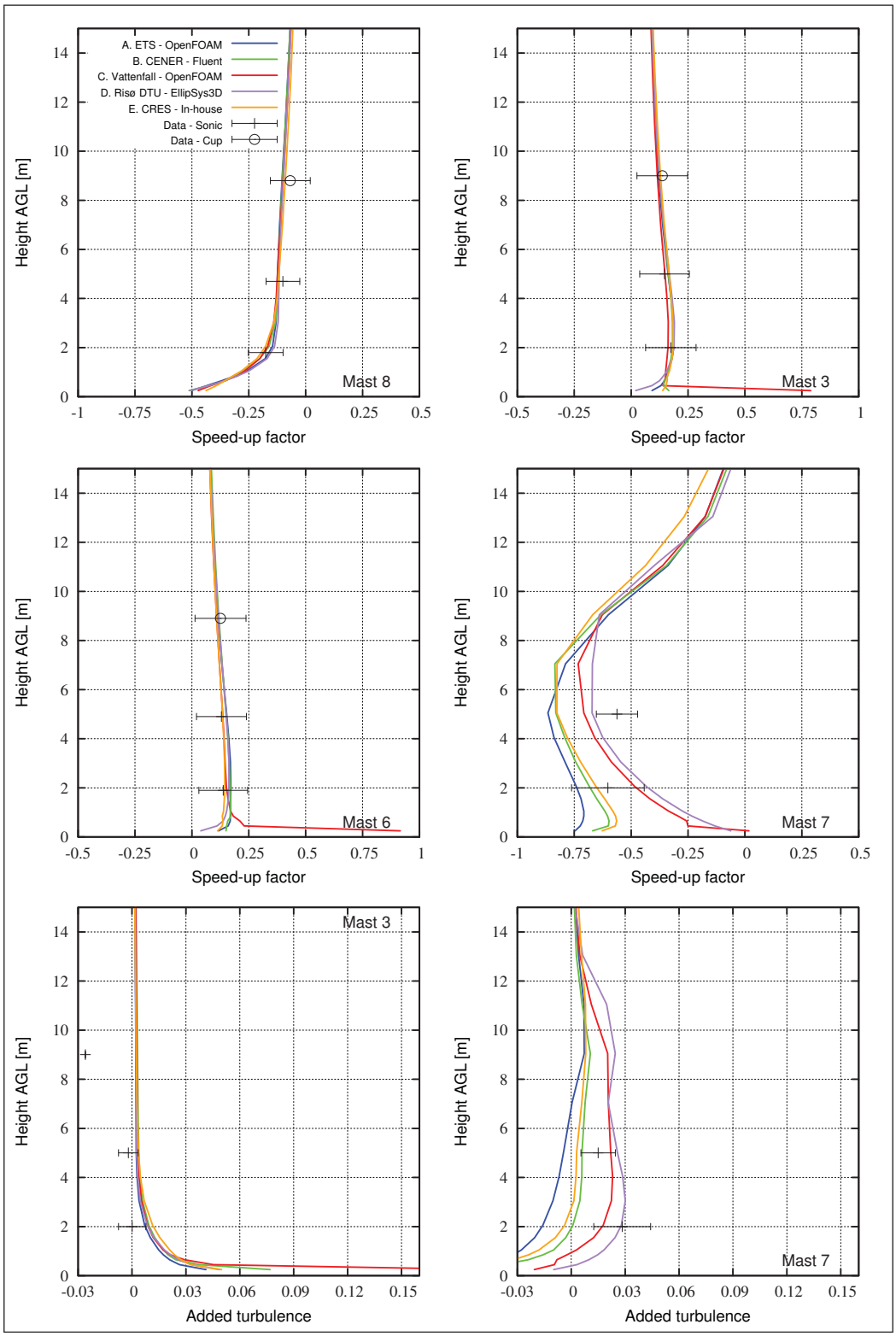

Figure-A I-10 Case 4 – Vertical distribution of speed-up factor at masts 3, 6, 7 and 8 and added turbulence at masts 3 and 7 for wind direction of 90°

speed-up factor error,

$$\zeta_{\Delta S} = \left|\Delta S_{model} - \Delta S_{exp}\right| \times 100 \qquad \text{(A I-25)}$$

where the fractional speed-up is given by equation A I-22. For the purposes of calculating errors, ΔS_{model} is linearly interpolated so as to coincide with measurements. Given the sometimes large discrepancies between cup and sonic anemometer measurements, only sonic data are used in the error analysis. Table I-4 summarizes the mean errors in predicted speed-up factor over all masts for all models and all cases at 2 and 5 m. Also included is the mean error at 5 m if masts located in the hill wake are neglected (*i.e.* masts 4, 5, 8 and 9 for cases 1–3 and masts 0, 1 and 7 for case 4).

Considering the ensemble, no model clearly stands out from the rest in terms of predictive capability. Ignoring the wake, the difference between the maximum and minimum errors for each case varies marginally between 0.4 and 2.1% at 5 m. Given the model similarities, this is perhaps to be expected and in some way reflects the maturity RANS/two-equation modelling has achieved in its application to atmospheric flows. The one outlier is case 3 where the lower near-ground wind speeds over the hill predicted by the ÉTS model result in a markedly lower error at 2 m. Given that the Risø DTU boundary conditions are nearly identical to those of ÉTS, the reason for the lower predicted wind speeds must stem from either the use of RNG closure or the discretization. Subsequent simulations by ÉTS using the $k-\varepsilon$ model have also yielded lower near-ground wind speeds just behind the cliff edge, which suggests discretization is playing a role and that results may not be grid independent. The lower error should be considered in this light.

Looking at the results case-by-case at 5 m without the wake, the case 4 configuration is by far the easiest to reproduce by the methods evaluated here: all models have errors less than 3%, contrary to the other cases where they are on the order of 5–10%.

Table-A I-4 Overall mean errors in speed-up factor

		A ÉTS OpenFOAM RNG $k-\varepsilon$	B CENER Fluent $k-\varepsilon$	C Vattenfall OpenFOAM $k-\varepsilon$	D Risø DTU EllipSys3D $k-\varepsilon$	E CRES In-house $k-\omega$
Case 1	2 m	13.8	13.4	15.9	14.5	11.9
	5 m	7.2	7.2	6.7	7.8	8.8
	5 m, no wake	6.6	4.5	5.2	5.2	6.2
Case 2	2 m	24.6	26.7	27.0	28.1	26.1
	5 m	17.1	16.6	16.8	17.4	16.4
	5 m, no wake	6.8	6.4	7.0	6.5	7.2
Case 3	2 m	9.6	22.5	21.2	21.1	20.2
	5 m	9.4	9.2	8.9	8.9	9.2
	5 m, no wake	9.4	7.6	8.0	7.9	8.1
Case 4	2 m	9.6	8.4	6.1	6.4	7.6
	5 m	11.3	8.8	6.0	5.0	6.3
	5 m, no wake	2.9	2.7	2.5	2.6	2.5

A similar analysis can be carried out for the turbulent kinetic energy by defining the increase in turbulence intensity as

$$\Delta I = \frac{\sqrt{k} - \sqrt{k_0}}{s_0}. \tag{A I-26}$$

The error is then normalized against the measured turbulent kinetic energy at the reference mast divided by the measured and *corrected* reference velocity, *i.e.*

$$\zeta_{\Delta I} = \frac{\left|\Delta I_{model} - \Delta I_{exp}\right|}{\left(\sqrt{k_0}/s_0\right)_{exp}} \times 100. \tag{A I-27}$$

Table I-5 summarizes the mean errors in predicted added turbulence.

Casual inspection of table I-5 suggests the turbulent kinetic energy is much more difficult to accurately resolve. The errors are much larger and the differences between models are also greater. Certainly, the use of the eddy viscosity concept and the imposition of isotropy are partly to blame; two-equation closure is fundamentally limited in the extent to which it can reproduce the turbulence structure of the atmospheric boundary layer. However, unlike for speed-up factor, one model does stand out from the rest. In every instance, the Risø DTU

Table-A I-5 Overall mean errors in predicted added turbulence

		A ÉTS OpenFOAM RNG $k-\varepsilon$	B CENER Fluent $k-\varepsilon$	C Vattenfall OpenFOAM $k-\varepsilon$	D Risø DTU EllipSys3D $k-\varepsilon$	E CRES In-house $k-\omega$
Case 1	2 m	46.0	47.5	46.1	44.6	50.2
	5 m	24.7	28.3	25.4	23.5	29.0
	5 m, no wake	32.5	33.0	26.0	23.6	26.2
Case 2	2 m	42.6	44.5	44.3	37.1	45.1
	5 m	33.5	33.5	30.7	28.8	28.4
	5 m, no wake	31.9	33.0	25.8	24.9	23.2
Case 3	2 m	29.4	36.8	40.0	32.4	39.7
	5 m	18.9	18.7	17.2	15.4	13.2
	5 m, no wake	25.8	28.2	21.5	20.0	17.2
Case 4	2 m	13.0	9.6	6.9	5.1	12.5
	5 m	9.4	6.0	7.1	6.0	9.1
	5 m, no wake	4.1	5.4	5.6	4.5	4.9

model has either the lowest or second lowest error in predicted added turbulence intensity. As for velocity, the errors for case 4 are by far the smallest.

5 Conclusions

The parameters of the blind comparison were not sufficiently controlled to formulate any best practice recommendations regarding turbulence modelling, grid generation, boundary conditions, *etc*. However, that is not to say that some general conclusions cannot be drawn from the results presented here.

First, it is evident that methods based on RANS/two-equation closure produce consistent results when applied correctly. Further research on turbulence modelling is clearly needed to improve agreement with measurements; however, the RANS flow predictions compare well with one another. This would likely be further improved if grid independency was formally evaluated by all modelers; the fixed deadline of the blind comparison made this difficult to carry out in some cases. In formulation, little distinguishes the models and, although this has yet to be formally verified, it is suspected that the majority of the differences observed in the results are related to the mesh.

Second, the models have greatest difficulty in the wake region. Certainly, two-equation closure is not ideal for recirculating flows; one might reasonably expect significant improvement with a second-order closure scheme. In the context of wind resource assessment for wind energy purposes, this is not so much of a concern for sites like Bolund as turbines would rarely be sited in topographic wakes or possible separation or recirculation zones in such terrain. However, these conditions may be unavoidable for more complex sites where accurate prediction of topographic wake properties then assumes greater importance.

Third, turbulence kinetic energy is generally more difficult to accurately predict than velocity. For wind resource assessment, the energy content is the most important parameter, but for siting purposes manufacturers require a more detailed description of the flow to assess turbine (fatigue) loads.

Lastly, although RANS-based modelling is fundamentally more valid than linearized approaches when dealing with complex sites, it is not a silver bullet. The Bolund site is only moderately complex and yet errors in predicted wind speed are still far from meeting the TPWind objectives. Furthermore, atmospheric stability has been ignored, a possibly important factor for both offshore and mountainous sites. With these facts in mind, the errors presented here might be considered lower bounds. Clearly, more research is required to handle even the simplest complex case if the requirements of TPWind are to be met.

Since Bolund, at least two more wind measurement campaigns have been undertaken by the community, both more challenging than the Bolund topography. CENER has organized one based on their experimental complex terrain wind farm Alaiz, while Risø DTU has instrumented a very mountainous site in India. It is hoped that the present work will in some way contribute to even better results of RANS/two-equation models in future blind tests.

ANNEX II

A CLOSER LOOK AT SECOND-ORDER CLOSURE FOR WIND FARM ANALYSIS

Jonathon Sumner[1], Daniel Cabezón[2], Christian Masson[1], Antonio Crespo[3],

[1]Département de Génie Mécanique, École de Technologie Supérieure, 1100 Notre-Dame Ouest, Montreal, Quebec, Canada H3C 1K3

[2]Wind Resource Assessment and Forecasting Service, National Renewable Energy Centre, c/ Somera 7-9, 28023 Madrid, Spain

[3]Escuela Técnica Superior de Ingenieros Industriales, Universidad Politéchnica de Madrid, c/ José Gutierrez Abascal 2, 28002 Madrid, Spain

This work has been presented at EuroMECH colloquium 528 on *Wind Energy and the Impact of Turbulence on the Conversion Process* and submitted for publication in its proceedings. The version presented here includes revisions based on the comments of the Board of Examiners.

Foreword

In all likelihood, the worst-case scenario for a wind energy yield analysis is represented by a dense wind farm sited in complex terrain where wake and topographic effects are important and interwoven. The complexity of such cases make them ideal for validation purposes and, so, the ability of several RANS closures and two actuator disk implementations to predict the energy yield of a medium-size wind farm situated in so-called *simple-complex* terrain is analyzed here. This work has been jointly carried out with the Wind Resource Assessment and Forecasting Service of CENER during an internship from August 2010 to June 2011.

Abstract

The atmospheric flow through a wind farm situated in moderately complex terrain is simulated in an effort to predict the energy capture of the park as a whole. The Reynolds-Averaged Navier–Stokes equations are used to model fluid motion while the effect of turbine rotors is modeled using the actuator disk concept wherein the rotor acts as a momentum sink. The performance of three RANS turbulence closure schemes (standard $k-\varepsilon$, RNG $k-\varepsilon$, and a Reynolds stress transport model) as well as two actuator disk implementations (which differ in how the reference wind speed is determined) are evaluated. Computational times are also briefly discussed.

1 Introduction

It has been shown that common two-equation RANS turbulence closures are not well adapted to actuator disk modelling of the wind turbine rotor (Réthoré, 2009). This combination of models is nonetheless incredibly popular for wind farm analyses given its relative economy and reasonably accurate velocity predictions for isolated rotors (see *e.g.* Barthelmie *et al.* (2009); Sanderse *et al.* (2011); Politis *et al.* (2012)). However, a fundamental change is likely needed to make significant improvements in velocity and turbulence predictions within a real wind farm. As the actuator disk representation of the rotor is by far the most economical (in comparison to actuator surface or line approaches) and is probably a mainstay, it is more appropriate to reconsider the closure. Of course, the greatest weakness of many lower-order turbulence models is the reliance on the eddy viscosity approximation which ties stresses to strain rates in the flow and imposes a single turbulent length scale. On the other hand, Reynolds stress transport models avoid these problems entirely by modelling each component of the stress tensor with its own transport equation and might be a promising alternative.

Traditionally, stress transport models have received relatively less attention as the closure problem still has to be dealt with and the additional equations add to the computational burden. Furthermore, some question remains as to whether the extra effort in fact yields more accurate predictions. But, in light of the possible benefits, second-order closure might be worth a closer

look and is investigated herein for the purposes of wind farm power performance analysis. This study presents a comparison of measured and predicted power ratios for a wind farm sited in moderately complex terrain using two common two-equation closures and a stress transport model. In addition, two actuator disk implementations are investigated.

2 Mathematical modelling

The objective of this study is to take a closer look at two important aspects of wind farm modelling in the context of popular RANS–actuator disk models: the turbulence closure and the actuator disk implementation. In general, the flow is considered steady and incompressible with the effect of turbulence on the transport of momentum being modeled with the Reynolds stress tensor and the effect of wind turbine rotors being represented by sink terms in the momentum equation.

Commonly, the turbulence closure is based on a two-equation parametrization of turbulence effects: the energy contained in the fluctuations and a measure of its rate of dissipation. These models are founded on the assumption that the momentum transport due to turbulence can be seen as stemming from an additional viscosity, generally orders of magnitude greater than the molecular viscosity, that may be deduced from local flow properties. The most popular two-equation RANS closure is the $k-\varepsilon$ model which is well known to provide poor estimates of wind turbine wake properties. Although modifications to the standard model have been proposed (El Kasmi and Masson, 2008; Cabezón *et al.*, 2011; Prospathopoulos *et al.*, 2011), a recent critique of eddy-viscosity-based models for wind turbine applications has shown that all models based on this formulation are probably weak. These arguments provide the impetus to consider second-order closures. Here, the standard $k-\varepsilon$ model, its RNG variant, and the Reynolds stress transport model (RSTM) of Gibson and Launder (1978) are tested. The model closure coefficients are calibrated for neutral surface layer flow where the von Karman constant, κ, is taken as 0.4187.

Concerning rotor modelling, the actuator disk method has been shown to yield nearly identical predictions of velocity defect as its higher-order counterpart the actuator line outside the very

near wake region (Réthoré *et al.*, 2011). It is thus expected to be an adequate representation of the rotor for the purposes of evaluating wind farm energy capture as only far wake wind speeds are of interest. While coupling the actuator disk model with blade-element/momentum theory is quite feasible, it is somewhat impractical (as global thrust and power curves are often the only information available) and is likely unnecessary for such large-scale analyses.

However, application of actuator disk modelling in complex terrain and in densely-packed wind farms poses a unique problem when the actuator disk implementation is based on thrust and power curves. The challenge lies in the proper estimation of the reference wind speed. In theory, this is the wind speed at the location of the wind turbine rotor that would be observed if the wind turbine was not present: it represents the quantity of energy available at the rotor location.

Two possibilities are immediately apparent. The first relies on establishing a relationship between the wind speed at some 'freestream' location and the reference wind speed at the rotor. In its simplest form, a one-to-one ratio might be supposed. A more evolved approach might invoke some assumption regarding axial induction at the rotor itself; so far, improvements yielded by such methods for wind farms in complex terrain have been modest Prospathopoulos *et al.* (2011). The first actuator disk implementation tested here follows this track and takes the wind speed two diameters directly upstream of the rotor as the reference wind speed. As the rotor thrust is determined iteratively as part of the flow solution it is referred to as an *elliptic* implementation.

The second possibility is to introduce the wind turbines sequentially in a row-by-row fashion such that the reference wind speeds for downstream turbines are calculated before their rotors are introduced. The advantage of such an approach is that the impacts of topography and wake recovery should be better captured although at the expense of longer run times. In this case, the rotor thrust is static and based only on upstream influences; it is thus referred to as a *parabolic* implementation.

In both cases, the elemental thrust introduced in the discretized momentum equations as a sink term is given by

$$\Delta\vec{T}_i = \frac{1}{2}\rho C_T \left(\|\hat{n}\cdot\vec{U}_\varnothing\|\right) U_\varnothing^2 A_\varnothing \frac{\Delta V_i}{V_\varnothing} \left(\hat{n}\cdot\hat{U}_\varnothing\right)^2 \hat{n} \tag{A II-1}$$

while the power is estimated using

$$P = \frac{1}{2}\rho C_P \left(\|\hat{n}\cdot\vec{U}_\varnothing\|\right) U_\varnothing^3 A_\varnothing \|\hat{n}\cdot\hat{U}_\varnothing\|^3 \tag{A II-2}$$

where ρ is the air density, C_P and C_T are the turbine power and thrust coefficients, $\hat{n}$ is the disk-normal direction, $A_\varnothing$ is the swept area, $\Delta V_i/V_\varnothing$ is the fraction of the total rotor volume occupied by cell i, and $\vec{U}_\varnothing$ is the reference wind velocity. The subscript $\varnothing$ refers to a quantity related to the actuator disk.

There remains the question of the best measure of energy content. An argument could be made that an average based on the wind speed cubed would be most representative. In standardized power performance testing however the hub height wind speed is presumed to be representative. For wake flow, this practice overly conservative: hub height wind speeds at the wake centre are at or near a minimum. As a first-order improvement, it is proposed to use the disk-averaged wind speed as the reference wind speed $U_\varnothing$.

3 Case study

The case study is based on a Spanish wind farm consisting of 43 wind turbines arranged in five rows with hub heights of 45 m and 55 m. The turbine thrust and power coefficient curves have been provided by the manufacturer. The terrain surrounding the wind farm is shown in figure II-1. A roughness length of $z_0 = 0.0082$ m is assumed for the entire site.

Observations have been filtered by sector and power as part of the European UPWIND project. The conditions for the present study correspond to a wind direction of $327^\circ \pm 5^\circ$, a wind speed at the reference turbine of 8.0 ± 0.5 m/s (by inverse power curve), and a turbulence intensity of roughly 12% at the meteorological mast at hub height.

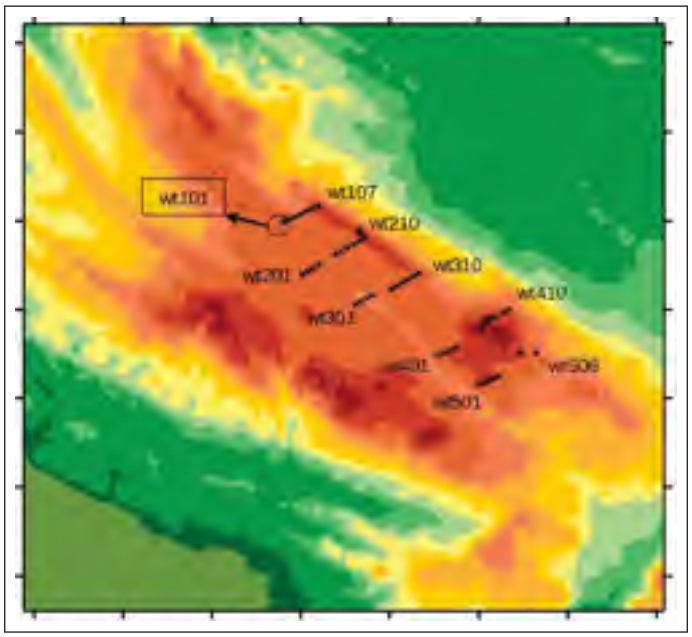

Figure-A II-1 Orography and layout of wind farm. Each contour level represents a 10-m change in elevation. Wind turbines are indicated by a cross while meteorological masts are represented by a triangle

4 Numerics

All simulations are run using OpenFOAM 1.7. The SIMPLE algorithm is used for pressure-velocity coupling. The convection terms in the momentum equation are discretized using a bounded version of QUICK; other convection terms use simple upwinding. All other terms are discretized with central differences. The simulations are run in parallel based on non-overlapping domain decomposition. Customized OpenFOAM solvers have been developed to introduce rotors "parabolically" and define reference wind speeds by the methods described above.

For the row-by-row introduction of rotors, the row convergence criteria are based on three parameters: the momentum equation residuals ($< 10^{-4}$), the maximum relative change in reference wind speed ($< 10^{-5}$), and a minimum number of iterations to ensure convection of upstream changes (500). For the elliptic actuator disk implementation, final convergence is based solely on normalized equation residuals; a tolerance of 10^{-5} is specified.

Equilibrium neutral surface-layer profiles of velocity, turbulent kinetic energy, dissipation rate, and stress tensor are specified at the inflow, located 11 km upstream of the wind farm. The friction velocity is calibrated to yield the measured power at the reference turbine. The outflow is placed 4 km downstream where a fully developed condition is assumed. The lateral boundaries, 2 km to each side of the wind farm, assume a symmetry condition. Freestream conditions are imposed at the upper boundary, roughly 1.5 km from the surface. Standard wall functions, with appropriate modifications for atmospheric flow (Blocken *et al.*, 2007), are used at the surface.

The domain is discretized using a structured mesh consisting of eight million cells with a near-wall cell height of 1 m; cell heights are expanded away from the wall. Each rotor is subdivided into roughly 40 cells.

5 Results & Conclusions

Figures II-2 and II-3 present the power ratios for the second and third rows of the wind farm. For the second row, the predictions of all models for nearly every turbine lie within one standard deviation of the observed power ratio. Significantly, no single combination of actuator disk implementation and turbulence closure stands out from the rest although the RSTM variants are generally somewhat more reliable than the two-equation closures. For row three, the agreement with measurement is not as impressive: all models over-predict the power production at turbine 7 with outliers also at 2, 3 and 5. Overall, the parabolic / RSTM model seems to provide the best agreement with measurements for this row, but only marginally so.

Returning to the original question regarding accuracy and computational effort related to the use of a stress transport model, the preliminary findings of this case study demonstrate that while some improvement in power predictions can be expected, it comes at a significant price: the run time (in terms of cpu-hours) for parabolic / RSTM was more than double that of parabolic / $k-\varepsilon$.

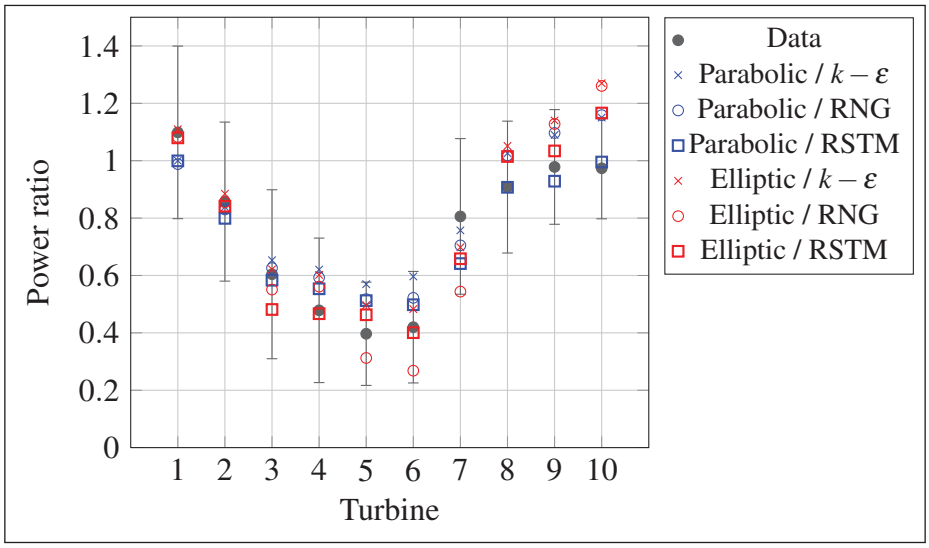

Figure-A II-2 Power ratios for turbines in second row. All results and measurements are normalized using the power output of the reference turbine (wt101)

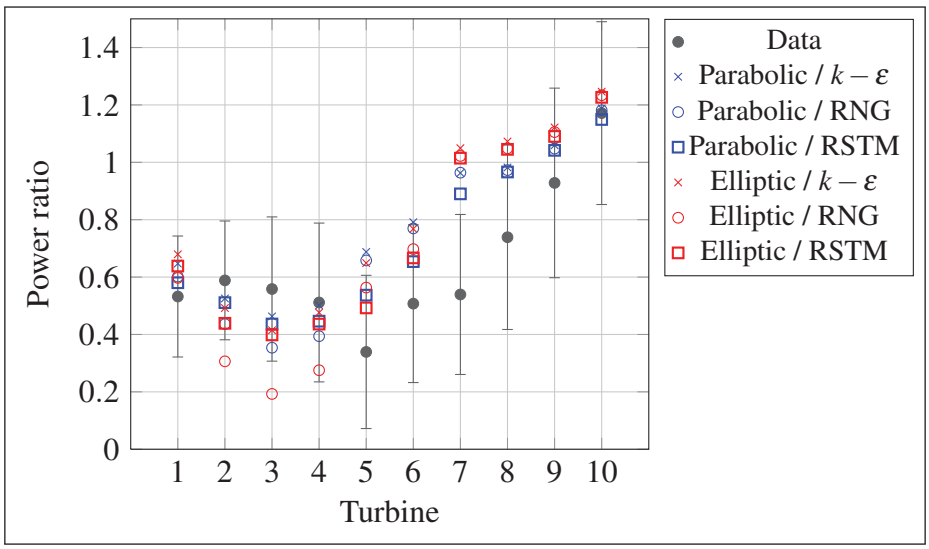

Figure-A II-3 Power ratios for turbines in third row. All results and measurements are normalized using the power output of the reference turbine (wt101)

APPENDIX 2

DERIVATION OF EXACT WEIGHTING FUNCTION FOR STABLE CONDITIONS

Recalling the general form for the weighting function

$$F = \frac{1}{\kappa^2}\left[\frac{d\ell_m}{dz}\frac{d\ell_\varepsilon}{dz} + \ell_m\frac{d^2\ell_\varepsilon}{dz^2} - 2\frac{\ell_m}{\ell_\varepsilon}\left(\frac{d\ell_\varepsilon}{dz}\right)^2\right]$$

and subsituting the following relationships

$$\ell_m = \frac{\kappa z}{\phi_m}, \tag{A 2-1}$$

$$\ell_\varepsilon = \frac{\kappa z}{\phi_\varepsilon}, \tag{A 2-2}$$

$$\phi_m = 1 + \beta\frac{z}{L}, \tag{A 2-3}$$

$$\phi_\varepsilon = 1 + (\beta - 1)\frac{z}{L}, \tag{A 2-4}$$

$$\frac{d\ell_m}{dz} = \frac{\kappa}{\phi_m}\left(1 - \frac{z}{\phi_m}\frac{d\phi_m}{dz}\right) = \frac{\kappa}{\phi_m^2}, \tag{A 2-5}$$

$$\frac{d\ell_\varepsilon}{dz} = \frac{\kappa}{\phi_\varepsilon^2}, \tag{A 2-6}$$

$$\frac{d^2\ell_\varepsilon}{dz^2} = -\frac{2\kappa}{\phi_\varepsilon^3}\frac{d\phi_\varepsilon}{dz}, \tag{A 2-7}$$

yields

$$F = \frac{1}{(\phi_m\phi_\varepsilon)^2} - \frac{2z}{\phi_m\phi_\varepsilon^3}\frac{d\phi_\varepsilon}{dz} - \frac{2}{\phi_m\phi_\varepsilon^3} \tag{A 2-8a}$$

$$= \frac{1}{(\phi_m\phi_\varepsilon)^2}\left[1 - \frac{2\phi_m}{\phi_\varepsilon}\left(1 + \frac{d\phi_\varepsilon}{dz}z\right)\right] \tag{A 2-8b}$$

$$= \frac{1}{(\phi_m\phi_\varepsilon)^2}(1 - 2\phi_m). \tag{A 2-8c}$$

Expressing F in terms of length scales gives

$$F = \frac{(\ell_m\ell_\varepsilon)^2}{(\kappa z)^4}\left(1 - \frac{2\kappa z}{\ell_m}\right). \tag{A 2-9}$$

Inverting equation (2.18) for z, substituting into the above and simplifying then leads to

$$F = -\left(\frac{\ell_\varepsilon}{\ell_m}\right)^2 \left(\frac{\ell_m}{\ell_{max}} + 1\right) \left(1 - \frac{\ell_m}{\ell_{max}}\right)^3, \qquad \text{(A 2-10)}$$

which is identical to equation (2.32) as the ratio of length scales is $(1 + R'_f)$.

REFERENCES

Alinot, C. and C. Masson. 2005. $k-\varepsilon$ model for the atmospheric boundary layer under various thermal stratifications. *Transactions of the ASME - Journal of Solar Energy Engineering*, vol. 127, no. 4, p. 438–443.

Ammara, I., C. Leclerc, and C. Masson. 2002. A viscous three-dimensional differential/actuator-disk method for the aerodynamic analysis of wind farms. *Transactions of the ASME - Journal of Solar Energy Engineering*, vol. 124, p. 345–356.

Apsley, D. and I. Castro. 1997. A limited-length-scale $k-\varepsilon$ model for the neutral and stably-stratified atmospheric boundary layer. *Boundary-Layer Meteorology*, vol. 83, no. 1, p. 75–98.

Aubrun, S., P. Devinant, and G. Espana. 2007. "Physical modelling of the far wake from wind turbines. Application to wind turbine interactions". In *Proceedings of EWEC 2007*. (Milan, Italy 2007), p. 1–8. European Wind Energy Association.

Ayotte, K. 2008. Computational modelling for wind energy assessment. *Journal of Wind Engineering and Industrial Aerodynamics*, vol. 96, p. 1571–1590.

Barth, T. and D. Jespersen. 1989. "The design and application of upwind schemes on unstructured meshes". AIAA paper 89-0366.

Barthelmie, R., K. Hansen, S. Frandsen, O. Rathmann, J. Schepers, W. Schlez, J. Phillips, K. Rados, A. Zervos, E. Politis, and P. Chaviaropoulos. 2009. Modelling and measuring flow and wind turbine wakes in large wind farms offshore. *Wind Energy*, vol. 12, no. 5, p. 431–444.

Barthelmie, R., J. Schepers, S. van der Pijl, O. Rathman, S. Frandsen, D. Cabezón, E. Politis, J. Prospathopoulos, K. Rados, K. Hansen, W. Schlez, J. Phillips, and A. Neubert. 2007. "Flow and Wakes in Complex Terrain and Offshore: Model Development and Verification in UpWind". In *Proceedings of EWEC 2007*. (Milan, Italy 2007), p. 1–10. European Wind Energy Association.

Barthelmie, R., S. Frandsen, O. Rathmann, K. Hansen, E. Politis, J. Prospathopoulos, J. Schepers, K. Rados, D. Cabezón, W. Chlez, A. Neubert, and M. Heath. 2011. *Flow and wakes in large wind farms: Final report for UpWind WP8*. Technical report. Risø DTU.

Baumert, H. and H. Peters. 2000. Second-moment closures and length scales for weakly stratified turbulent shear flows. *Journal of Geophysical Research*, vol. 105, no. C3, p. 6453–6468.

Bechmann, A., N. Sørensen, J. Berg, J. Mann, and P.-E. Réthoré. 2011. The Bolund experiment, Part II: Blind comparison of microscale flow models. *Boundary-Layer Meteorology*, vol. 141, no. 2, p. 245–271.

Bechmann, A. and N. Sørensen. 2010. Hybrid RANS/LES method for wind flow over complex terrain. *Wind Energy*, vol. 13, no. 1, p. 36–50.

Bechmann, A., J. Johansen, and N. Sørensen. 2007. *The Bolund experiment - Design of measurement campaign using CFD*. Technical Report R-1623(EN). Risø, 20 p.

Berg, J., J. Mann, A. Bechmann, M. Courtney, and H. Jørgensen. 2011. The Bolund experiment, Part I: Flow over a steep, three-dimensional hill. *Boundary-Layer Meteorology*, vol. 141, no. 2, p. 219–243.

Betts, P. and V. Haroutunian. 1983. *A $k-\varepsilon$ finite element simulation of buoyancy effects in the atmospheric surface layer*. Technical Report 83-WA/HT-32. American Society of Mechanical Engineers, 8 p.

Bitsuamlak, G., T. Stathopoulos, and C. Bedard. 1999. Numerical evaluation of wind flow over complex terrain: Review. *Journal of Aerospace Engineering*, vol. 17, no. 4, p. 135–145.

Blackadar, A. 1962. The vertical distribution of wind and turbulent exchange in a neutral atmosphere. *Journal of Geophysical Research*, vol. 67, no. 8, p. 3095–3102.

Blocken, B., T. Stathopoulos, and J. Carmeliet. 2007. CFD simulation of the atmospheric boundary layer: wall function problems. *Atmospheric Environment*, vol. 41, no. 2, p. 238–252.

Blocken, B., P. Moonen, T. Stathopoulos, and J. Carmeliet. 2008. Numerical study on the existence of the Venturi effect in passages between perpendicular buildings. *Journal of Engineering Mechanics*, vol. 134, no. 12, p. 1021–1028.

Bradley, E. 1980. An experimental study of the profiles of wind speed, shearing stress and turbulence at the crest of a large hill. *Quarterly Journal of the Royal Meteorological Society*, vol. 106, no. 447, p. 101–123.

Brasseur, J. and T. Wei. 2010. Designing large-eddy simulation of the turbulent boundary layer to capture law-of-the-wall scaling. *Physics of Fluids*, vol. 22, no. 2, p. 1–21.

Brockmann, U., K. Eberlein, K. Huber, H.-J. Neubert, G. Radach, and K. Schulze. 1984. "JONSDAP '76: FLEX/INOUT ATLAS Vol. I & II". (Copenhagen, Denmark 1984). ICES Oceanographic Data Lists and Inventories.

Brodeur, P. and C. Masson. 2008. Numerical site calibration over complex terrain. *Transactions of the ASME - Journal of Solar Energy Engineering*, vol. 130, no. 3, p. 1–12.

Burchard, H. and H. Baumert. 1995. On the performance of a mixed-layer model based on the $k-\varepsilon$ turbulence closure. *Journal of Geophysical Research*, vol. 100, no. C5, p. 8523–8540.

Businger, J., J. Wyngaard, Y. Izumi, and E. Bradley. 1971. Flux-profile relationships in the atmospheric surface layer. *Journal of the Atmospheric Sciences*, vol. 28, no. 2, p. 181–189.

Cabezón, D., J. Sanz, I. Martí, and A. Crespo. 2009. "CFD modelling of the interaction between the surface boundary layer and rotor wake: Comparison of results obtained with different turbulence models and mesh strategies". In *Proceedings of EWEC 2009*. (Marseilles, France 2009), p. 1–7. European Wind Energy Association.

Cabezón, D., E. Migoya, and A. Crespo. 2011. Comparison of turbulence models for the computational fluid dynamics simulation of wind turbine wakes in the atmospheric boundary layer. *Wind Energy*, vol. 14, no. 7, p. 909–921.

Castro, F., J. Palma, and A. Silva Lopes. 2003. Simulation of the Askervein flow. Part I: Reynolds averaged Navier–Stokes equations ($k-\varepsilon$ turbulence model). *Boundary-Layer Meteorology*, vol. 107, no. 3, p. 501–530.

Cebeci, T. and P. Bradshaw, 1977. *Momentum transfer in boundary layers*. New York : Hemispere Publishing Corporation, 407 p.

Chen, Y. and S. Kim. 1987. *Computation of turbulent flows using an extended $k-\varepsilon$ turbulence closure model*. Technical Report CR-179204. NASA, 30 p.

Cheng, Y. and W. Brutsaert. 2005. Flux–profile relationships for wind speed and temperature in the stable atmospheric boundary layer. *Boundary-Layer Meteorology*, vol. 114, no. 3, p. 519–538.

Chien, K.-Y. 1982. Predictions of channel and boundary-layer flows with a low-Reynolds-number turbulence model. *AIAA Journal*, vol. 20, no. 1, p. 33–38.

Chow, F. and R. Street. 2009. Evalution of turbulence closure models for large-eddy simulation over complex terrain: Flow over Askervein hill. *Journal of Applied Meteorology and Climatology*, vol. 48, no. 5, p. 1050–1065.

Chow, F. and R. Street. 2004. "Evaluation of turbulence models for large-eddy simulations of flow over Askervein hill". In *16th Symposium on Boundary Layers and Turbulence*. (Portland, US 2004), p. 381–388. American Meteorological Society.

Chow, F., A. Weigel, R. Street, M. Rotach, and M. Xue. 2006. High-resolution large-eddy simulations of flow in a steep alpine valley. i. Methodology, verification, and sensitivity experiments. *Journal of Applied Meteorology*, vol. 45, no. 1, p. 63–86.

Comte-Bellot, G. and S. Corrsin. 1966. The use of a contraction to improve the isotropy of grid-generated turbulence. *Journal of Fluid Mechanics*, vol. 25, no. 4, p. 657–682.

Crespo, A., F. Manuel, D. Moreno, E. Fraga, and J. Hernandez. 1985. "Numerical analysis of wind turbine wakes". In *Delphi Workshop on Wind Energy Applications*. (Delphi, Greece 1985), p. 15–25.

Crespo, A., J. Hernandez, and S. Frandsen. 1999. Survey of modelling methods for wind turbine wakes and wind farms. *Wind Energy*, vol. 2, no. 1, p. 1–24.

Cuxart, J., G. Morales, E. Terradellas, and C. Yague. 2002. Study of coherent structures and estimation of the pressure transport terms for the nocturnal stable boundary layer. *Boundary-Layer Meteorology*, vol. 105, no. 2, p. 305–328.

Dalpé, B. and C. Masson. 2008. Numerical study of fully developed turbulent flow within and above a dense forest. *Wind Energy*, vol. 11, no. 5, p. 503–515.

Detering, H. and D. Etling. 1985. Application of the $E-\varepsilon$ turbulence model to the atmospheric boundary layer. *Boundary-Layer Meteorology*, vol. 33, no. 2, p. 113–133.

Durbin, P. 1996. On the $k-\varepsilon$ stagnation point anomaly. *International Journal of Heat and Fluid Flow*, vol. 17, no. 1, p. 89–90.

Eidsvik, K. 2005. A system for wind power estimation in mountainous terrain. Prediction of Askervein hill data. *Wind Energy*, vol. 8, no. 2, p. 237–249.

El Kasmi, A. and C. Masson. 2008. An extended $k-\varepsilon$ model for turbulent flow through horizontal-axis wind turbines. *Journal of Wind Engineering and Industrial Aerodynamics*, vol. 96, no. 1, p. 103–122.

El Kasmi, A. and C. Masson. 2010. Turbulence modeling of atmospheric boundary layer flow over complex terrain: A comparison of models at wind tunnel and full scale. *Wind Energy*, vol. 13, no. 8, p. 689–704.

Emeis, S., M. Højstrup, and N. Jensen. 1993. *Hjardemål experiment data report*. Technical report. Risø DTU.

ESDU. 1985. *Engineering sciences data item 85020*. Technical report. 251-259 Regent Street, London : Engineering Sciences Data Unit.

Espana, G. 2009. "Étude expérimentale du sillage lointain des éoliennes à axe horizontal au moyen d'une modélisation simplifiée en couche limite atmosphérique". PhD thesis, Université d'Orléans, 314 p. In French.

Ferziger, J. and M. Perić, 2002. *Computational methods for fluid dynamics*. Ed. 3. Springer-Verlag, 423 p.

Franke, J., W. Hellsten, H. Schlunzen, and B. Carissimo. 2007. *Best practice guideline for the CFD simulation of flows in the urban environment*. Technical report. Brussels : COST Office, 52 p.

Freedman, F. and M. Jacobson. 2003. Modification of the standard ε-equation for the stable ABL through enforced consistency with Monin-Obukhov similarity theory. *Boundary-Layer Meteorology*, vol. 106, no. 3, p. 383–410.

Frenzen, P. and C. Vogel. 2001. Further studies of atmospheric turbulence in layers near the surface: scaling the TKE budget above the roughness sublayer. *Boundary-Layer Meteorology*, vol. 99, no. 2, p. 173–206.

Gatski, T. and C. Rumsey. 2002. Linear and non-linear eddy viscosity models. Launder, B. and N. Sandham, editors, *Closure strategies for turbulent and transitional flows*, chapter 1, p. 9–46. Cambridge University Press.

Gatski, T. and C. Speziale. 1993. On explicit algebraic stress models for complex turbulent flows. *Journal of Fluid Mechanics*, vol. 254, p. 59–78.

Gibson, M. and B. Launder. 1978. Ground effects on pressure fluctuations in the atmospheric boundary layer. *Journal of Fluid Mechanics*, vol. 86, p. 491–511.

Gómez-Elvira, R., A. Crespo, E. Migoya, F. Manuel, and J. Hernández. 2005. Anisotropy of turbulence in wind turbine wakes. *Journal of Wind Engineering and Industrial Aerodynamics*, vol. 93, no. 10, p. 797–814.

Gorlé, C., J. Vanbeeck, P. Rambaud, and G. Van Tendeloo. 2009. CFD modelling of small particle dispersion: The influence of the turbulence kinetic energy in the atmospheric boundary layer. *Atmospheric Environment*, vol. 43, no. 3, p. 673–681.

Hackman, L. 1982. "A numerical study of the turbulent flow over a backward facing step using a two equation turbulence model". PhD thesis, University of Waterloo.

Hargreaves, D. and N. Wright. 2007. On the use of the $k-\varepsilon$ model in commercial CFD software to model the neutral atmospheric boundary layer. *Journal of Wind Engineering and Industrial Aerodynamics*, vol. 95, no. 5, p. 355–369.

Hartogensis, O. and H. Bruin. 2005. Monin–Obukhov similarity functions of the structure parameter of temperature and turbulent kinetic energy dissipation rate in the stable boundary layer. *Boundary-Layer Meteorology*, vol. 116, no. 2, p. 253–276.

Hashimoto, T., S. Yoshida, and O. Iso. 2007. "Wind farm layout optimization in complex terrains". In *Proceedings of EWEC 2007*. (Milan, Italy 2007). European Wind Energy Association.

IEA. 2010a. *World Energy Outlook 2010 – Executive Summary*. Technical report. International Energy Agency, 18 p.

IEA. 2010b. *Projected costs of generating electricity*. Technical report. International Energy Agency, 218 p.

IEA. 2011. *Clean energy progress report*. Technical report. International Energy Agency, 71 p.

Jasak, H. 1996. "Error analysis and estimation for the finite volume method and applications to fluid flows". PhD thesis, Imperial College, 394 p.

Jenkins, G., P. Mason, W. Moores, and R. Sykes. 1981. Measurements of the flow structure around Ailsa Craig, a steep, three-dimensional, isolated hill. *Quarterly Journal of the Royal Meteorological Society*, vol. 107, no. 454, p. 833–851.

Jimenez, A., A. Crespo, E. Migoya, and J. Garcia. 2007. " Advances in large-eddy simulation of a wind turbine wake ". In *Proceedings of The Science of Making Torque from Wind (2nd conference)*. (Danish Technical University, DK 2007), p. 1–13. Journal of Physics: Conference Series 75.

Jones, W. and B. Launder. 1972. The prediction of laminarization with a two-equation model of turbulence. *International Journal of Heat and Mass Transfer*, vol. 15, no. 2, p. 301–314.

Kaimal, J. and J. Finnigan, 1994. *Atmospheric boundary layer flows*. New York : Oxford University Press, 289 p.

Kalitzin, G., G. Medic, G. Iaccarino, and P. Durbin. 2005. Near-wall behaviour of RANS turbulence models and implications for wall functions. *Journal of Computational Physics*, vol. 204, no. 1, p. 265–291.

Katul, G., L. Mahrt, D. Poggi, and C. Sanz. 2004. One- and two-equation models for canopy turbulence. *Boundary-Layer Meteorology*, vol. 113, no. 1, p. 81–109.

Khosla, P. and S. Rubin. 1974. A diagonally dominant second-order accurate implicit scheme. *Computers & Fluids*, vol. 2, p. 207–289.

Kim, H. and V. Patel. 2000. Test of turbulence models for wind flow over complex terrain with separation and recirculation. *Boundary-Layer Meteorology*, vol. 94, no. 1, p. 5–21.

Kim, H., V. Patel, and C. Lee. 2000. Numerical simulation of wind flow over hilly terrain. *Journal of Wind Engineering and Industrial Aerodynamics*, vol. 87, no. 1, p. 45–60.

Kitada, T. 1987. Turbulence structure of sea breeze front and its implication in air pollution transport - Application of $k-\varepsilon$ turbulence model. *Boundary-Layer Meteorology*, vol. 41, no. 1–4, p. 217–239.

Lam, C. and K. Bremhorst. 1981. A modified form of $k-\varepsilon$ model for predicting wall turbulence. *Journal of Fluids Engineering*, vol. 103, p. 456–460.

Landberg, L., L. Myllerup, O. Rathmann, E. Petersen, B. Jørgensen, J. Badger, and N. Mortensen. 2003. Wind resource estimation - An overview. *Wind Energy*, vol. 6, no. 3, p. 261–271.

Laporte, L. 2008. " Application d'un code CFD atmosphérique à l'estimation du productible éolien en terrain complexe ". PhD thesis, Université Paris-Est, 246 p. In French.

Launder, B. and D. Spalding. 1974. The numerical computation of turbulent flows. *Computer Methods in Applied Mechanics and Engineering*, vol. 3, p. 269–289.

Leclerc, C. 1998. " Simulation numérique de l'écoulement tridimensionnel turbulent dans un parc éolien ". Master's thesis, École Polytechnique de Montréal, 121 p. In French.

Leonard, B. 1979. A stable and accurate convective modelling procedure based on quadratic upstream interpolation. *Computer Methods in Applied Mechanics and Engineering*, vol. 19, no. 1, p. 59–98.

Lopes da Costa, J., F. Castro, J. Palma, and P. Stuart. 2006. Computer simulation of atmospheric flows over real forests for wind energy resource evaluation. *Journal of Wind Engineering and Industrial Aerodynamics*, vol. 94, no. 8, p. 603–620.

Lun, Y., A. Mochida, S. Murakami, H. Yoshino, and T. Shirashawa. 2003. Numerical simulation of flow over topographic features by revised $k-\varepsilon$ models. *Journal of Wind Engineering and Industrial Aerodynamics*, vol. 91, no. 1–2, p. 231–245.

Lun, Y., A. Mochida, H. Yoshino, and S. Murakami. 2007. Applicability of linear type revised $k-\varepsilon$ models to flow over topographic features. *Journal of Wind Engineering and Industrial Aerodynamics*, vol. 95, no. 5, p. 371–384.

Mason, P. and J. King. 1985. Measurements and predictions of flow and turbulence over an isolated hill of moderate slope. *Quarterly Journal of the Royal Meteorological Society*, vol. 111, no. 468, p. 617–640.

Maurizi, A. 2000. Numerical simulation of turbulent flows over 2-D valleys using three versions of the $k-\varepsilon$ closure model. *Journal of Wind Engineering and Industrial Aerodynamics*, vol. 85, no. 1, p. 59–73.

Meyers, J. and C. Meneveau. 2012. Optimal turbine spacing in fully developed wind farm boundary layers. *Wind Energy*, vol. 15, no. 2, p. 305–317.

Michelsen, J. 1992. *Basis3D – A platform for development of multiblock PDE solvers*. Technical report. Technical University of Denmark.

Michelsen, J. 1994. *Block structured multigrid solution of 2D and 3D elliptic PDE solvers*. Technical report. Technical University of Denmark.

Mickle, R., N. Cook, A. Hoff, N. Jensen, J. Salmon, P. Taylor, G. Tetzla, and H. Teunissen. 1988. The Askervein hill project: Vertical profiles of wind and turbulence. *Boundary-Layer Meteorology*, vol. 43, no. 1–2, p. 143–169.

Mikkelsen, R. 2003. "Actuator Disc Methods Applied to Wind Turbines". PhD thesis, Technical University of Denmark, 121 p.

Muramaki, S., A. Mochida, and S. Kato. 2003. Development of local area wind prediction system for selecting suitable site for windmill. *Journal of Wind Engineering and Industrial Aerodynamics*, vol. 91, no. 12–15, p. 1759–1776.

Nagano, Y. and H. Hattori. 2003. "A new low-Reynolds-number turbulence model with hybrid time-scales of mean flow and turbulence for complex wall flows". In *Proceedings of the Fourth International Symposium on Turbulence, Heat and Mass Transfer*. (Antalya, Turkey 2003). ICHMT.

Nagano, Y., H. Hattori, and T. Irikado. 2001. "Prediction of flow over complex terrain using turbulence model". In *Proceedings of the TED-Conference '01*. (Japan 2001). Japan Society of Mechanical Engineers.

Nielsen, M., L. Landberg, N. Mortensen, R. Barthelmie, and A. Joensen. 2001. " Application of the Measure-Correlate-Predict approach for wind resource assessment ". In *Proceedings of EWEC 2001*. (Copenhagen, Denmark 2001), p. 773–776. European Wind Energy Association.

OpenCFD. 2009a. *OpenFOAM: The Open Source CFD Toolbox – Programmer's Guide v1.6*.

OpenCFD. 2009b. *OpenFOAM: The Open Source CFD Toolbox – User Guide v1.6*.

Pahlow, M., M. Parlange, and F. Porté-Agel. 2001. On Monin–Obukhov similarity in the stable atmospheric boundary layer. *Boundary-Layer Meteorology*, vol. 99, no. 2, p. 225–248.

Palma, J., F. Castro, L. Ribeiro, A. Rodrigues, and A. Pinto. 2008. Linear and nonlinear models in wind resource assessment and wind turbine micro-siting in complex terrain. *Journal of Wind Engineering and Industrial Aerodynamics*, vol. 96, no. 12, p. 2308–2326.

Panofsky, H. and J. Dutton, 1984. *Atmospheric Turbulence*. John Wiley & Sons, 397 p.

Parente, A., C. Gorlé, J. van Beeck, and C. Benocci. 2011. Improved k–ε model and wall function formulation for the RANS simulation of ABL flows. *Journal of Wind Engineering and Industrial Aerodynamics*, vol. 99, no. 4, p. 267–278.

Patankar, S., 1980. *Numerical Heat Transfer and Fluid Flow*. Hemisphere Publishing Corporation, 197 p.

Patankar, S. and D. Spalding. 1972. A calculation procedure for heat, mass and momentum transfer in three-dimensional parabolic flows. *International Journal of Heat and Fluid Flow*, vol. 15, p. 1787–1806.

Patel, M., 1999. *Wind and Power Solar Systems*. Boca Raton : CRC Press, 351 p.

Piomelli, U. 2008. Wall-layer models for large-eddy simulations. *Progress in Aerospace Sciences*, vol. 44, no. 6, p. 437–446.

Piomelli, U. and E. Balaras. 2002. Wall-layer models for large-eddy simulations. *Annual Review of Fluid Mechanics*, vol. 34, p. 349–374.

Politis, E., J. Prospathopoulos, D. Cabezón, K. Hansen, P. Chaviaropoulos, and R. Barthelmie. 2012. Modelling wake effects in large wind farms in complex terrain: the problem, the methods and the issues. *Wind Energy*, vol. 15, no. 1, p. 161–182.

Pope, S., 2000. *Turbulent flows*. Cambridge University Press, 771 p.

Prospathopoulos, J., E. Politis, K. Rados, and P. Chaviaropoulos. 2009. " Enhanced CFD modelling of wind turbine wakes ". In *Extended Abstracts for Euromech Colloquium 508 on Wind Turbine Wakes*. (Madrid, Spain 2009). European Mechanics Society.

Prospathopoulos, J., E. Politis, K. Rados, and P. Chaviaropoulos. 2011. Evaluation of the effects of turbulence model enhancements on wind turbine wake predictions. *Wind Energy*, vol. 14, no. 2, p. 285–300.

Prospathopoulos, J. and S. Voutsinas. 2006. Implementation issues in 3D wind flow predictions over complex terrain. *Transactions of the ASME - Journal of Solar Energy Engineering*, vol. 128, no. 4, p. 539–553.

Pullen, A. and S. Sawyer, eds. 2010. *Global wind report: Annual market update 2010*. Technical report. Global Wind Energy Council, 67 p.

Raithby, G., G. Stubley, and P. Taylor. 1987. The Askervein hill project: A finite control volume prediction of three-dimensional flows over the hill. *Boundary-Layer Meteorology*, vol. 39, no. 3, p. 247–267.

Réthoré, P.-E. 2009. "Wind turbine wake in atmospheric turbulence". PhD thesis, Aalborg University, 187 p.

Réthoré, P.-E., N. Troldborg, F. Zahle, and N. Sørensen. 2011. "Comparison of the near wake of different kinds of wind turbine CFD models". In *Wake Conference Book of Abstracts*. (Visby, Sweden 2011), p. 33–38. Gotland University.

Rhie, C. 1981. "A numerical study of the flow past an isolated airfoil with separation". PhD thesis, University of Illinois.

Richards, P. and R. Hoxey. 1993. Appropriate boundary conditions for computational wind engineering models using the $k-\varepsilon$ turbulence model. *Journal of Wind Engineering and Industrial Aerodynamics*, vol. 46 & 47, p. 145–153.

Richards, P. and S. Norris. 2011. Appropriate boundary conditions for computational wind engineering models revisited. *Journal of Wind Engineering and Industrial Aerodynamics*, vol. 99, no. 4, p. 257–266.

Richards, P. and B. Younis. 1990. Comments on 'Prediction of wind generated pressure distribution around buildings'. *Journal of Wind Engineering and Industrial Aerodynamics*, vol. 34, p. 107–110.

Richards, P., A. Quinn, and S. Parker. 2002. A 6 m cube in an atmospheric boundary-layer flow. Part 2. Computational studies. *Wind and Structure*, vol. 5, no. 2–4, p. 177–192.

Riddle, A., D. Carruthers, A. Sharpe, C. McHugh, and J. Stocker. 2004. Comparisons between FLUENT and ADMS for atmospheric dispersion modelling. *Atmospheric Environment*, vol. 38, no. 7, p. 1029–1038.

Rodi, W. 1987. Examples of calculation methods for flow and mixing in stratified fluids. *Journal of Geophysical Research*, vol. 92, no. C5, p. 5305–5328.

Sagaut, P., 2006. *Large Eddy Simulation for Incompressible Flow*. Ed. 3. Springer.

Salmon, J., H. Teunissen, R. Mickle, and P. Taylor. 1988. The Kettles Hill Project: Field observations, wind-tunnel simulations and numerical model predictions for flow over a low hill. *Boundary-Layer Meteorology*, vol. 43, p. 309-343.

Sanderse, B., S. van der Pijl, and B. Koren. 2011. Review of computational fluid dynamics for wind turbine wake aerodynamics. *Wind Energy*, vol. 14, no. 7, p. 799–819.

Sanz Rodrigo, J., D. Cabezón, I. Martí, P. Patilla, and J. van Beeck. 2008. "Numerical CFD modelling of non-neutral atmospheric boundary layers for offshore wind resource assessment based on Monin-Obukhov theory". In *Proceedings of EWEC 2008*. (Brussels, Belgium 2008). European Wind Energy Association.

Shih, T., J. Zhu, and J. Lumley. 1995. A new Reynolds stress algebraic equation model. *Computer Methods in Applied Mechanics and Engineering*, vol. 125, no. 1–4, p. 287–302.

Silva Lopes, A. and J. Palma. 2002. "Large eddy simulation of flow around the Askervein hill". In *Proceedings of 3rd Theoretical Fluid Mechanics Meeting*. (St. Louis, US 2002). American Institute of Aeronautics and Astronautics.

Silva Lopes, A., J. Palma, and F. Castro. 2007. Simulation of the Askervein flow. Part 2: Large-eddy simulations. *Boundary-Layer Meteorology*, vol. 125, no. 1, p. 85–108.

Snyder, W. 1981. *Guideline for fluid modelling of atmospheric diffusion*. Technical Report EPA-600/8-81-009. US Environment Protection Agency, 185 p.

Sogachev, A. and O. Panferov. 2006. Modification of two-equation models to account for plant drag. *Boundary-Layer Meteorology*, vol. 121, p. 229–266.

Sørensen, J., W. Shen, and X. Munduate. 1998. Analysis of wake states by a full-field actuator disc model. *Wind Energy*, vol. 1, no. 2, p. 73-88.

Sørensen, N. 1995. "General purpose flow solver applied to flow over hills". PhD thesis, Risø DTU. Risø-R-827(EN).

Sørensen, N. 1998. *HypGrid2D – a 2-D mesh generator*. Technical report. Risø DTU.

Sørensen, N., A. Bechmann, L. Myllerup, and P. Botha. 2007. "Identification of severe wind conditions using a Reynolds averaged Navier-Stokes solver". In proceedings of the European Wind Energy Association/EAWE special topic conference: The Science of Making Tourque from Wind.

Sumner, J., C. Sibuet Watters, and C. Masson. 2010. CFD in wind energy: The virtual, multiscale wind tunnel. *Energies*, vol. 3, no. 5, p. 989–1013.

Svensson, U. and K. Häggkvist. 1990. A two-equation turbulence model for canopy flows. *Journal of Wind Engineering and Industrial Aerodynamics*, vol. 35, p. 201–211.

Taylor, P. and H. Teunissen. 1987. The Askervein hill project: Overview and background data. *Boundary-Layer Meteorology*, vol. 39, no. 1–2, p. 15–39.

Taylor, P., J. Walmsley, and J. Salmon. 1983. A simple model of neutrally-stratified boundary-layer flow over real terrain incorporating wavenumber-dependent scaling. *Boundary-Layer Meteorology*, vol. 26, no. 2, p. 169–189.

Townsend, A., 1976. *The Structure of Turbulent Shear Flow*. Ed. 2nd. Cambridge : Cambridge University Press, 448 p.

TPWind. 2008. *Strategic research agenda: Market deployment strategy 2008–2030*. Technical report. European Wind Energy Technology Platform, 52 p.

Troen, I. and E. Petersen, 1989. *The European Wind Atlas*. Roskilde, Denmark : Risø National Laboratory, 656 p.

Uchida, T. and Y. Ohya. 1999. Numerical simulation of atmospheric flow over complex terrain. *Journal of Wind Engineering and Industrial Aerodynamics*, vol. 81, no. 1–3, p. 283–293.

Uchida, T. and Y. Ohya. 2003. Large-eddy simulation of turbulent airflow over complex terrain. *Journal of Wind Engineering and Industrial Aerodynamics*, vol. 91, no. 1–2, p. 219–229.

Uchida, T. and Y. Ohya. 2006. Application of LES technique to diagnosis of wind farm by using high resolution elevation data. *JSME International Journal*, vol. 49, no. 3, p. 567–575.

Undheim, O., H. Andersson, and E. Berge. 2006. Non-linear, microscale modelling of the flow over Askervein hill. *Boundary-Layer Meteorology*, vol. 120, no. 3, p. 477–495.

VDI. 2000. *Physical modelling of flow and dispersion processes in the atmospheric boundary layer - Application to wind tunnels*. Technical Report VDI 3783/12. Verein Deutscher Ingenieure.

Vermeer, L., J. Sørensen, and A. Crespo. 2003. Wind turbine wake aerodynamics. *Progress in Aerospace Sciences*, vol. 39, no. 6–7, p. 467–510.

Wilcox, D., 1998. *Turbulence Modeling for CFD*. La Canada : DWC Industries, 522 p.

Wood, N. 2000. Wind flow over complex terrain: A historical perspective and the prospect for large-eddy modelling. *Boundary-Layer Meteorology*, vol. 96, no. 1–2, p. 11–32.

Yakhot, V. and L. Smith. 1992. The renormalization group, the ε-expansion and derivation of turbulence models. *Journal of Scientific Computing*, vol. 7, no. 1, p. 35–61.

Yakhot, V. and S. A. Orszag. 1986. Renormalization group analysis of turbulence. I. Basic theory. *Journal of Scientific Computing*, vol. 1, no. 1, p. 3–51.

Yang, Y., M. Gu, S. Chen, and X. Jin. 2009. New inflow boundary conditions for modelling the neutral equilibrium atmospheric boundary layer in computational wind engineering. *Journal of Wind Engineering and Industrial Aerodynamics*, vol. 97, no. 2, p. 88–95.

Ying, R., V. Canuto, and R. Ypma. 1994. Numerical simulation of flow data over two-dimensional hills. *Boundary-Layer Meteorology*, vol. 70, no. 4, p. 401–427.

Zeman, O. and N. Jensen. 1987. Modification of turbulence characteristics in flow over hills. *Quarterly Journal of the Royal Meteorological Society*, vol. 113, p. 55–80.